Design Optimization and Knowledge Mining for Turbomachinery

	Tohoku University
URL	http://hdl.handle.net/10097/39936

Design Optimization and Knowledge Mining for Turbomachinery

（ターボ機械の最適化と設計知識マイニング）

by

Kazuyuki SUGIMURA

January 16, 2009

Design Optimization and Knowledge Mining
for Turbomachinery

Kazuyuki Sugimura

Abstract

Turbomachinery is widely used for exchanging mechanical energy and fluid energy continuously. It can be classified into several categories, *i.e.*, fans, blowers, compressors, turbines, pumps, and water mills, according to the types of fluid media and directions of energy exchange. They are used in various situations in power plants, industrial machines, consumer products, *etc*. There is increasing social demand for minimizing energy consumption to reduce carbon dioxide emissions and suppress global warming. Therefore, the aerodynamic performance of turbomachinery, particularly aerodynamic efficiency, has to be improved as much as possible. A great deal of effort has been already made to improve the aerodynamic performance of turbomachinery used in power plants and industrial machines, where the amounts of energy consumption are relatively large. In contrast, there have been fewer efforts for turbomachinery used in consumer products. In these products, centrifugal configuration is often used because of its ability to provide higher pressure increases in a more compact body.

One solution for improving the performance is the application of numerical design optimization methods. Design optimization methods for turbomachinery have been investigated since the 1990s. However, there are several problems to apply these existing methods to practical designs in industry, particularly to the designs of centrifugal turbomachinery used for consumer products. One problem is the short design turnaround time. As product life cycles are short and computational resources are limited, it is necessary to develop efficient design optimization methods capable of reducing the design lead time. Another problem arises from uncertainties in practical designs. Designers are often faced with uncertainties in design decisions and design conditions, which cannot be defined deterministically at the start of the designs. The uncertainty in design decisions is defined as freedom of choosing trade-off balance among multiple design objectives. The uncertainty in design conditions is defined as variance in products, such as dimensions and material properties. Practical design optimization methods have to be capable of handling these uncertainties. Another problem is concerned with how to reinforce the design knowledge of designers. Unlike academic applications, industrial designers must repeat and improve design routines. Therefore, it is necessary to develop knowledge-oriented design methods, with which designers can discover design insights such as important design parameters and design rules applicable to subsequent steps in the design process.

Design exploration methods, which combine design optimization and data mining, have been used to facilitate knowledge-oriented design optimization. Thus, the objectives of this research include the proposal and development of practical design exploration methods for centrifugal turbomachinery configurations capable of resolving the problems described above. This research is composed of four stages of developments to achieve this final goal.

In the first stage, single-objective design exploration methods were developed. An efficient method for three-dimensional shape parameterization of centrifugal turbomachinery was developed using a minimum set of non-uniform rational B-Spline curves. These curves

were assigned only to the enclosed boundaries of the blades consisting of the hub, shroud, leading edge, and trailing edge profiles. In other words, traditional multi-sectional definition of the blade profile was avoided and the number of design variables was reduced. An efficient single-objective global optimization method was developed by combining simulated annealing and artificial neural network. The neural network adaptively learned the simulation results collected by simulated annealing. The trained neural network, as an approximation model, periodically predicted a possible global optimum to shorten optimization lead time. Simulated annealing itself explored the design space independently of the neural network in case the neural network learning failed. This ensured a robust and fully automatic optimization. With these methods, the required design turnaround time was reduced, although the degree of reduction depended on the prediction accuracy of the neural network. As the first step of data mining, the global characteristics of the design space were analyzed using regression analysis. The analysis was attempted to extract useful information such as sensitivity and non-linearity of the design space. The design exploration methods developed in this stage were applied to the design problems of centrifugal impeller and diffuser for a vacuum cleaner. The optimized impeller had a unique S-shaped leading edge profile, which effectively controlled secondary flows and improved the flow uniformity at the impeller exit. The optimized diffuser had a unique bending trailing edge with a wedge-shaped gap, which generated a streamwise vortex and prevented boundary layer separation. The regression analysis revealed important design variables that were related to these unique shapes of the optima.

In the second stage, multi-objective design exploration methods were developed. A multi-objective optimization approach was taken to handle the uncertainty in design decisions, *i.e.,* the variety in trade-off balance among objective functions. A multi-objective genetic algorithm was employed with enhancements of convergence to widespread non-dominated solutions. It enabled the acquisition of multiple design candidates with different trade-off balance, from which the best design candidate can be chosen according to the requirement specified afterward. This method was applied to the design of a low-specific-speed centrifugal impeller with a vaned diffuser for a vacuum cleaner. The design objectives were set to improve both aerodynamic efficiency and aerodynamic stability. Computational fluid dynamics were conducted for a combined model of blade-to-blade regions of an impeller and a diffuser. A time-averaged and spatially distributed flow was modeled at the mixing plane to evaluate the flow uniformity, which affected aerodynamic stability. Seven non-dominated solutions were obtained, and the improvements in both design objectives were confirmed by experiments with a selected non-dominated solution. Data mining methods, namely decision tree analysis and rough set theory, were applied to extract quantitative design rules for improving each of the objective functions to the maximum limit. The obtained rules indicated that dimensions such as inlet blade angle, vane-less diffuser height, and blade load balance were important for the extreme designs, helping designers correlate important design variables with underlying flow physics. It was also clarified that decision tree analysis generally extracts a single rule of *necessary condition*, while rough set theory mines multiple rules of *sufficient conditions*. Decision tree analysis extracts a single but yet simple rule, while rough set theory extracts multiple but yet complicated rules.

In the third stage, multi-objective robust design exploration (MORDE) methods were developed. The previously developed method was extended to a multi-objective *robust* optimization method to handle the uncertainty in design conditions, *i.e.*, the variance in product's properties. Probabilistic representations of design parameters were introduced to the multi-objective genetic algorithm to model these variances. The parameter representation was generalized in such a way that it was compatible with that in the Taguchi method. Kriging models were adopted as approximation models to conduct large number of response calculation among design parameters swiftly. Data mining methods, namely Self-organizing maps and association rules, were used to clarify the design rules for achieving certain

trade-off balance among multiple objective functions. The combined use of the association rule with an aspiration vector, which specified the desired trade-off balance, was proposed to analyze multi-objective design space. The MORDE was applied to a centrifugal fan design problem of a washer-dryer. This design was aimed toward improving the means and standard deviations of the resultant statistical distributions of fan efficiency and turbulence noise level. The variances were assumed to exist in the fan's dimensions due to mass production. It was demonstrated that designers could obtain the best design candidate and quantitative rules that met with the required trade-off balance. It was also demonstrated that traditional non-robust optimal design as well as quality-weighted design such as the Taguchi method were simultaneously accomplished with the MORDE. It was clarified that association rule generally reveals multiple and quantitative design rules, while it is difficult to perform the same analysis with Self-organizing map. Association rules can be either *necessary* or *sufficient conditions* according to the control parameters for rule extraction. The design turn around time necessary for this fan design was only two weeks and was considered to be practical. Based on these investigations, it was concluded that practical design exploration methods were established with the MORDE, with which knowledge-oriented design optimization under the uncertainties became feasible within short design turnaround time.

In the final stage, another practical design exploration method was further developed. Because design rules represent key structures in multi-objective design space, they were considered to be useful in determining the optimum setup of design variables. Therefore, a new rule-based multi-objective parameter design method was proposed. This method utilized a database of design rules obtained by the following data mining methods, namely analysis of variance, Self-organizing maps, decision tree analysis, rough set theory, and association rule. Comparative studies of these methods revealed the strengths and weaknesses of each method, and a systematic procedure was developed for applying these methods in a complementary way. Firstly, analysis of variance was applied to determine dominant main and interaction effects of design variables, which were used in the latter process of data mining. Self-organizing maps or alternative visualization methods were used to find qualitative low-order correlations, particularly trade-off relationships between objective functions. Then, design rule extraction methods were applied to obtain quantitative rule sets. Decision tree analysis could be applied to extract an easy-to-understand rule. However, decision tree analysis could be skipped because the rule could not distinguish main and interaction effects. Both rough set theory and association rule were applied to extract multiple design rules that distinguished main and interaction effects. While rules from rough set theory were only *sufficient conditions*, association rules could be either of *sufficient* or *necessary conditions*. However, rough set theory had an advantage in capability of automatic finding the minimum rule length, which had to be specified manually in the case of association rule. Therefore, the usage of association rule, after obtaining the proper rule length by rough set theory, was recommended. Once the design rule database was obtained, the proposed method first used predominant main effects of different design variables for optimizing different objective functions. Then, it used predominant interaction effects to resolve any remaining trade-off conflicts. The capability of this method was demonstrated using the same design optimization problem of a washer-dryer's fan. It was confirmed that this method was superior to the Taguchi method in its capability of performing multi-objective design.

Based on the developments of design optimization and data mining methods described above, design exploration for centrifugal turbomachinery configurations has become practical for industrial applications. The methods were successfully applied to actual products of a vacuum cleaner and a washer-dryer in Hitachi Ltd., which suggested the methods' capabilities in real-world applications.

Table of Contents

List of Figures

List of Tables

Chapter 1

Introduction

1.1 Background and Previous Work

Turbomachinery is widely used for exchanging mechanical energy and fluid energy continuously, and can be classified into several categories, *i.e.*, fans, blowers, compressors, turbines, pumps, and water mills, according to the types of fluid media and directions of energy exchange (Table 1-1). They are used in various situations in power plants, industrial machines, consumer products, *etc.*

There is increasing social demand for minimizing energy consumption to reduce carbon dioxide emissions and suppress global warming. According to the Kyoto Protocol [1], Japan must reduce environmentally harmful gas emissions by 6% of that in 1990 by 2012. Therefore, the aerodynamic performance of turbomachinery, particularly aerodynamic efficiency, must be improved as much as possible. A great deal of effort has been made to improve the aerodynamic performance of turbomachinery used in power plants and industrial machines, where the levels of energy consumption are relatively large.

In contrast, there have been fewer efforts for turbomachinery used in consumer products. In these products, centrifugal configurations are often used because they can provide higher pressure increases in a more compact body than various other types of turbomachinery. Thus, at the start of this research, the main focus was centrifugal fans and blowers, and the goal was to develop design optimization methods for achieving extreme performance of these types of turbomachinery.

Before 1990, industrial designs of turbomachinery were mainly conducted using one-, two-, or quasi-three-dimensional performance prediction tools that formulated simplified governing equations of fluid. Then, designs using fully three-dimensional analysis became available during the 1990s with the significant improvements in computer hardware and commercial computational fluid dynamics (CFD) software incorporating advanced numerical techniques. Many experimental approaches were replaced with CFD in industry during this period. In the latter half of the 1990s, some researchers in public research institutes began to use numerical optimization techniques that combined CFD and optimization algorithms.

For example, Pierrt [2] developed a blade raw design system using Reynolds-averaged

Navier-Stokes flow simulations and an artificial neural network. This was an expert system that accumulated results of expensive flow simulations as a design database, which were then learned by the artificial neural network to predict better design candidates. Although optimization was attempted, the targets of this design system were two-dimensional axial turbomachinery configurations. Dennis *et al.* [3] applied a genetic algorithm and sequential quadratic programming to a two-dimensional axial airfoil design problem to accelerate global optimization. Although a significant reduction of total pressure loss was achieved, many expensive Navier-Stokes simulations were required to determine the optimum solutions. Benini and Tourlidakis [4] applied genetic algorithms to two-dimensional centrifugal diffuser design, but this work also required expensive computations.

Most of the previous works focused on optimization of axial turbomachinery configurations, and fewer studies were found for centrifugal ones. More importantly, computations for merely two-dimensional designs were too expensive to carry out design optimizations for consumer products, for which short design turnaround times were required. It was another characteristic of these previous works that they mainly aimed at obtaining optimal solutions and paid less attention to analysis of reasons for achieving the optimality. Regarding to the short design turnaround time, a practical approach was taken by Advanced Design Technology [5], which used an inverse design method for turbomachinery. Although the computational cost was drastically reduced for designing centrifugal turbomachinery, the method was only based on inviscid flow simulations.

Figure 1-1 illustrates the problems of applying existing design optimization methods to practical designs of consumer products, using the design of a vacuum cleaner as an example. As shown in Fig. 1-1, the product was developed through the processes of conceptual design, basic design, detailed design, trial, and production.

The first problem was the need for a short design turnaround time. The turnaround time could be reduced by numerically efficient optimization methods as well as reduction of redesign cycles necessary for modifications. Thus, it was necessary to represent the turbomachinery shape with sufficient flexibility with as a few design variables as possible. It was also necessary to conduct global optimization using as few CFD evaluations as possible.

The second problem was the existence of uncertainties in practical designs. Uncertainties exist in both design decisions and design conditions. The uncertainty in design decisions is defined as the variations in trade-off balance among multiple design objectives (objective functions). For example, the sales points of a vacuum cleaner may include high suction power, low noise, and light weight, and the designer usually assumes a certain balance between these sales points. However, the balance is essentially determined through

negotiations between suppliers, buyers (customers), and competitors during or after the design stage. If the assumptions made are not correct, time-consuming redesign cycles then become necessary.

The uncertainty in design conditions is defined as the variances in the properties of a product (design variables). The variances appear in dimensions, material properties, environmental conditions, and degree of aged deteriorations. The variances are important for mass-produced consumer products. For example, the suction power of a vacuum cleaner varies due to variances in dimensions of centrifugal blowers. A designer usually assumes certain statistics for the variances based on experience and previous records. If the variances exceed the allowable limits, redesign cycles again become necessary.

Thus, practical designs had to deal with these uncertainties, which could not be handled by existing deterministic optimization methods. As design optimization involves solving a mathematically defined problem, the quality of the design depends on the quality of the problem definition. Therefore, a design optimization method that could model and handle these uncertainties is required.
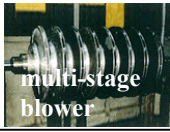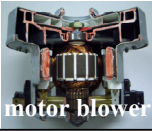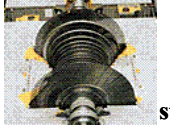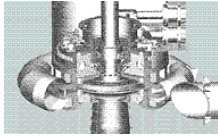
The third problem was the demand for design knowledge reinforcement. The design process shown in Fig. 1-1 was repeated as the product life cycle, and we expected a new design to be improved by using previously acquired design knowledge. Thus, some mechanisms of reinforcing design knowledge in design routines were necessary in practical designs. That is, a practical design optimization method should aim at reason-oriented design, not result-oriented design as used in previous work.

Figure 1-2 shows a new design paradigm for solving these problems in comparison with the traditional paradigm. In the traditional approach, the performance of the product is optimized in a step-by-step manner by trial-and-error. The resultant solution is a local optimum and is risky to the uncertainties. In contrast, the new design paradigm uses the following two steps. The first step is efficient global optimization, taking multiple design objectives and even the effects of variances into account. As the result of this step, a design database is obtained, which consists of non-dominated solutions and design-of-experiment (DOE) data. In the second step, data mining is conducted with the design database to analyze the design space and obtain design knowledge. The resultant solution is a global optimum that can be adapted to the uncertainties. Moreover, design knowledge can be obtained systematically.

This combination of design optimization and data mining to facilitate knowledge-oriented design optimization is called design exploration [6]. The present study took the design exploration approach and develops practical methods for this approach.

Table 1-1 Categories of turbomachinery

type	fluid media	direction of energy exchange	examples
fan	gas	mechanical energy → fluid energy	tunnel jet fan cooling fan
blower	gas	mechanical energy → fluid energy	multi-stage blower motor blower
compressor	gas	mechanical energy → fluid energy	multi-stage compressor
turbine	gas	fluid energy → mechanical energy	steam turbine
pump	liquid	mechanical energy → fluid energy	mixed-flow pump
water mill	liquid	fluid energy → mechanical energy	Francis turbine
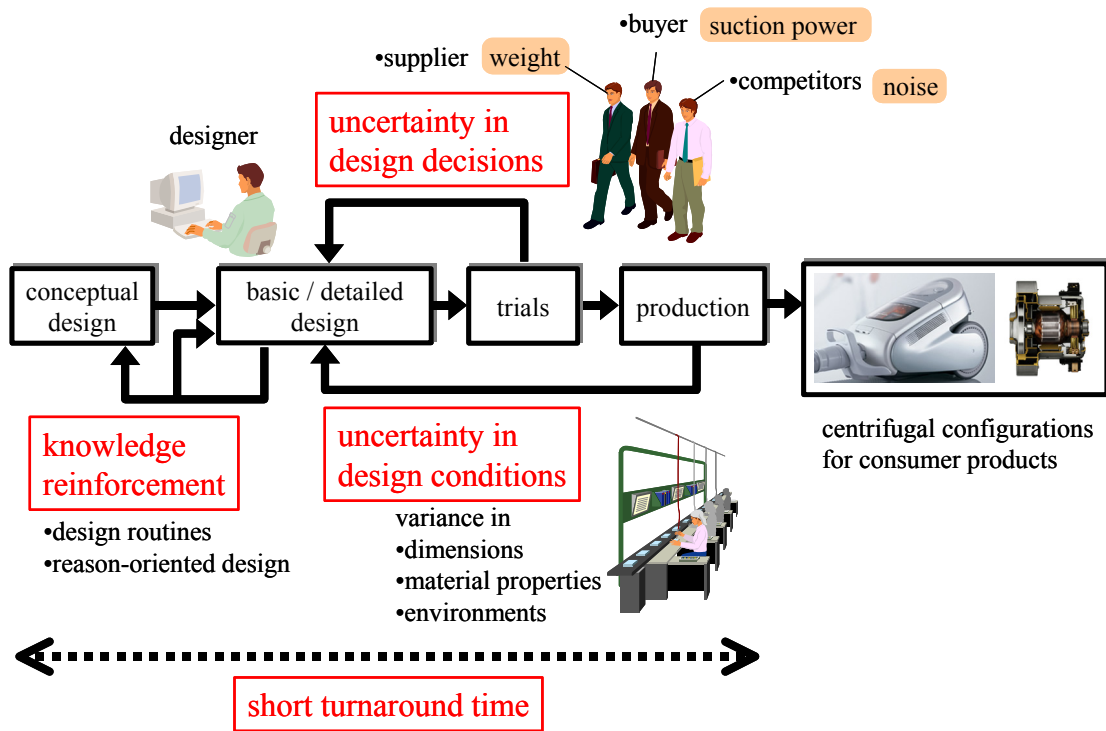
Figure 1-1 Problems in practical design

Traditional paradigm
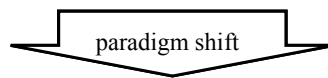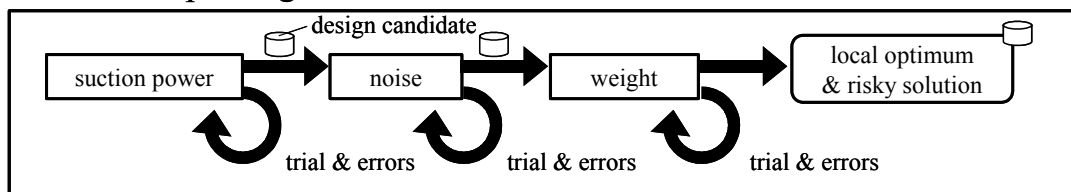
New paradigm
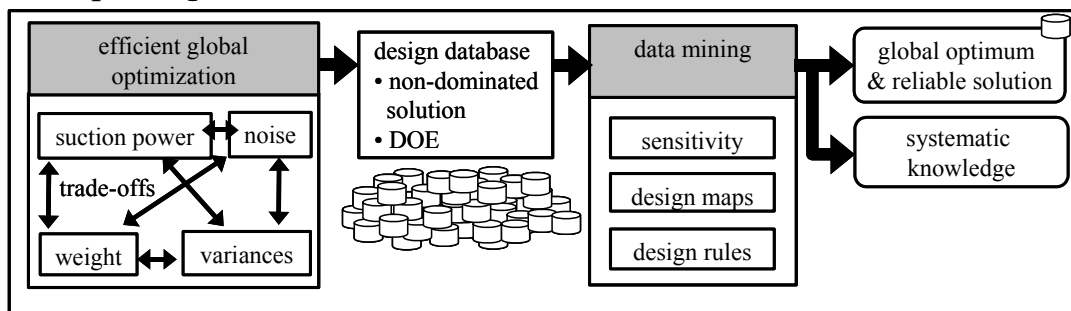
Figure 1-2 Paradigm shift in engineering design

1.2 Research Objectives

The objective of this research was to develop and propose practical design exploration methods that can solve the problems described in the previous section. The capabilities of the developed methods were examined with industrial applications of centrifugal turbomachinery for consumer products.

This final goal was achieved by taking the following stages of development.

I.   Stage 1

- Efficient shape parameterization for centrifugal turbomachinery configurations.
- Single-objective efficient global optimization.
- Analysis of global characteristics of design space.

II.   Stage 2

- Multi-objective optimization.
- Extraction of design rules for achieving extreme designs.

III. Stage 3

- Multi-objective robust optimization using approximation models.
- Extraction of design rules for controlling trade-off balance.

IV.   Stage 4

- Comparative study of data mining methods.
- Practical parameter design method based on cooperative data mining.

1.3 Organization of Thesis

The chapters of this thesis are assigned to the development stages described in the previous section. Chapter 2 describes an efficient shape parameterization method tailored for centrifugal turbomachinery configurations. The shape is modeled with non-uniform rational B-Spline curves for reducing the number of design variables necessary. This chapter also describes a single-objective efficient optimization algorithm that combines simulated annealing with artificial neural network for reduction of computational costs. The fundamental characteristics of the global design space, such as sensitivity and non-linearity, are analyzed using regression analysis with a neural network. These methods are applied to the design of centrifugal impeller and diffuser for a vacuum cleaner.

Chapter 3 describes a multi-objective optimization method that can handle the uncertainty in design decisions, *i.e.*, the varieties in trade-off balance among multiple objective functions. A multi-objective genetic algorithm is developed to efficiently obtain widespread non-dominated solutions. Design rules to improve each objective function are extracted using decision tree analysis and rough set theory to find key design points and relate them to flow physics. These methods are applied to the design of a centrifugal impeller accompanied with a diffuser for a vacuum cleaner.

Chapter 4 explains a multi-objective robust optimization method that can additionally handle the uncertainty in design conditions, *i.e.*, the variance in design variables. A probabilistic representation of design parameters is incorporated into the multi-objective optimization method developed in Chapter 3. Kriging approximation models are adopted for rapidly evaluating statistical responses among design parameters. Design rules for controlling trade-off balance in high-dimensional objective function space are extracted using Self-organizing maps and association rules. The combined use of association rules with "aspiration vectors" is newly proposed, which helps in the decision-making process. These methods are applied to the design of centrifugal fan for a washer-dryer.

Chapter 5 summarizes the data mining methods investigated in Chapters 2, 3, and 4, adding analysis of variance to quantify the effects of design variables on objective functions. Based on comparative studies on these data mining methods, the strengths and weaknesses of each method are clarified and a new rule-based multi-objective parameter design method is proposed as a practical design optimization method. The capabilities of this method are demonstrated with the same design problem as discussed in Chapter 4.

Chapter 6 repeats the conclusions of each chapter and presents the final conclusions of

this thesis. It also comments on possible future work.

Appendix A gives the detailed explanation on non-uniform rational B-spline curve used for shape parameterization of centrifugal turbomachinery.

References

[1] Abstract of Kyoto Protocol, http://www.env.go.jp/earth/cop6/3-2.html.

[2] Pierrt, S., Van den Braembussche, R. A., Turbomachinery Blade Design using a Navier-Stokes Solver and Artificial Neural Network, ASME paper 98-GT-04, 1998.

[3] Dennis, B. H., Dulikravich G. S., Han, Z. X., Constrained Shape Optimization of Airfoil Cascades using a Navier-Stokes Solver and a Genetic/SQP Algorithm, ASME Paper No. 99-GT-441, 1999.

[4] Benini, E., Tourlidakis A., "Design Optimization of Vaned Diffusers for Centrifugal Compressors Using Genetic Algorithm", AIAA-2001-2583, 2001.

[5] Turbo Design[-1], http://www.adtechnology.co.uk/, Advanced Design Technology, UK, 1999.

[6] Obayashi, S., Jeong, S., Chiba, K., and Morino, H., Multi-Objective Design Exploration and its Application to Regional-Jet Wing Design, Transaction of the Japan Society for Aeronautical and Space Science, Vol. 50, No. 167, pp.1-8, May 2007.

Chapter 2

Single-objective Design Exploration
using Simulated Annealing, Neural Network,
and Regression Analysis

2.1 Introduction

Centrifugal fans (or blowers) are suitable to transport gas in compact mechanical systems such as consumer products because they can provide higher pressure-rises than other types of similar-sized turbomachinery. They generally consist of centrifugal impellers, diffusers, volutes, and/or collectors. Unlike high-grade centrifugal compressors used in jet engines or gas turbines, centrifugal fans in consumer products must be developed quickly and produced inexpensively. Nevertheless, there has been a strong need to improve their aerodynamic efficiency.

Recently, numerical optimization techniques have been employed in turbomachinery designs in order to improve performance and shorten lead-time. For example, Pierrt [1][2] used artificial neural network for blade raw design. Dennis [3] used genetic algorithm and sequential quadratic programming for cascade design. Benini [4] and Platt [5] used genetic algorithm for designs of centrifugal configurations of turbomachinery. These previous works were concerned with high-grade turbomachinery.

However, there are several difficulties in applying such optimization techniques to inexpensive centrifugal fans. First, designers need a simplified but flexible shape parameterization method, because these fans usually have two-dimensional shapes, rather than complex three-dimensional ones. This means the parameterization methods must be able to represent innovative two-dimensional shapes that can be easily produced but yet promise better performance. Second, the optimum design should be automated and efficiently conducted, because the allowable design time is short. This requires us not only to use an automatic and efficient global optimization algorithm for a one-time design cycle, but also to establish a knowledge-based engineering process to achieve technological maturity over the course of the design cycles.

Samareh [6][7] reviewed various shape-parameterization techniques for design and optimization. Nowadays, CAD-oriented modeling and morphing (e.g. free form deformation) seem to be the most versatile approaches in the sense that they don't limit the design targets. However, CAD-oriented modeling still has defects in automatic mesh generation, and morphing suffers from the problems of collapsed meshes, which frequently occurs when deformed hexahedral mesh is used for flow simulations. Once these problems arise, it becomes very difficult to automate the design process. In contrast, shape parameterization with polynomial and partial differential equations has been shown to be good for modeling and meshing standardized geometries such as those of airplanes and turbomachinery. Even when the geometry becomes slightly more complex, the combination of this shape parameterization and unstructured mesh generation enables to conduct shape optimization, as investigated by Newman [8].

Therefore, the author employed a non-uniform rational B-spline (NURBS) curve [9], which is a type of polynomial equation. In Section 2.2, the author introduces a NURBS-based shape parameterization method for two-dimensional centrifugal fans, particularly for enhancing flexibility at blade edges.

For efficient global optimization, a two-step approach has become popular: it consists of (step 1) construction of a response surface (or a meta-model), and (step 2) global optimization on the response surface. For example, Pierrt [10] developed a blade design system for axial compressors using an artificial neural network and simulated annealing. This system stores Navier-stokes simulation results, which are then used to build a response surface represented by the neural network. Design optimization on the response surface is conducted using the simulated annealing algorithm afterwards. It has been verified by many researchers that these types of two-step approaches are very efficient. However, we need special care to the accuracy of the response surfaces and robustness in building these models. Otherwise, as the result of trusting the model excessively, we sometimes obtain incorrect optimums or suffer from bankrupcty of automated design processes. These problems may arise when the design space is too complex to be approximated by the model. This is actually the case for centrifugal fans in which the inner flow is more complicated than those of axial fans.

For these reasons, the author chose an approach, whereby the construction and utilization of a response surface and exploration using a global optimization algorithm is conducted independently but collaboratively. It is worth noting that this approach does not as strongly rely on the response surface as the ordinary two-step approaches. The response surface would rather be used to support the global optimization algorithm. The author also attempted to extract knowledge about the design space by means of statistical analysis. These methods are

described in Section 2.3.

Section 2.4 and 2.5 describe the application of proposed design method to two turbomachinery design problems: optimum design of a centrifugal impeller and a centrifugal diffuser.

2.2 Shape Parameterization using Non-uniform Rational B-Spline Curves

Among the variety of components that make up a centrifugal fan, the impeller and (vaned) diffuser were chosen for design optimization. The shape parameterization methods for them are explained using Figure 2-1 and 2-2.

As shown in Fig. 2-1, an inexpensive centrifugal impeller is usually made of metallic plates of a hub plate, a shroud plate and several blades. Its shape is entirely determined if all of the meridian, blade and blade-edge (e.g. leading edge and trailing edge) shapes are given. It is generally the case for low-specific-speed impellers to define two blade sectional profiles, one of which is for the hub surface and the other for the shroud surface. Intermediate parts in the spanwise direction are generated by linear interpolation. Nevertheless, in the proposed method, the blade's leading and trailing edges can be flexibly deformed via the blade-edge-shape definition described later.

The meridian shape is defined by two NURBS curves: hub and shroud. The blade shape (section) is defined by a combination of two NURBS curves and two circles, tangentially connected to each other. These NURBS curves represent the pressure and suction sides of the blade, while the circles represent the head and tail of the blade. The control points of these NURBS curves are at the coordinates calculated from the blade camber and thickness distributions. In order to keep two-dimensionality, a common camber distribution is used, and the thickness of the blade is kept constant in spanwise direction. The leading or trailing edge consists of one NURBS curve, which starts from the hub surface and ends at the shroud.

Design variables for optimization are related to the coordinates of the NURBS control points, or to the parameters defining the blade camber distribution. Note that the number of blades is kept constant in this study. Once the shape is defined, the curves is then discretized and surfaces and a hexahedral mesh for computational fluid dynamics (CFD) is generated algebraically.
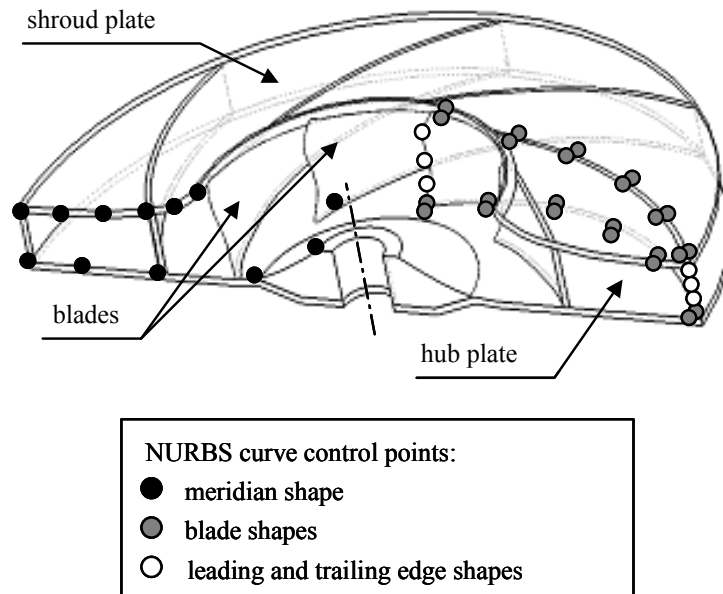
Figure 2-1 Shape parameterization of an impeller
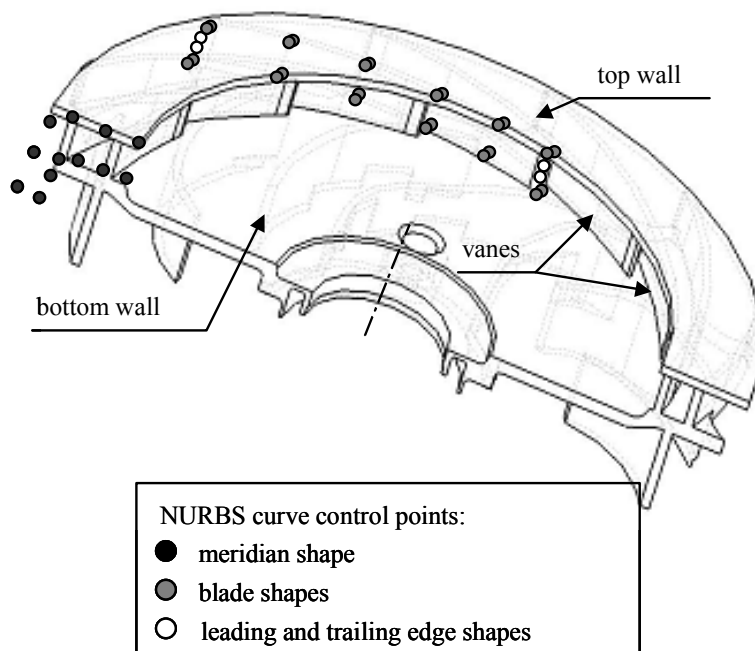
Figure 2-2 Shape parameterization of a diffuser

An inexpensive centrifugal diffuser could be made of injection-molded plastic. For example, as shown in Fig. 2-2, the bottom (or top) wall and the vanes are molded together, and the top (or bottom) wall is attached to the vanes to prevent leakage. The parameterization method for a diffuser is the same as the one for the impellers.

See Appendix A for more details on NURBS curve representation.

2.3 Design Exploration Method

2.3.1 Hybrid Algorithm of Simulated Annealing and Neural Network

Figure 2-3 shows the proposed hybrid optimization process [11]. A simulated annealing algorithm (SA) [12] is coupled with an artificial neural network (NN) [13] for synergetic optimization.

In the SA, the next search point is randomly perturbed around the temporary optimum according to the following probability density function (normal distribution):

$$p(x_i) = \frac{1}{\sqrt{2\pi}\sigma_i} \exp\left\{-\frac{\left(x_i - x_i^*\right)^2}{2\sigma_i^2}\right\} \quad \left(i = 1, 2, \cdots, n_{DV}\right), \tag{2-1}$$

where x_i, x_i^* and σ_i are i-th design variable, its temporary optimum value and its standard deviation respectively. Total number of design variables corresponds to n_{DV}. The standard deviation is defined by

$$\sigma_i = \sigma_0 \cdot \left(x_i^{max} - x_i^{min}\right) \cdot r^n, \tag{2-2}$$

where max and min denote the upper and lower boundaries of the design variable, n a temperature-stage count and r a reduction ratio. The σ_0 is set to 1.0 in this study. In the beginning of the optimization, σ is set to be large enough to encourage uniform global exploration of design space. On the other hand, near the end of the optimization, σ becomes small to converge at the optimum as quickly as possible.
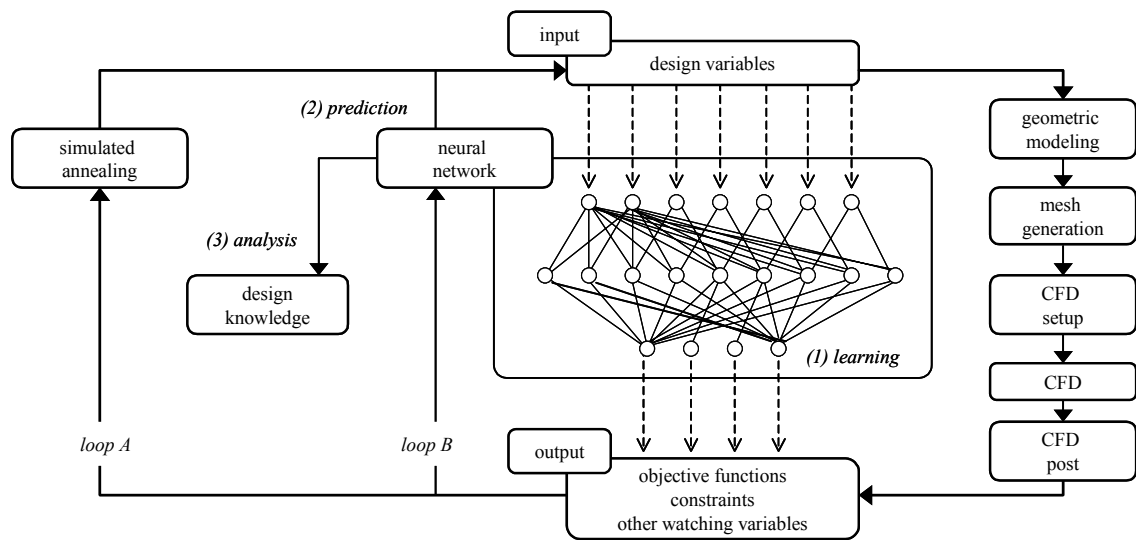
Figure 2-3 Hybrid optimization process
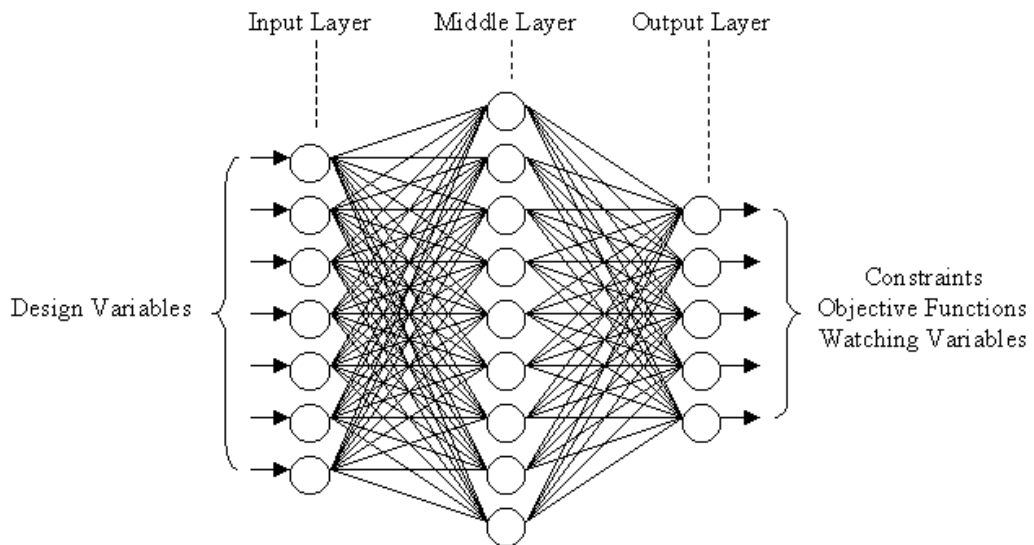
Figure 2-4 Architecture of neural network

An acceptance probability for permitting a worse solution in the SA is defined by

$$p_{accept} = \exp\left(-\frac{\Delta f}{T}\right),$$
(2-3)

where Δf is variation in the objective function's values and T current temperature. The temperature is gradually reduced according the following equation:

$$T = T_0 \cdot r_{temp}^n .$$
(2-4)

The NN is three-layered, and the number of neurons in the input and output layer corresponds to the number of input and output parameters of the design problem, respectively (Fig. 2-4). The number of neurons in the middle layer is empirically decided according to complexity of the design space. Each neuron has multiple inputs and one output, and the output is calculated through sigmoid function defined as follows:

$$f(s,t) = \frac{1}{1 + \exp\{-(s-t)\}} .$$
(2-5)

Using the sigmoid function, the neuron model is defined as

$$x_{ip} = f(z_{ip}, h_i),$$
(2-6)

where x_{ip}, z_{ip} and h_i are i-th neuron's output, input and a threshold. The p implies the p-th teacher signal. The input to the i-th neuron is equal to the weighted sum of neuron outputs in the previous layer and is calculated as

$$z_{ip} = \sum_j w_{ij} y_{jp} ,$$
(2-7)

where w_{ij} and y_{jp} are connecting weights and output from the j-th neuron in the previous layer.

The teacher signals are obtained by normalizing the CFD results. The weights and

threshold are calculated using a back-propagation learning rule. The goal of learning is to minimize the total error function defined as follows:

$$E = \sum_p E_p = \sum_p \left\{ \frac{1}{2} \sum_i \left(\overline{x}_{ip} - d_{ip} \right)^2 \right\},$$

(2-8)

where E_p is an error function for p-th teacher signal and d_{ip} the corresponding output of the teacher signal. The minimizing algorithm is a steepest descent method which uses the gradient vectors of E in terms of w_{ij} and h_i. Regarding w_{ij}, the gradient vector is defined as

$$\frac{\partial E}{\partial w_{ij}} = \sum_p \frac{\partial E_p}{\partial w_{ij}} = \sum_p \left(\frac{\partial E_p}{\partial z_{ip}} \frac{\partial z_{ip}}{\partial w_{ij}} \right) = \sum_p \left(\frac{\partial E_p}{\partial z_{ip}} y_{jp} \right)$$

$$= \sum_p \left(\frac{\partial E_p}{\partial x_{ip}} \frac{\partial x_{ip}}{\partial z_{ip}} y_{jp} \right) = \sum_p \left(\frac{\partial E_p}{\partial x_{ip}} \frac{\partial f_i}{\partial z_{ip}} y_{jp} \right) = -\sum_p \delta_{ip} y_{jp},$$

(2-9)

where

$$\delta_{ip} = -\frac{\partial E_p}{\partial x_{ip}} \frac{\partial f_i}{\partial z_{ip}}.$$

(2-10)

When i stands for the output layer,

$$\delta_{ip} = -\left(\overline{x}_{ip} - d_{ip} \right) \frac{\partial f_i}{\partial z_{ip}},$$

(2-11)

otherwise,

$$\delta_{ip} = \frac{\partial f_i}{\partial z_{ip}} \sum_k \delta_{kp} w_{ki}.$$

(2-12)

Using the gradient vectors defined above, the connection weights are iteratively calculated as follows:

$$\vec{w}^{(m+1)} = \vec{w}^{(m)} - \left(1 - \alpha\right)\left(\eta \frac{\partial E_p}{\partial \vec{w}}\right)^{(m)} + \alpha\left(\vec{w}^{(m)} - \vec{w}^{(m-1)}\right). \qquad (2\text{-}13)$$

The third term in the right hand side is the inertial term to improve learning convergence. The η is a relaxation factor and α is a mixing ratio of the steepest descent term and the inertial term. Note that the learning algorithm for thresholds is similarly formulated as that of the connection weights.

The SA has the major role in the collaborative optimization process. The 80%, for instance, of all the iterations (i.e. four times every five iterations) are controlled by the SA (loop A in Figure 2-3). However, the SA not only searches for a global optimum; it also stores the teacher signals for the NN to learn later. In the remaining 20%, the NN controls the process, and determines a next search point (loop B in Figure 2-3). This search point is chosen as a tentative global optimum by solving a sub-optimization problem on a response surface represented by the learned NN. To solve this sub-optimization problem, a simulated annealing algorithm is used with an ideal annealing schedule, because neural networking is much faster than CFD. The NN learns all the teacher signals that have been obtained so far. The initial conditions of the weights and thresholds are set to the previously learned results in order to improve learning performance. When the learning fails, initial values of the weights and thresholds are randomly perturbed from the previous results and the back propagation rule is applied again.

Using the NN response surface enables us to search for a global optimum much faster than with a single SA. Using the SA enables us to sample the design space globally and to provide a mechanism to jump out of an incorrect optimum that may be predicted by an inaccurate response surface. Even if a response surface can't be constructed, the automatic optimization process can still survive by a single SA. The complimentary roles of the SA and NN thus enable robust and collaborative optimization.

The performance of the hybrid algorithm is verified using a test function defined as

$$f = -10 \cdot \exp\left\{ -\left(\frac{x_1 - \pi}{10} \right)^2 \right\} \cdot \cos(x_1 - \pi)$$

$$-10 \cdot \exp\left\{ -\left(\frac{x_2 - 0.5 \cdot \pi}{10} \right)^2 \right\} \cdot \cos(x_2 - 0.5 \cdot \pi),$$

(2-14)

subject to $0 \le x_i \le 4\pi \, (i = 1,2)$. The optimum (minimum solution) is

$$f^* = -20 \, (x_1 = \pi, x_2 = 0.5 \cdot \pi).$$

(2-15)

This is a multi-modal function as shown in Fig. 2-5, in which the objective function is normalized. Figure 2-6 compares the performance of the hybrid algorithm (SA+NN) with that of single SA given the same conditions for SA algorithm. The NN is active during 20% of all the iterations. The figure suggests that the hybrid algorithm finds the global optimum much faster than the single SA does.
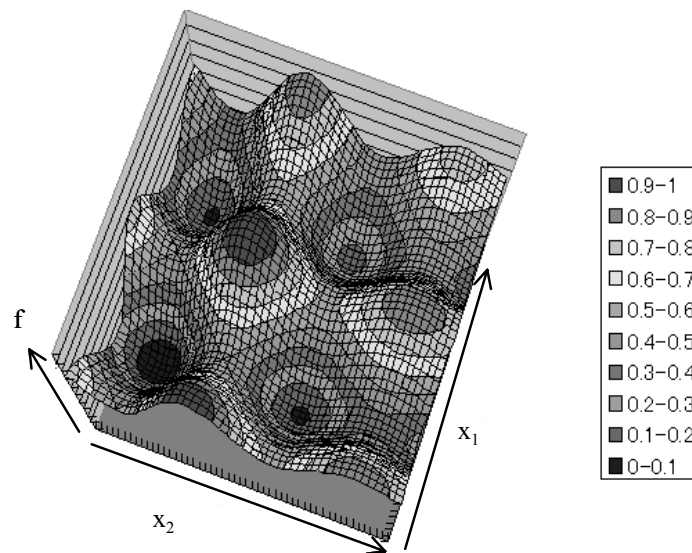
Figure 2-5 Test function
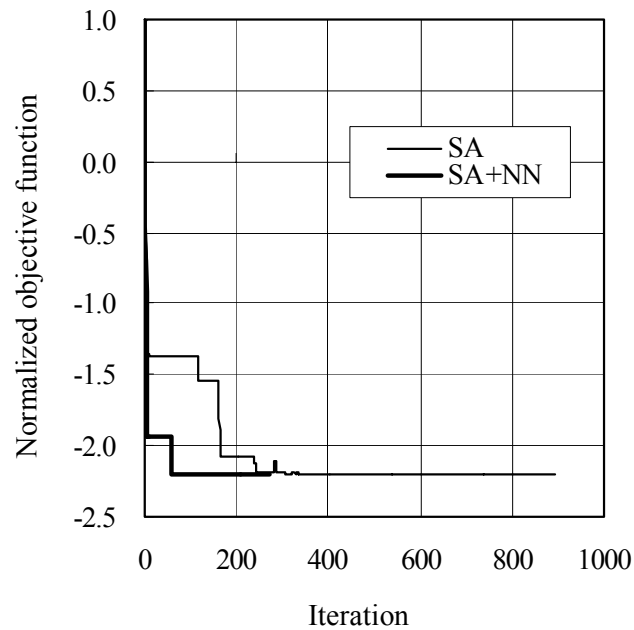
Figure 2-6 Comparison of optimization histories

2.3.2 Regression Analysis of Design Space

Another feature of the proposed method is that it automatically conducts a statistical analysis of the response surface. This analysis aims to identify important design variables, thereby helping a designer to understand the design problem. This information is defined as "design knowledge" in this study.

The analysis calculates two statistical values, sensitivity and non-linearity. Figure 2-7 visualizes the three-dimensional design space of the two design variables and one objective function as a simple example. Several points sampled by SA are plotted on the response surface of the NN. At the current sampling point, the response surface is cut into orthogonal two cross sections. Figure 2-8 shows the profile of a cross section, where the section has been numerically discretized. The regression line shows the global tendency between the objective function and the design variable. The sensitivity is calculated as the gradient of the regression line after re-scaling the abscissa by the distance between the upper and lower limits of the design variable X. The non-linearity is defined as the mean square deviation of the cross section from the regression line. Sensitivity suggests the importance of a design variable,

while non-linearity indicates the difficulty in examining the design variable.

In the hybrid algorithm, the SA randomly searches in a neighborhood around a temporary optimum for better solutions. This neighborhood covers the whole design space at first, after which it is gradually narrowed according to the progress of optimization. Therefore, the positions of the cross sections mentioned above vary randomly within the whole design space before they gather round the final optimum. The knowledge mining calculates and averages the two statistical values for every iteration. Thus, the averages are expected to show global characteristics at first and local characteristics near the final optimum lastly. It is expected that these averaging operations cancel noise due to the immaturity of the response surface.
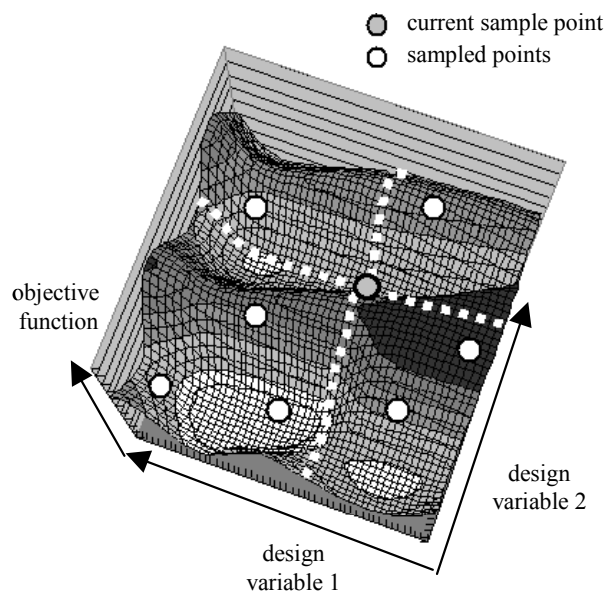
Figure 2-7 Example of design space
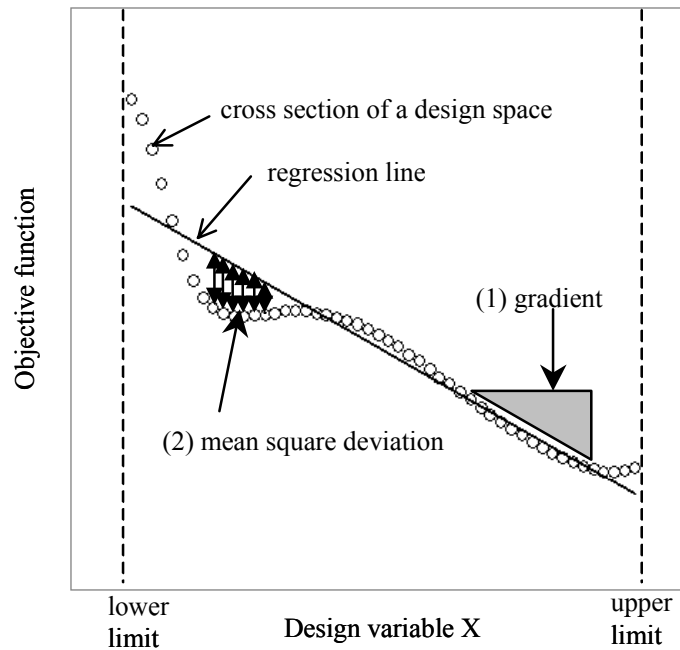
Figure 2-8 Definition of statistical indexes

2.4 Design Optimization of Centrifugal Impeller

Centrifugal fans of vacuum cleaners are typical examples of inexpensive fans. In the Japanese market, a law limits the maximum input power of a vacuum cleaner. Therefore, we have to develop aerodynamically efficient fans in order to increase the units' suction power. In this section, the proposed optimization method is applied to a centrifugal impeller with a specific speed of 120 [min^{-1}, m^3/min, m] (see Figure 2-1).

2.4.1 Design Problem Definition

The single objective function is defined as adiabatic efficiency:

$$\eta_{ad} = \frac{G \cdot C_p \cdot T_1 \left\{ \left(\dfrac{P_2}{P_1} \right)^{\frac{\kappa-1}{\kappa}} - 1 \right\}}{W_{axis}}, \tag{2-16}$$

where G, C_p, T, P, W_{axis}, κ are mass flow rate, specific heat under constant pressure, total temperature, total pressure, axial input power, and specific heat ratio, respectively. The subscripts 1 and 2 designate the entrance and exit of the impeller, respectively.

The design variables are prepared according to the parameterization method described in Section 2.2. The trailing edge profile is a line, while the leading edge is flexibly deformed. The number of design variables is 27. The initial shape follows an ordinary two-dimensional design method.

The axial input power is treated as a constraint, and it is considered to be feasible if its value is within 1% of the target. The constraint is taken into consideration by means of a penalty function.

The hybrid algorithm's frequency of using NN is set at 20%. Note that the flows were simulated using commercial software, "STAR-CD^{TM} (CD-adapco JAPAN Co., LTD.) [14], " solving RANS equations with $k - \varepsilon$ turbulence model combined with standard wall function.

2.4.2 Results and Discussion

Figure 2-9 shows the history of the adiabatic efficiency normalized by the initial value. Individual solution is plotted in circular marks. The line shows tentative optimums, which the SA keeps inside. The normalized efficiency is improved by 2.7% at the optimum. The hybrid algorithm using SA and NN find better solutions, but NN accounts for 62% of all the findings in this case. This clearly shows that the hybrid algorithm has a great advantage in efficient design exploration over a single SA.

Figure 2-10 compares flow fields of the initial and optimum shapes. The flow fields are visualized with surface-restricted streamlines, which show flow directions near wall surfaces. The regions near the leading edges are shown in the upper half of the figure, and hub surfaces are shown in the bottom half.

A significant difference in shapes is found at the leading edges. The linear leading edge of the initial shape changes into a unique "S-shaped" one in the optimum shape. In the optimum shape, the inclined edge near the hub surface generates a streamwise vortex as shown in the figure. This streamwise vortex, together with the horseshoe vortex, sweeps out a low-energy flow from the corner of the hub surface and the blade's suction side.
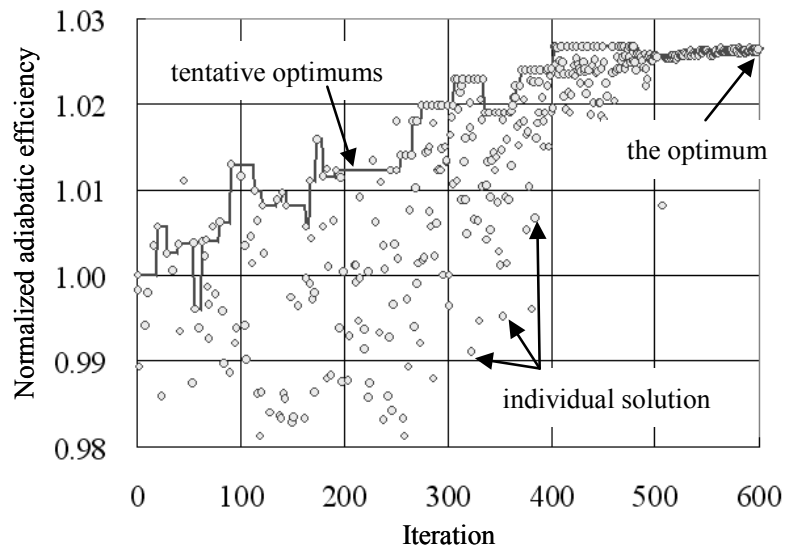
Figure 2-9 History of the objective function (impeller)

(a) Initial shape   (b) Optimum shape
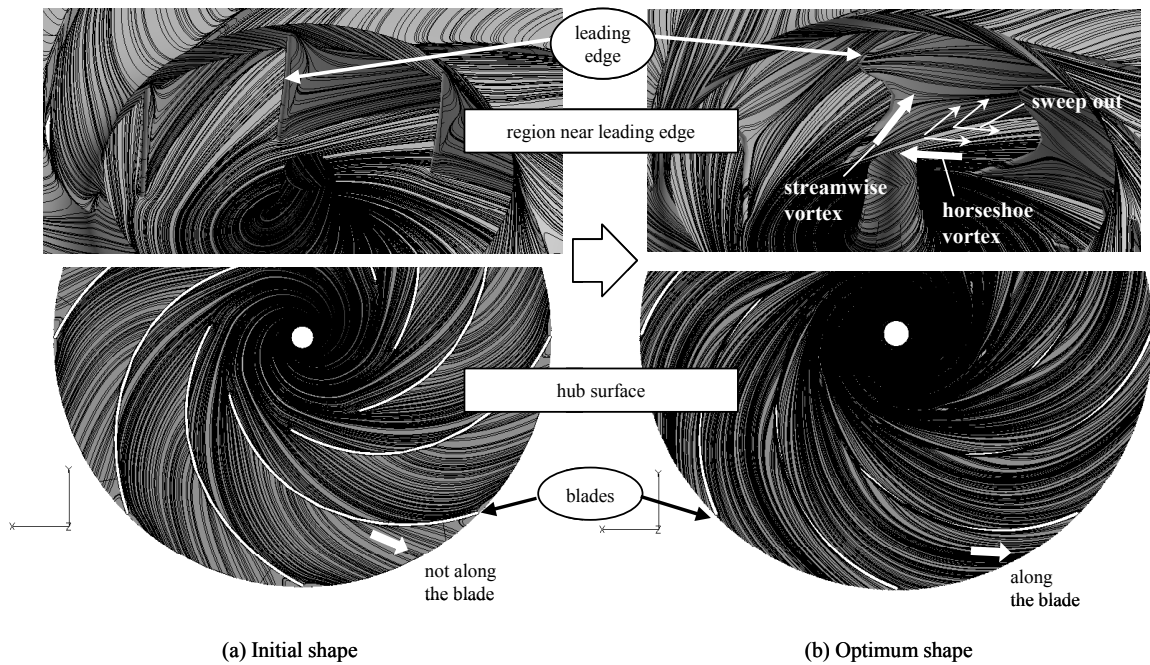
Figure 2-10 Comparison of restricted streamlines
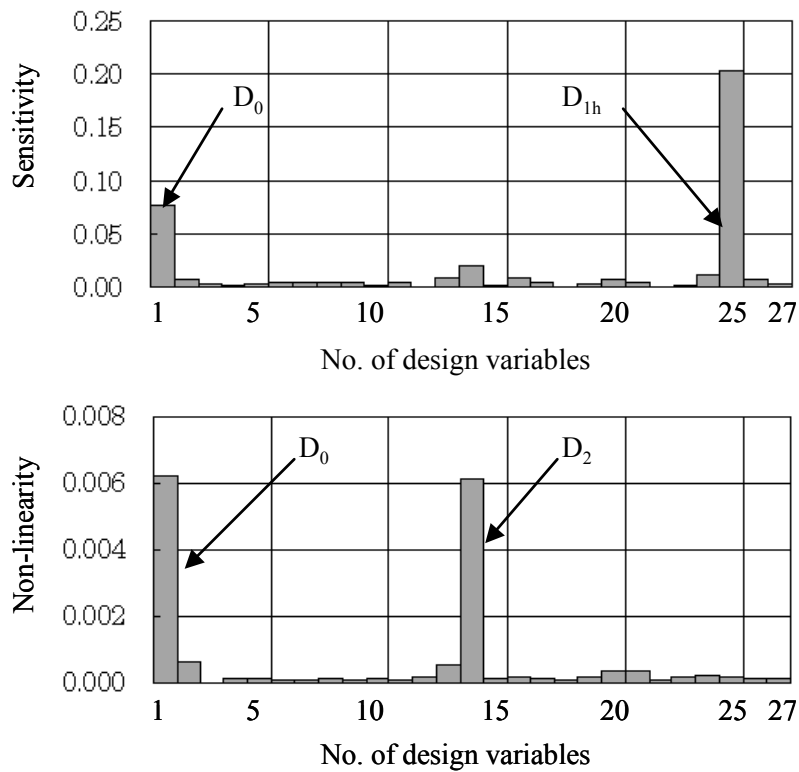
Figure 2-11 Design space characteristics (impeller)

The initial impeller tends to have low-energy fluid at this corner, resulting in non-uniform flow at the impeller exit. In fact, the near-wall flow direction at the exit is not along the blade in Figure 2-10. In contrast, as the result of controlling the secondary flow in the upstream region, the optimum shape ensures that the outflow is completely along the blade. The more uniform outflow reduces secondary flow loss and improves adiabatic efficiency.

Figure 2-11 shows the results of the statistical analysis of the design space. The average sensitivity and non-linearity converge during the optimization process, and the figure plots the last values for each design variable.

Two design variables, D_0 and D_{1h}, are found to have large sensitivity to the adiabatic efficiency. D_0 is the inlet diameter of the impeller, and D_{1h} is the hub-side diameter of the blade's leading edge. In terms of non-linearity, D_0 and D_2 have large values (D_2 is the outlet diameter of the impeller).

2.5 Design Optimization of Centrifugal Diffuser

The inflow condition for this diffuser (Figure 2-2) is calculated from the average CFD results of the optimum impeller described in Section 2.4. The inflow condition is assumed to be uniform. The outer diameter of the diffuser is kept constant in the optimum design.

2.5.1 Design Problem Definition

The objective function is defined as static pressure recovery at the diffuser as follows:

$$\Delta P = p_{exit} - p_{entrance}.$$ (2-17)

The number of design variables is 26. The blade thickness is allowed to have a non-uniform distribution in this case, but the distribution form is kept constant throughout the optimization. Skew is not allowed, as in the impeller case. Regarding the blade edges, the leading edge is assumed to be linear while the trailing edge is deformed flexibly using a NURBS curve. The initial shape is decided based on a traditional two-dimensional design method.

Other conditions for the hybrid algorithm and the flow solver are set similarly to those of the impeller's case.

2.5.2 Results and Discussion

Figure 2-12 shows the history of the objective function normalized by the initial value. The optimum design improves the normalized pressure recovery by nearly 10%.

In this case, the NN finds only 6% of all the better solutions. Although there is still a slight improvement in exploration efficiency, it is not as much as in the impeller's case. This is because the non-linearity of the design space is so strong (as described later) that the accuracy of the response surface deteriorates.

Figure 2-13 compares static pressure contours of the initial and optimum shapes. The optimum shape has a smoothly bending blade-tail profile, in which the upper side of the blade is stretched downward. A pressure gradient is naturally established since more pressure is recovered on the upper side than on the lower side. This gradient helps the mainstream to bend smoothly and avoid flow separation.
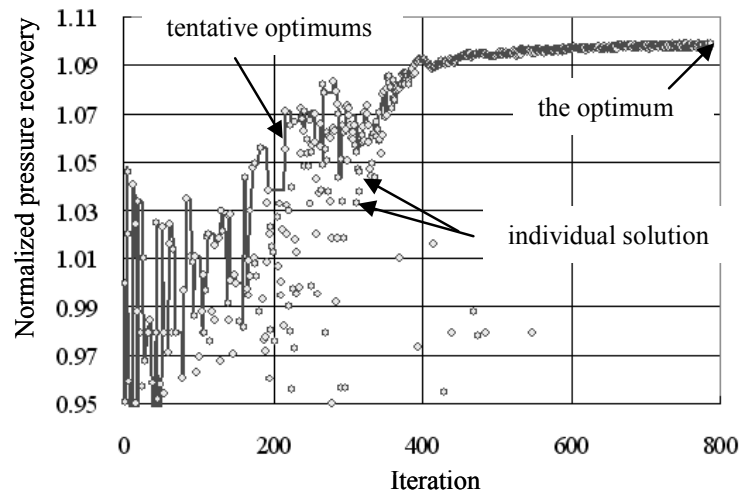
Figure 2-12 History of the objective function (diffuser)

(a) Initial shape
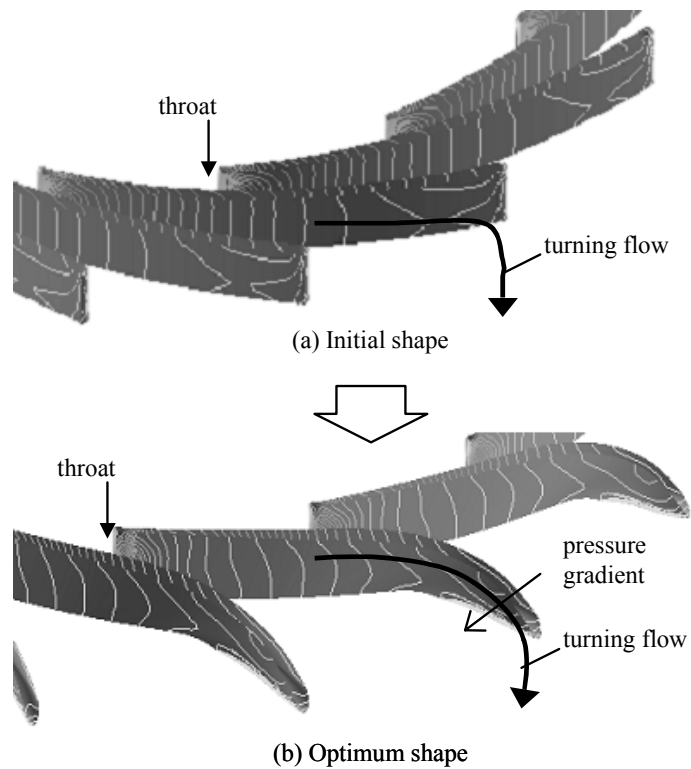
(b) Optimum shape

Figure 2-13 Comparison of pressure distributions
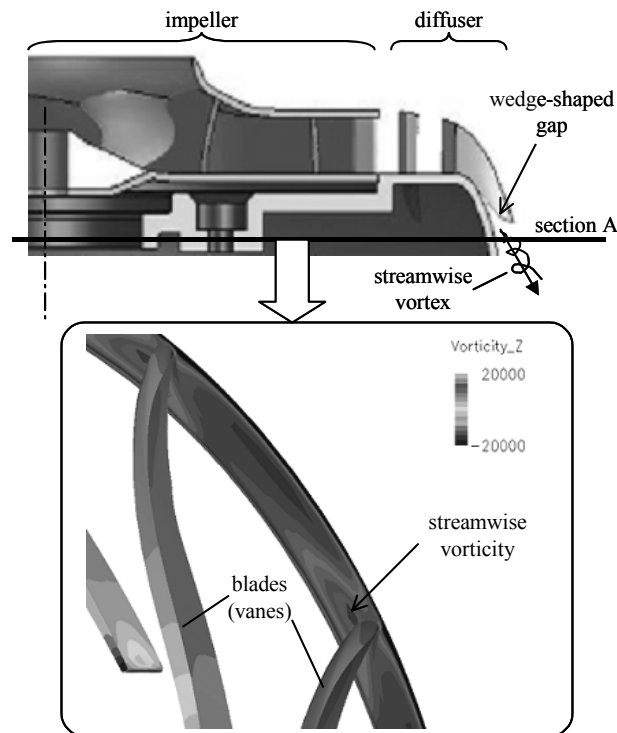
Figure 2-14 Streamwise vortex

Another feature of the optimum shape can be explained with help of Figure 2-14, which shows a section of the optimum impeller and diffuser. The trailing edge of the diffuser blade forms a wedge-shaped gap. In this gap, a streamwise vortex is generated by pressure drop over the diffuser blade. This is shown in the lower figure, which visualizes axial vorticity distribution in section A.

The mainstream, where energy is high, is supported by the above-mentioned pressure gradient. However, near-wall flow, where energy is low, needs more assistance. The streamwise vortex then mixes the low and high-energy flow regions, suppressing the boundary layer growth.

In the upstream region near the throat, the flow field for the optimum shape is too strongly diffused to be stable aerodynamically. The current problem definition allows that a flow is diffused as long as it is not separated. This means that stability of an optimum solution strongly depends on the accuracy of the flow solver. We need to make further investigations to be able to devise better problem definitions.
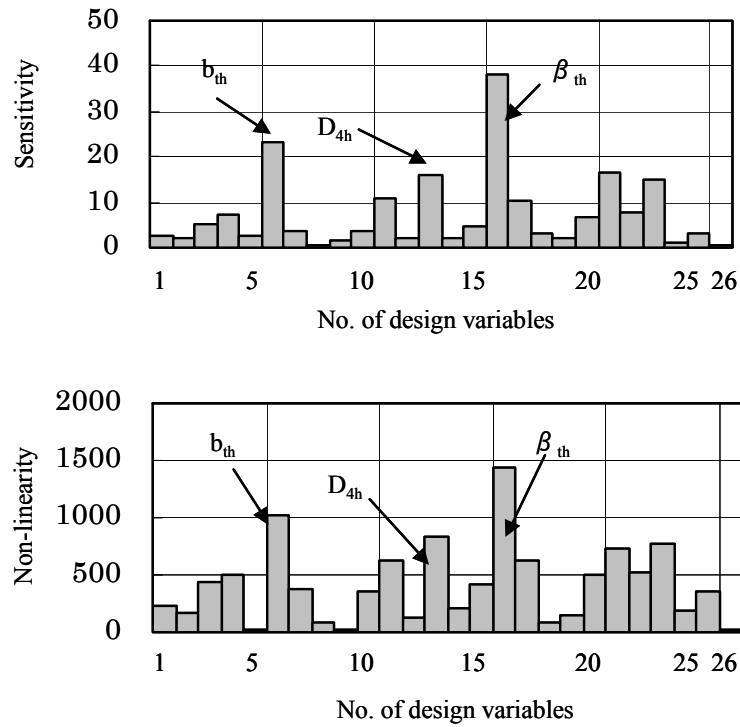
Figure 2-15 Design space characteristics (diffuser)

Figure 2-15 summarized the results of the design space analysis. Unlike the impeller's case, many design variables show a large sensitivity and large non-linearity at the same time. In fact, designing a diffuser always faces problems of flow separation, which is a typical non-linear phenomenon. These results imply some difficulties in designing a diffuser, which is in agreement with common sense regarding turbomachinery design. The β_{th}, b_{th} and D_{4h} are good candidates for important design variables. The β_{th} and b_{th} are the blade angle and blade height near the throat, respectively. The throat is where the section area of flow paths becomes the smallest, as designated in Figure 2-13. It is well known that the throat has the greatest impact on the aerodynamic performances of a diffuser. D_{4h} is the diameter of the trailing edge on the hub surface, where the streamwise vortex is generated.

It is interesting that the proposed knowledge mining method is able to identify all the design variables, which are related to the throat and the wedge-shaped gap, as important parameters.

2.6. Conclusion

This chapter described a single-objective global design optimization method suitable for centrifugal fans. The shapes of centrifugal impellers and diffusers are parameterized by using NURBS curves. This method has an advantage in modeling the blade's leading and trailing edges flexibly, keeping two-dimensional simplicity as a whole.

A hybrid algorithm combining SA and NN was developed for efficient and automatic design exploration. The NN learns the CFD results that were collected by the SA. The NN is then used as a response surface to accelerate the global search. The SA explores the design space independently of the NN, ensuring robust and automatic optimization. Statistical analysis for the purpose of knowledge mining is conducted with the NN.

The proposed method was applied to the impeller and diffuser design problems. The resulting impeller design had a unique S-shaped leading edge profile, which effectively controls secondary flow. The diffuser design gave a smoothly bending trailing edge profile with a remarkable wedge-shaped gap, which generates a streamwise vortex and effectively prevents boundary layer separation.

The design process of both designs were surely accelerated, but speedup depended on how strongly non-linear the design space was. The statistical analysis revealed important parameters for new shapes and these confirmed to what designers take to be common sense when drawing up turbomachinery designs.

Based on these results, the author concludes that the proposed design method is suitable for automatically finding innovative shapes and useful design knowledge of centrifugal fans. Note that the design problem, the result of which strongly depends on accuracy of a flow solver, should be defined more properly than was done in this paper. For example, in the diffuser design problem, several constraints are necessary to secure aerodynamic stability. The author believes that such constraints should be treated as objective functions and that a multi-objective optimization problem should be solved, in order to avoid problems of simulation accuracy as much as possible. Tacking these issues will be the topic of the next work.

References

[1] Pierrt, S., Multi-objective and Multi-Disciplinary Optimization of Three-dimensional Turbomachinery Blades, Proceedings of 6th World Congresses of Structural and multidisciplinary Optimization, 2005.

[2] Pierret, S., Three-dimensional Blade Design by means of an Artificial Neural Network and Navier-Stokes Solver, von Karman Institute for Fluid Dynamics Lecture Series 1999-02 Turbomachinery Blade Design System, 1999.

[3] Dennis, B. H., Dulikravich G. S., Han, Z. X., Constrained Shape Optimization of Airfoil Cascades using a Navier-Stokes Solver and a Genetic/SQP Algorithm, ASME Paper No. 99-GT-441, 1999.

[4] Benini, E., Tourlidakis, A., Design Optimization of Vaned Diffusers for Centrifugal Compressors Using Genetic Algorithm, AIAA-2001-2583, 2001.

[5] Platt, M. J., Marsh, M., Multidisciplinary Optimization of a LH2 Turbopump Design in an Agile Engineering Environment, AIAA-2003-4765, 2003.

[6] Samareh, J. A., Status and Future of Geometry Modeling and Grid Generation for Design and Optimization, Journal of Aircraft, Vol.36, No.1, pp.97-104, 1999.

[7] Samareh, J. A., Survey of Shape Parameterization Techniques for High-Fidelity Multidisciplinary Shape Optimization, AIAA Journal, Vol. 39, No.5, pp.877-884, 2001.

[8] Newman, J. C., Taylor, A. C., Barnwell, R. W., Newman, P. A., Hou, G. J. W., Overview of Sensitivity Analysis and Shape Optimization for Complex Aerodynamic Configurations, Journal of Aircraft, Vol. 36, No. 1, pp.87-96, 1999.

[9] Rogers, D. F., Adams, J. A., Mathematical Elements for Computer Graphics, McGrawHill, 1990.

[10] Pierrt, S., Van den Braembussche, R. A., Turbomachinery Blade Design using a Navier-Stokes Solver and Artificial Neural Network, ASME paper 98-GT-04, 1998.

[11] Sugimura, K., Savill, A. M., Dawes, W. N., Development of Emerging Design Optimization System using Neural Network and its Application for Turbomachinery Blade Design, the proceedings of OPTIS, 2002 (in Japanese).

[12] William H. Press, Brian P. Flannery, Saul A. Teukolsky, and William T. Vetterling, Nemerical Recipe in C, Cambridge University Press, 1988.

[13] Phil Picton, Neural Networks, palgrave, 2000.

[14] CD-Adapco Japan Co. Ltd., http://www.cdaj.co.jp/

Chapter 3

Multi-objective Design Exploration
using Multi-objective Genetic Algorithm,
Decision Tree Analysis, and Rough Set Theory

3.1 Introduction

In Chapter 2, a single-objective global optimization method for centrifugal turbomachinery configurations was developed to find innovative shapes that can improve aerodynamic performance in short turn-around-time. It was also confirmed that characteristics of design space, which were revealed by regression analysis, helps designers to understand important design variables to be investigated carefully.

However, extreme design regarding an explicit single objective function often ignores other implicit design objectives or constraints. For example, more efficient fans are usually noisier. Fans with higher efficiency at a design flow rate usually have worse efficiencies at off-design flow rates. In this sense, the single-objective optimization approach is only useful when we can reduce multiple design criteria into a single objective properly with reasonable assumptions. When these assumptions are not available, we need to optimize multiple objective functions directly. It is indeed beneficial to have multiple design candidates as non-dominated solutions from multi-objective optimization, because designers can choose the best solution according to design requirements specified afterwards. This makes it possible to design products under the uncertainty in design requirements.

In this chapter, therefore, a multi-objective optimization method is developed using real-coded multi-objective genetic algorithm. The author also attempts to extract design rules from multi-objective design space for finding governing design rules for achieving extreme improvement in each objective function. While the sensitivity and non-linearity of design space discussed in Chapter 2 are concerned with general information on the global characteristics, the design rules are related to particular information on conditions to achieve a certain design objective. The developed methods are applied to a design problem of centrifugal impeller accompanied with a vaned diffuser.

Figure 3-1 shows a motor blower used for a vacuum cleaner. The blower consists of a centrifugal impeller, vaned-diffuser, and return guide. Its specific speed is as low as 120 $[(min^{-1})(m^3/min)^{0.5} (m)^{-0.75}]$ at the design point. The design objective of these blowers is to achieve higher aerodynamic efficiency over a wide range of operating flow rates in such a way that the vacuum cleaners have high suction power regardless of dust amount.

However, the blower size is not large enough for designers to investigate the inner flow field experimentally. For instance, the throat size of the diffuser is only a few millimeters. Therefore, the predominant design approach for these blowers is now computational fluid dynamics (CFD) and numerical optimization techniques. In addition, there has been increasing demand for design knowledge acquisition from these numerical investigations as a substitute for experimentation.

Although there were many multi-objective optimization studies of aerodynamic configurations [1][2][3][4], there have not been many studies on this type of low-specific-speed blower that accompanies a vaned diffuser. Benini et. al [5] optimized the shape of a vaned diffuser by using Reynolds-averaged Navier Stokes (RANS) simulation and a multi-objective genetic algorithm (MOGA). However, the inflow to the diffuser was assumed to be uniform and so the interaction effect with the impeller was ignored. This approach cannot be used to evaluate aerodynamic stability because the non-uniform inflow to the diffuser plays an important role on aerodynamic stall. Khelladi et al. [6] computed flows of a high-fidelity CFD model, which included an impeller, diffuser, and return guide. Although the interaction effect was considered, design optimization was not conducted.

The intention of this study is to optimally design aerodynamically efficient and stable centrifugal impellers. This goal is achieved by multi-objective shape optimization of a centrifugal impeller, where the time-averaged and spatially non-uniform interaction effect with the diffuser can be investigated. Although it is widely recognized that the multi-objective optimization is computer intense, a lot of simulation results and optimal design solutions can be made available as a design database instead. The author therefore believes that multi-objective optimization is not costly, if we can extract additional information from the database by means of data mining.
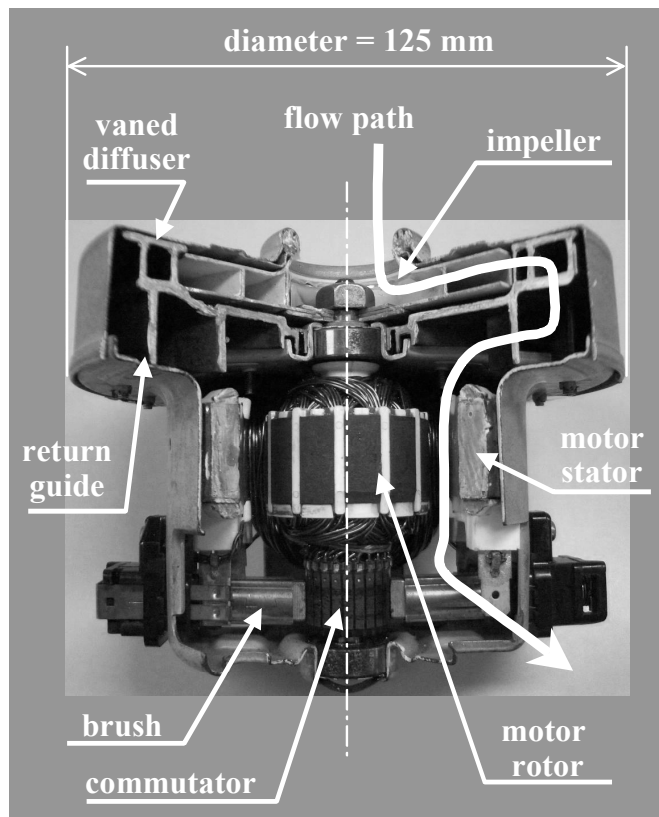
Figure 3-1 Motor blower for vacuum cleaner

Nomenclature

D_{2h}	=	outer diameter of impeller blade on hub side [mm]
D_{2s}	=	outer diameter of impeller blade on shroud side [mm]
D_2	=	mean of D_{2h} and D_{2s} [mm]
D_{0s}	=	outer diameter of impeller inlet [mm]
D_{0h}	=	inner diameter of impeller inlet [mm]
D_{1h}	=	inner diameter of impeller blade on hub side [mm]
D_{1s}	=	inner diameter of impeller blade on shroud side [mm]
r_D_{1h}	=	ratio for determining D_{1h}
r_D_{1s}	=	ratio for determining D_{1s}
R	=	radius corresponding to diameter D [mm]
b_0	=	height of impeller inlet [mm]
b_2	=	height of impeller exit [mm]

b_3	=	height of diffuser inlet [mm]
R_{01}	=	radius of first circle consisting of the shroud line [mm]
r_R_{01}	=	ratio for determining R_{01}
R_{tan}	=	radius of connecting point between second circle and line on shroud line [mm]
r_R_{tan}	=	ratio for determining R_{tan}
β_{in}	=	blade angle of first NURBS control point in blade angle distribution [degree]
β_{max}	=	blade angle of second NURBS control point in blade angle distribution [degree]
β_{out}	=	blade angle of third NURBS control point in blade angle distribution [degree]
r_β_{max}	=	ratio of determining radial location of β_{max}
D_{le1}	=	diameter of first NURBS control point for leading edge definition (near hub line) [mm]
D_{le2}	=	diameter of second NURBS control point for leading edge definition [mm]
D_{le3}	=	diameter of third NURBS control point for leading edge definition (near shroud line) [mm]
D_m	=	mean of D_{1h} and D_{1s} [mm]
r_R_{le1}	=	ratio of determining D_{le1}
r_R_{le2}	=	ratio of determining D_{le2}
r_R_{le3}	=	ratio of determining D_{le3}
Q	=	flow rate [m³/min]
η_{blower}	=	blower efficiency
p	=	averaged static pressure [Pa]
W_{ax}	=	shaft power [W]
i_b	=	incidence angle [degree]
σ	=	standard deviation
g_i	=	mass flow rate at mesh cell i on diffuser inlet [kg/s]
β_{4_i}	=	inlet flow angle at mesh cell i on diffuser inlet [degree]
β_{4b}	=	inlet blade angle at diffuser inlet (constant) [degree]
n	=	number of mesh cells on the diffuser inlet boundary
DV	=	design variable(s)
OF	=	objective function(s)
A	=	criteria in terms of design variable(s)
B	=	criteria in terms of objective function(s)
W	=	relative velocity [m/s]
U	=	peripheral velocity [m/s]
C	=	absolute velocity [m/s]

3.2 Design Exploration Method

3.2.1 Procedure of Design Exploration

Design exploration processes are divided into two steps, as shown in Fig. 3-2. In the first step, the optimization problem is solved by the multi-objective genetic algorithm (MOGA), which is explained in the next section. We then investigated the obtained sample data and non-dominated solutions. Non-dominated solutions are optimal solutions in multi-objective optimization problems in the sense that no other solutions in the objective function space are superior to them when all objective functions are considered. In other words, a non-dominated solution has at least one superior objective function's value compared with all the other non-dominated solutions.

In the second step, data mining techniques, decision tree analysis and rough set theory, are applied to the CFD database accumulated in the first step. This is done to extract dominant design variables and their levels to be maintained to improve design objectives. If the database of the sample data is used, the resultant rules are characterized as general rules. If the database of non-dominated solutions is used, trade-off control rules are obtained. In this Chapter, extraction of general rules is attempted. Extraction of trade-off control rules is mentioned in Chapter 4.
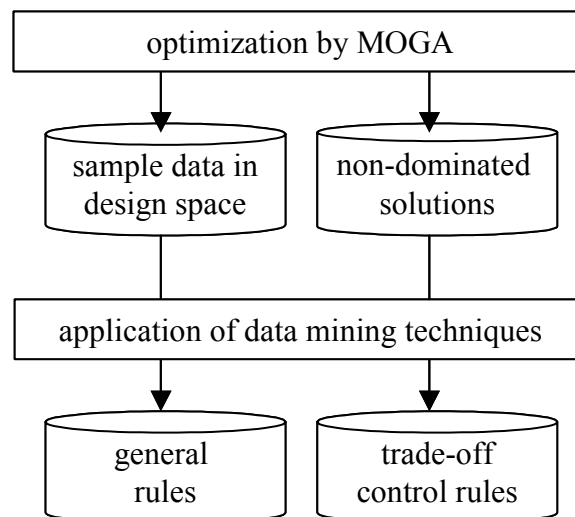
Figure 3-2 Flowchart of design exploration

3.2.2 Multi-objective Genetic Algorithm

Genetic algorithm (GA) [8] mimics an evolutionary process of natural selection as shown in Fig. 3-3. After forming initial population, where each individual represents design candidate, CFD are conducted to evaluate multiple objective functions (evaluation). By making a scalar function called "fitness" from these objective functions (fitness assignment), superior individuals are chosen according to the magnitude of fitness (selection). The feature of multi-objective genetic algorithm [9] is the way of defining this scalar function. Elitist strategy is used in the process of generation alternation for accelerating convergence (generation alternation). New population is created by means of exchanging (crossover) and perturbing (mutation) genetic information. In the followings, the methods used in the developed optimization system are explained.

Initial population is generated using Latin hypercube sampling, which is a kind of design of experiment.

The MOGA uses an evaluation method based on Pareto-ranking and fitness sharing [10] to obtain widely spread non-dominated solutions. Pareto-ranking method evaluates fitness of each population referring to its rank number that adds the number of dominating solutions and one. Consequently, the rank numbers for non-dominated solutions become ones (Fig. 3-4). Fitness sharing method gives smaller fitness for solutions gathering together in the objective function space so that widely spread solutions can be obtained as a result of evolution.

In the evaluation process, each objective function f_i is first normalized as follows.

$$f_i = \frac{f_i - f_i^{\min}}{f_i^{\max} - f_i^{\min}} \quad \left(i = 1, \cdots, nOF\right).$$

(3-1)

In case of $f_i^{\max} = f_i^{\min}$, f_i is set to one. Rank number is thus calculated.

Average fitness is calculated using obtained rank number as,

$$F_i = \frac{\sum_{j=1}^{nRnk_i}\left(nPop - j\right)}{nRnk_i} \quad \left(i = 1, \cdots, \max Rnk\right),$$

(3-2)

where $nPop$ and $nRnk_i$ are number of population in total and each rank, respectively.

The fitness is corrected according to convergence in local area in the objective function space using sharing function $sh(d_{k,j})$ as follows.

$$F_k = \frac{F_k}{\sum_{j=1}^{nRnk_k} sh(d_{k,j})} .$$

(3-3)

Sharing function is calculated as

$$sh(d_{k,j}) = \begin{cases} 1 - \left(\dfrac{d_{k,j}}{\sigma_{sh}}\right)^{\alpha_{sh}} & \left(d_{k,j} < \sigma_{sh}\right) \\ 0 & \left(d_{k,j} \geq \sigma_{sh}\right) \end{cases} ,$$

(3-4)

where Euclid distance $d_{k,j}$ between the individual k and j is calculated as follows:

$$d_{k,j} = \sqrt{\sum_{i=1}^{nOF}\left(f_i^{k} - f_i^{j}\right)^2} .$$

(3-5)

σ_{sh} in Eq. (3-4) is basis distance, which is used for judging degree of the gathering, and calculated as follows:

$$nPop \cdot \left(\sigma_{sh}\right)^{nOF-1} - \frac{\prod_{i=1}^{nOF}\left(f_i'^{\max} - f_i'^{\min} + \sigma_{sh}\right) - \prod_{i-1}^{nOF}\left(f_i'^{\max} - f_i'^{\min}\right)}{\sigma_{sh}} = 0 .$$

(3-6)

where f' is objective function before it is normalized. In the normalized form,

$$nPop \cdot \left(\sigma_{sh}\right)^{nOF-1} - \frac{\left(1 + \sigma_{sh}\right)^{nOF} - 1}{\sigma_{sh}} = 0 .$$

(3-7)

Since the average fitness of Eq. (3-2) changes due to the sharing operation, it is corrected as

$$F_k'' = \frac{\sum\limits_{j=1}^{nRnk_k} F_j}{\sum\limits_{j=1}^{nRnk_k} F_k'} F_k' ,\tag{3-8}$$

in order that the sums of average fitness stay the same. Here, F are F' fitness values before and after sharing operation, respectively.

All the design parameters are treated as real numbers in the MOGA and real-coded genetic operations, a roulette wheel selection method, a BLX-α (α = 0.5) crossover method, and a non-uniform mutation method are used [8].

In the BLX-α crossover method, a pair of new individual is created as follows:

$$x_i^{(1,t+1)} = (1-\gamma)x_i^{(1,t)} + \gamma x_i^{(2,t)} ,\tag{3-9}$$

$$x_i^{(2,t+1)} = \gamma x_i^{(1,t)} + (1-\gamma)x_i^{(2,t)} , \text{ and}\tag{3-10}$$

$$\gamma = (1+2\alpha_{crs})u_i - \alpha_{crs} \qquad (\alpha_{crs} = 0.5) .\tag{3-11}$$

The α_{crs} is set to 0.5 for balancing global and local optimum searches.

In the non-uniform mutation, disturbance of mutation is controlled as it is large and small in the former and later processes of evolution, respectively.

$$x_i^{(1,t+1)} = x_i^{(1,t+1)} + \tau(x_i^{\max} - x_i^{\min})(1 - u_i^{(1-t/nGen)^b}) \quad .\tag{3-12}$$

To improve convergence of the MOGA, the Pareto-optimality-based constraint handling technique [11] and the Best-N strategy [7] are employed in the MOGA code. The Pareto-optimality-based constraint handling technique introduces Pareto-ranking concept further to the constraint space so that it can avoid the use of penalty functions that need factitious parameters. Since solutions violating the constraints are given a larger rank number in this method, these solutions are gradually diminished. The Best-N strategy chooses the best N population from the previous two generations (2*N population) so that this generation alternation assures steady improvement of an average of an objective function over a generation.

```
┌─────────────────────────────────────┐
│     initialization of population     │
└─────────────────────────────────────┘
                  │
                  ▼
┌─────────────────────────────────────┐
│             evaluation              │◀──────────┐
└─────────────────────────────────────┘           │
                  │                                │
                  ▼                                │
┌─────────────────────────────────────┐           │
│          fitness assignment          │           │
│   (Pareto ranking + fitness sharing) │           │
└─────────────────────────────────────┘           │
                  │                                │
                  ▼                                │
┌─────────────────────────────────────┐           │
│        generation alternation        │           │
│          (best-N strategy)           │           │
└─────────────────────────────────────┘           │
                  │                                │
                  ▼                                │
Yes      ◇ convergence judgment ◇                  │
  ◀──────────────                                  │
          │   No                                   │
          ▼                                        │
┌─────────────────────────────────────┐           │
│      selection (roulette selection)  │           │
└─────────────────────────────────────┘           │
                  │                                │
                  ▼                                │
┌─────────────────────────────────────┐           │
│         crossover（BLX-α）           │           │
└─────────────────────────────────────┘           │
                  │                                │
                  ▼                                │
┌─────────────────────────────────────┐           │
│   mutation（non-uniform mutation）   │───────────┘
└─────────────────────────────────────┘

                  ▼
                Finish
```
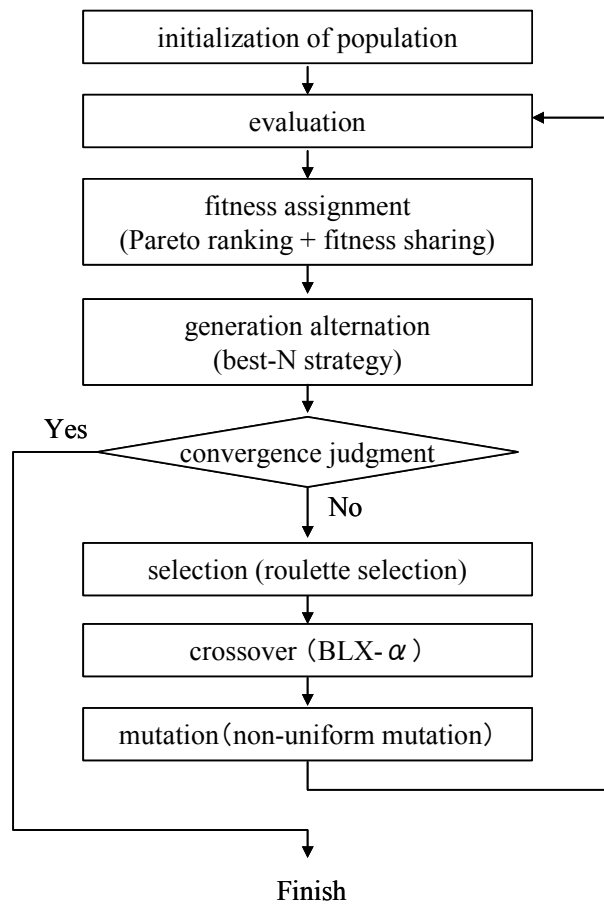
Figure 3-3 Flowchart of genetic algorithm
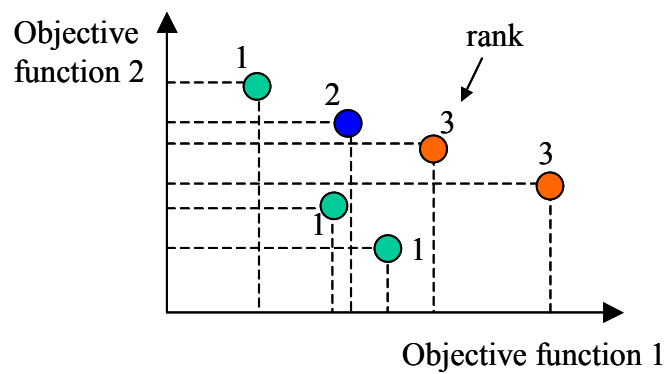
Figure 3-4 Pareto-ranking method (example of two objective function space)

41

3.2.3 Design Rule Mining with Decision Tree Analysis

Decision tree analysis [12] is an application of analysis of variance in statistical science. This method has been widely used as a decision-making method based on statistical analysis of multivariate data. In this study, this method is newly applied to an engineering design database that can be obtained by multi-objective optimization.

The goal of decision tree analysis is to extract a single design rule (decision rule) that is expressed in the following if-then form:

$$\text{if } (DV1 > A1) \text{ and } (DV2 < A2) \text{ and } \dots, \text{ then } (B1 < OF < B2). \tag{3-13}$$

Decision tree analysis iteratively divides a group of data into two sub-groups of data so as to distinguish one group from the other as clearly as possible (Fig. 3-5). The variance of means of objective function of each group is used as a criterion for determining the clearness of the division. The procedure for decision tree analysis is as follows.

1. Decide a criterion Ai for design variable DVi, where i denotes an index number of a design variable.
2. Divide original data group P into two sub-groups Q and R, in such a way that DVi is bigger and lower than Ai in Q and R, respectively.
3. Calculate the variances of data in Q and R from the mean of the original data group P.
4. Go back to 1) until the maximum variance is found.
5. Divide the group P into Q and R by the determined criterion. Go back to 1) and apply the same process to each of the sub-groups.

As a consequence of this procedure, a tree diagram shown in Fig. 3-6 is obtained. The grouping criteria are shown in the boxes, which correspond to diagram nodes. Design variables appear from the top box in order of sensitivity to the design objective so that, usually, the dominant main effects of these design variables can be extracted. A design rule is obtained by tracing a path to reach a desired node. In Fig. 3-6, a rule to maximize the objective function is shown with a thick lined path as an example. Decision tree analysis is characterized by its single and probabilistic design rule. The commercial software JMP (SAS Institute) [13] is used to calculate decision tree diagrams.
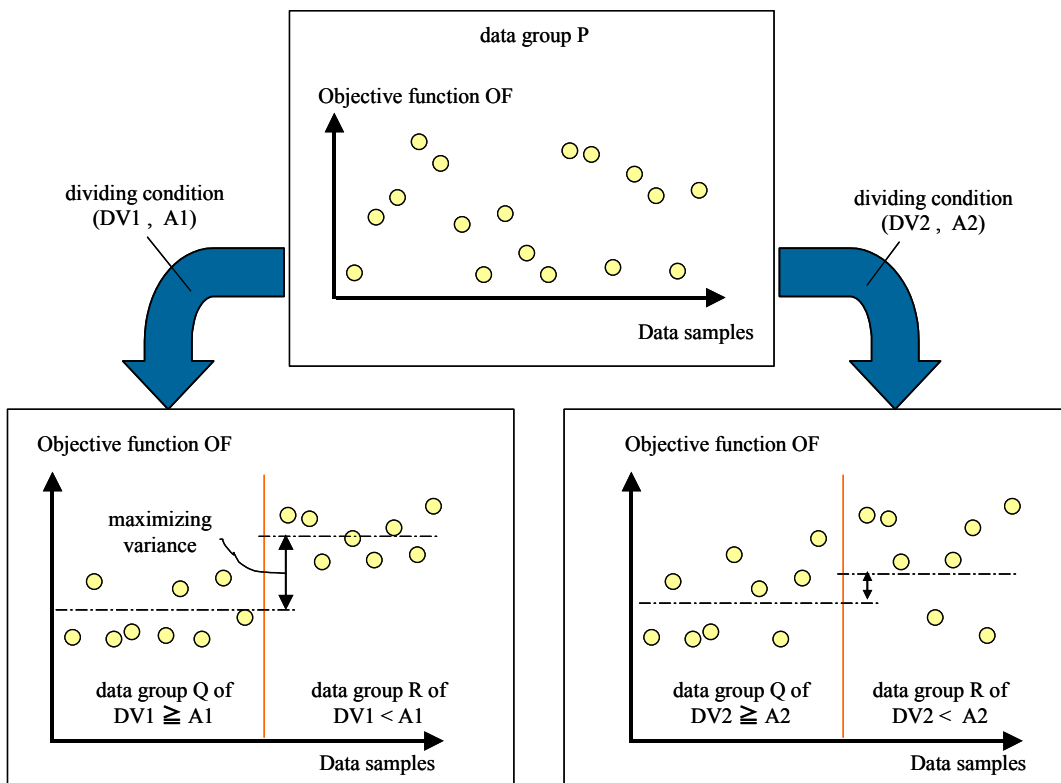
Figure 3-5 Division of data group by decision tree analysis
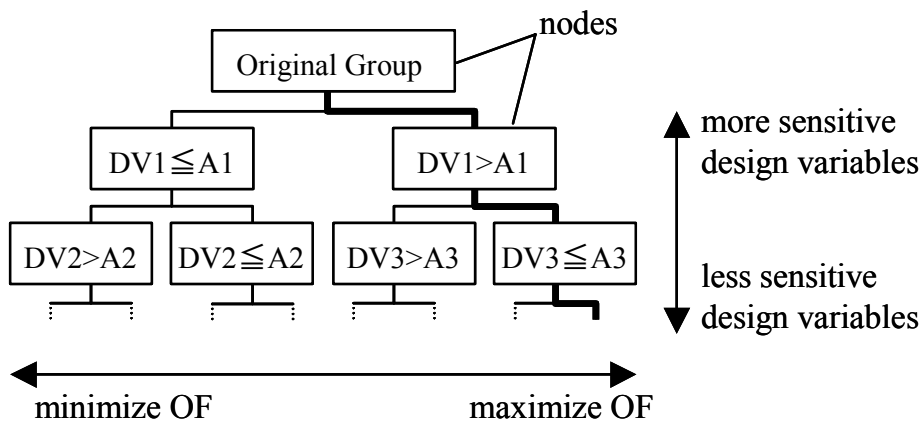
Figure 3-6 Decision tree diagram

3.2.4 Design Rule Mining with Rough Set Theory

Rough set theory was originally developed by Pawlak [14]. This mathematical method has been applied to human sense analysis because rough set theory is capable of handling ambiguous data and extracting underlying rules from that data. Because simulation data is deterministic, only the latter function is used. Rough set theory extracts design rules (decision rules) through the classification of set elements and set operations. As shown Fig. 3-7, any combination of design variable X's levels, and an objective function Y's level are assigned to set elements, and sufficient conditions are determined by examining inclusion relationship of these set elements [14][15]. In rough set theory, included elements are named as "lower approximation," while elements that partially share the same area but are not included are called "upper approximation." Rough set theory uses the lower approximation to extract design rules.

The concept and flowchart of applying rough set theory to an engineering design database are explained using Fig. 3-8. First, the CFD data samples with continuous variables are discretized to make logical set operation possible. Consequently, design variables (DVs) and objective functions (OFs) are categorized into several levels as the table in Fig. 3-8. Here, a level is assigned to a range of values of a design parameter in such a way that, for instance, the level 1,2 and 3 corresponds to the minimum, middle and maximum ranges, respectively. For multi-objective optimization cases, any clustered group, such as a group of the same rank number, can be a discrete category instead of these levels. Each line in the table is then regarded as a deterministic rule describing conditions and results. Hence, all the data becomes a collection of rule sets.

However, the rule sets still have as many conditions as the number of design variables, making it difficult for designers to understand them. Since some design variables do not affect the results or decisions, reducing the number of design variables required to obtain the same results is possible. This operation used for the purpose of obtaining minimum sets of conditions to determine the desired decision attributes is called "reduction", which makes obtaining simple rules with fewer conditions possible. This reduction is done using set operations. After obtaining reduced rule sets, the rule sets are filtered on the basis of the frequency with which the same rules are extracted. This is done because the reduction process still produces many rule sets, from which dominant rule sets must be determined. Finally, the meaning of the filtered rule sets is interpreted. Unlike decision tree analysis, rough set theory can extract multiple and deterministic design rules. The open software ROSSETA [16][17] is used for the necessary calculations.
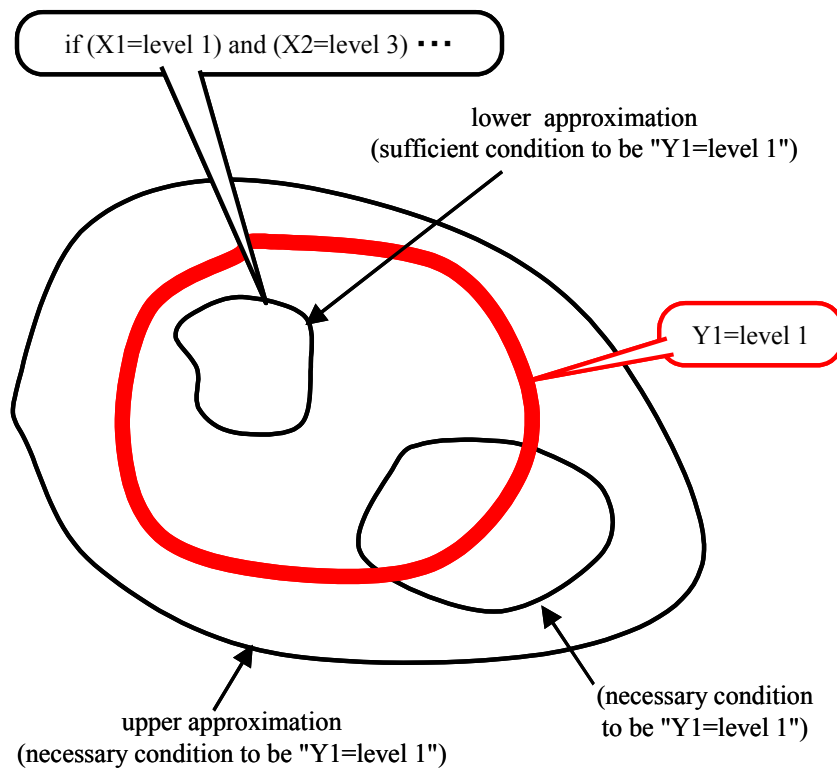
Figure 3-7 Rule extractions with rough set theory

	Condition attribute		Decision attribute
DV1	DV2	DV3	OF1
Level 3	Level 2	Level 3	Level 3
Level 2	Level 3	Level 1	Level 2

Discretization

Reduction --- Obtaining simple rules containing minimum sets of conditions

Filtering --- Selection of dominant rule sets

Interpretation --- Statistical evaluation of rule sets
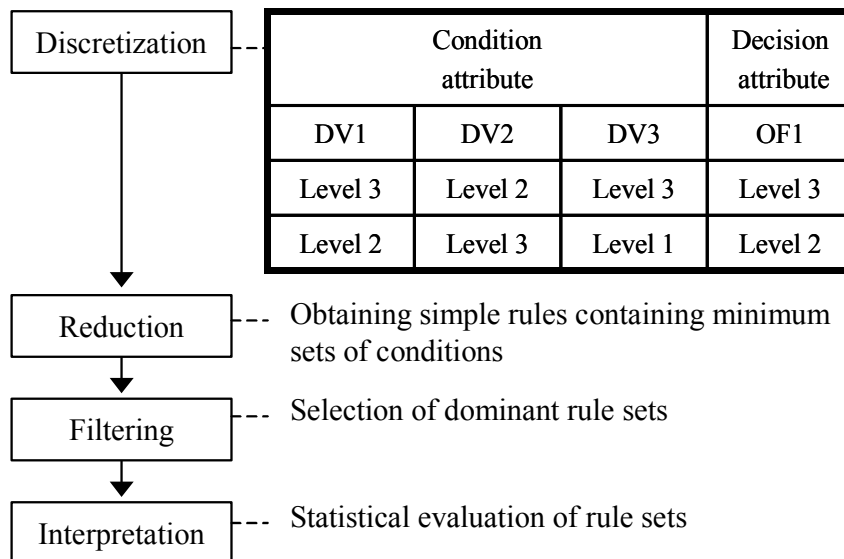
Figure 3-8 Application procedure of rough set theory

3.3 Design Optimization of Centrifugal Impeller
accompanied with Diffuser

3.3.1 Shape Parameterization

The shape of a low-specific-speed impeller is often designed two-dimensionally as a result of balancing performance-gain with production cost. Therefore, the shape parameterization method developed in Chapter 2 is used for defining the centrifugal fan of a vacuum cleaner [18]. In this section, detailed explanation is given about how to determine NURBS control points.

The shape of a centrifugal impeller is defined by a meridional profile and several blade profiles, i.e., blade sections. The fundamental concept of the method is that only two blade sections corresponding to the hub and shroud surfaces are defined and connected by two NURBS curves assigned to the blade's leading and trailing edges. Since this method does not require those multiple blade sections to be defined, the number of design variables can be reduced. Moreover, the method is capable of providing adequate spanwise three-dimensionality of the blade by deforming the connecting NURBS curves.

The meridional profile of the impeller is defined as shown in Fig. 3-9, where the vaned diffuser and the connecting vane-less diffuser are also shown. The hub and shroud lines are represented by NURBS curves, onto which the two blade sections mentioned above are projected. For simplicity, features such as lines and circles are directly used, and the resultant geometries are then fitted by these NURBS curves with a sufficient number of control points. In this study, the hub line was fixed, and the shroud line is modeled with two circles and a line. These features are tangentially connected to each other. As shown in Fig. 3-9, each of the blade's leading and trailing edges is represented by a NURBS curve with five control points. The locations of the control points at the ends are determined by blade profile definitions so that three control points in the middle can be moved. Notice that the trailing edge is assumed to be straight in this study to avoid highly distorted flow at the trailing edge.
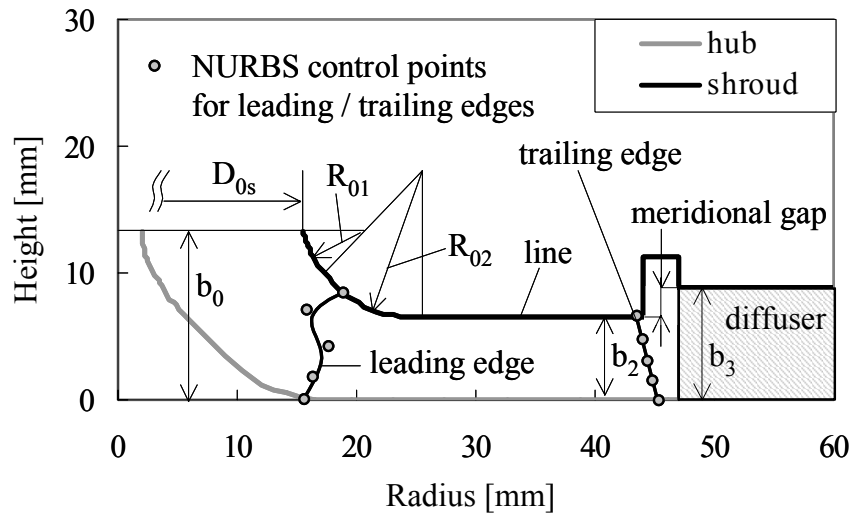
Figure 3-9 Meridional profile definition
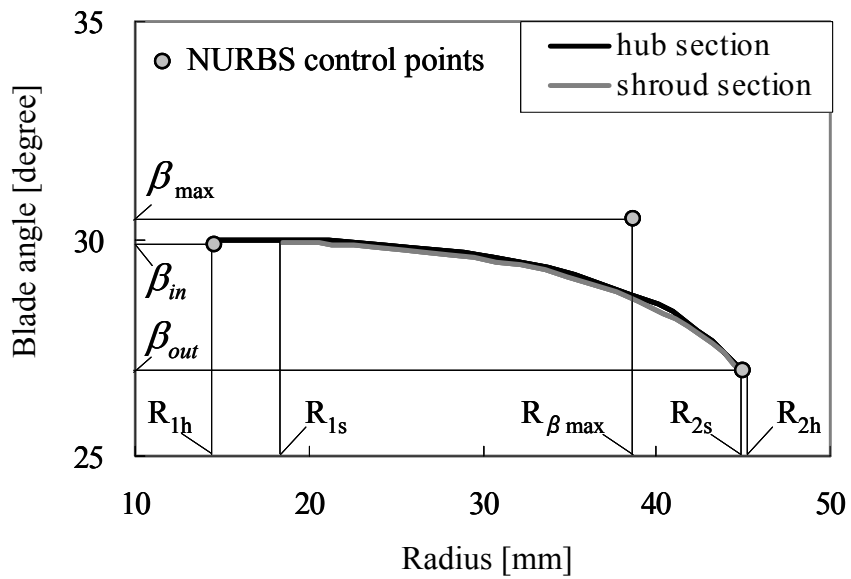
Figure 3-10 Definition of blade angle distribution function

47

The blade profile is built using camber and thickness definitions. The camber is defined by a distribution function of blade angle to the radius, as shown in Fig. 3-10. Here, the blade angle is defined as an angle made by tangential lines to the blade camber and to the circumferential line. This function is modeled by a NURBS curve with three control points. The distribution function for thickness is also defined in the same manner. On the basis of these functions, discretized points on the blade surface are calculated numerically. The leading edge and trailing edge on the blade section are modeled using circles. Notice that the blade profile uses NURBS curves indirectly while the meridional profile uses them directly for geometry representation. Although this method is capable of modeling quasi-three-dimensional skewed blades, the same distribution functions are used in this study for both the hub and shroud sections to build two-dimensional shapes for easier mass production. Thus, we only defined one NURBS curve for blade angle distribution, which are commonly used for both the hub and shroud sections (Fig. 3-10). The blade angle corresponding to R_{1h} (in the case of $R_{1h} > R_{1s}$) or R_{1s} (in the case of $R_{1h} < R_{1s}$) is automatically calculated. Blade thickness was taken to be constant.

This parameterization method is similarly used for modeling a vaned diffuser, although the diffuser shape is fixed during the design optimization. Once an impeller and diffuser are modeled, they are combined with a vane-less diffuser region.

3.3.2 Computational Fluid Dynamics

The computational domain is defined as a combination of the blade-to-blade regions of the impeller and diffuser to take the time-averaged interaction effect into consideration. A computational grid is shown in Fig. 3-11. The multi-block grids are automatically generated by an in-house tool that uses an algebraic generation algorithm. The mesh is structured and generated by specifying the least mesh size on the block boundaries and the numbers of meshes in I-J-K directions. Mesh density in the intermediate regions is controlled using geometric series calculations. The blocks for the impeller and vaned-diffuser parts are modeled according to the shape parameterization methods that are shown in Fig. 3-9 and 3-10. The blocks for the inlet duct, vane-less diffuser, and outlet duct parts are additionally modeled by specifying duct heights, radiuses, and the corresponding mesh sizes. Multi-rotating reference frame modeling is used, and the mixing plane is taken as being at the interface between the impeller and vane-less diffuser (#4 in Fig. 3-11). The number of revolution is 43,000 [min-1]. The unstructured-mesh-based RANS solver STAR-CD^{TM}

(CD-adapco) calculates a steady flow of compressible air using the standard $k-\varepsilon$ turbulence model and a wall function. The spatially second-order MARS scheme is applied for discretization of governing equations, and the resultant non-linear equations are solved by the SIMPLE algorithm and the conjugate gradient method. The number of mesh cells was decided as 224,952 after confirming that almost the same CFD results were obtained with 566,256. Computational fluid dynamics is conducted at the prescribed design point of $Q = $ 1.5 [m^3/min] at ambient condition. The numbers of the impeller blades and diffuser vanes are 8 and 13, respectively.

At the inlet, axial uniform inflow is assumed and the mass flow rate and temperature are fixed. Static pressure is extrapolated from the downstream to the inlet to calculate inflow density. Static pressure is fixed at the outlet. At the mixing plane, the same grids are used for both the impeller side and diffuser side. Flow properties at the mixing plane are averaged in the circumferential direction, but not in the spanwise direction so that spanwise non-uniform inflow to the diffuser can be considered. The impeller and vaned diffuser are aligned in the axial direction in such a way that both hub surfaces have the same axial position. This causes a meridional gap on the shroud side due to $b_3 > b_2$, as described in Fig. 3-9.
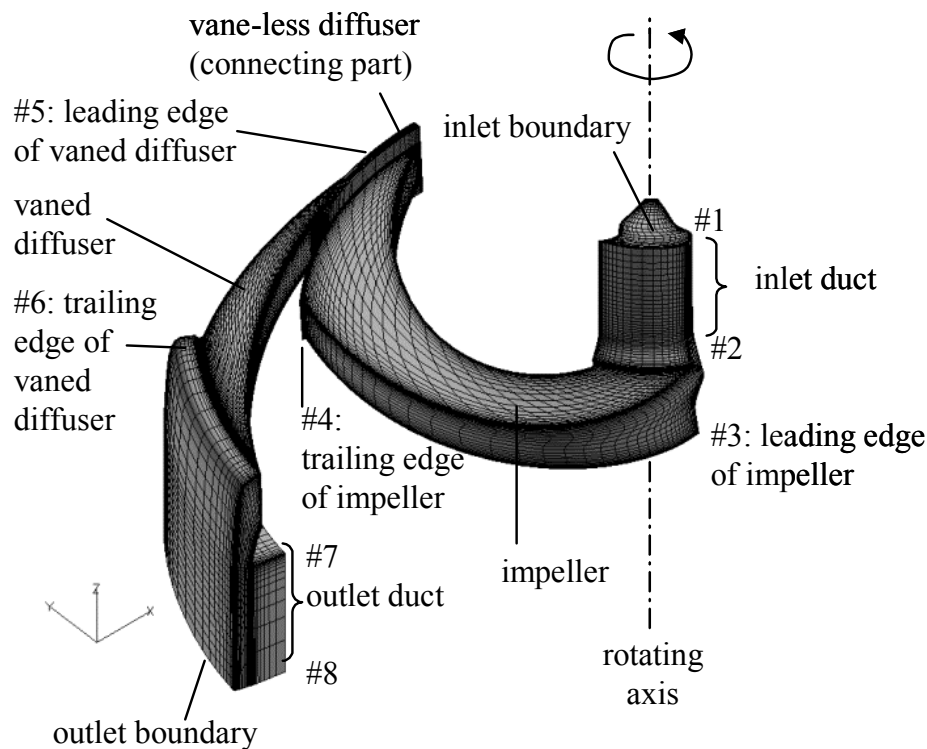
Figure 3-11 CFD model (# indicates locations)

3.3.3 Design Problem Definition

The optimization was performed only for the impeller's shape whereas CFD was performed for the combined configuration. This design policy attempts to design impellers that make the most of the potential performance of the combined diffuser. The author used this policy because of a difficulty in optimizing diffuser shapes. Optimizing a vaned diffuser in terms of pressure-rise generally results in an aerodynamically unstable shape, with which the flow is about to separate. However, with present technologies, RANS simulation cannot predict flow separation precisely without fine mesh and careful model tuning, which are undoubtedly not suitable for parameter surveys.

As mentioned earlier, the design objective is improving aerodynamic efficiency and stability against the varying flow rate. The uniformity of inflow incidence to the vaned diffuser is used to evaluate stability. Namely, the author assumed that a more uniform inflow to the diffuser at the design point also results in a more stable flow at the off-design points, because the incidence at the diffuser inlet has enough safety margins against flow angle variations.

The objective functions are then defined as follows.

■ Blower efficiency:

$$\eta_{blower} = \frac{Q(p_7 - p_1)}{W_{ax}}.$$

$$(3\text{-}14)$$

The product of the flow rate Q and the pressure rise $p_7 - p_1$ is divided by the shaft power W_{ax}. The subscripts of p denote the locations of the flow path (see # in Fig. 3-11).

■ The root mean square of the incidence angle ($i_b = \beta_{4\_i} - \beta_{4b}$) distribution at the vaned diffuser inlet:

$$\sigma(i_b) = \sqrt{\frac{\sum_{i=1}^{n} g_i \left(\beta_{4\_i} - \beta_{4b}\right)^2}{\sum_{i=1}^{n} g_i}} \, .$$

$$(3\text{-}15)$$

The summation is weighted by the local mass flow rate g_i at the mesh cell i. The inlet angle of the diffuser vane β_{4b} is constant in this study because the diffuser shape is two-dimensionally manufactured by means of molding and is fixed during design optimization.

Table 3-1 Design parameters

type	No	symbol	min.	max.	note
design variables	1	D_{2h} [mm]	89.5	90.5	$2*R_{2h}$
	2	D_{2s} [mm]	89.5	90.5	$2*R_{2s}$
	3	D_{0s}/D_2	0.31	0.37	$D_2=0.5(D_{2h}+D_{2s})$
	4	r_D_{1h}	0.22	0.36	$(D_{1h}-D_{0h})/(D_{2h}-D_{0h})$ $D_{1h}=2*R_{1h}$
	5	r_D_{1s}	0.0	0.1	$(D_{1s}-D_{0s})/(D_{2s}-D_{0s})$ $D_{1s}=2*R_{1s}$
	6	b_2 [mm]	6.0	6.6	-
	7	b_0/b_2	1.8	2.5	-
	8	r_R_{01}	0.05	0.95	$R_{01}/(b_0-b_2)$
	9	r_R_{tan}	0.1	0.8	$(R_{tan}-R_{1s}+R_{01})$ $/(R_{2s}-R_{1s}+R_{01})$
	10	β_{in} [deg.]	10.0	30.0	$\min(R_{1h},R_{1s})$
	11	β_{max} [deg.]	30.0	60.0	-
	12	r_β_{max}	0.10	0.90	$(R_{\beta max}-R_{in})$ $/(R_{out}-R_{in})$
	13	β_{out} [deg.]	20.0	30.0	$\max(R_{2h},R_{2s})$
	14	r_R_{le1}	0.95	1.05	D_{le1}/D_m $D_m=0.5(D_{1h}+D_{1s})$
	15	r_R_{le2}	0.95	1.05	D_{le2}/D_m
	16	r_R_{le3}	0.95	1.05	D_{le3}/D_m
objective functions	1	η_{blower}	maximize		-
	2	$\sigma(i_b)$ [deg.]	minimize		-
constraint	1	W_{ax} [W]	875.0	895.0	-

The shaft power W_{ax} was taken as a constraint because the maximum energy consumption of a vacuum cleaner is regulated. Geometrical parameters are assigned to design variables using the dimensions shown in Figs. 3-9 and 3-10. Table 3-1 summarizes all the definitions of these design variables and their allowable definition regions, together with the constraint and the objective functions. Major dimensions regarding radiuses and heights are related to the design variables from Nos. 1 to 9. The blade angles are related to those from Nos. 10 to 13. The remaining Nos. 14, 15, and 16 define the leading edge's deformation. Most of design variables are defined in normalized forms as shown in Table 1 in order to make the automatic geometry modeling and mesh generation possible, avoiding definitions of infeasible or highly distorted geometries.

3.4 Results and Discussion

3.4.1 Non-dominated Solutions

The population of MOGA was set to 40, and 12 generations were altered within the allowed turn around time. The obtained non-dominated and associated dominated solutions are shown in Fig. 3-12. As described in Fig. 3-12, an apparent trade-off relationship was found between two objectives, i.e. higher blower efficiency resulted in higher non-uniformity (less aerodynamic stability), and vice versa. In this calculations, seven non-dominated solutions A, B, …, and G were determined on the trade-off line. The impeller's shapes corresponding to these non-dominated solutions are also visualized, shown in Fig. 3-12 as the axial view, side view, and bird view near the leading edges. Efficiency and stability-weighted design candidates are shown toward the right and left, respectively.

Clear distinctions in shapes cannot be found from these figures except from the leading edges. However, identifying a tendency of these leading edges remains difficult. Therefore, choosing dominant design variables to the trade-off is attempted by means of correlation analysis. Table 3-2 summarizes coefficients of correlation between the design variables and objective functions. If a design variable is related to the trade-off, the corresponding two correlation coefficients must have different signs. Taking this into consideration, the author chose the dominant design variables D_{2h}, D_{2s}, b_2, and r_β_{max} as a consequence of filtering those with magnitudes of correlation coefficients lower than 0.7.
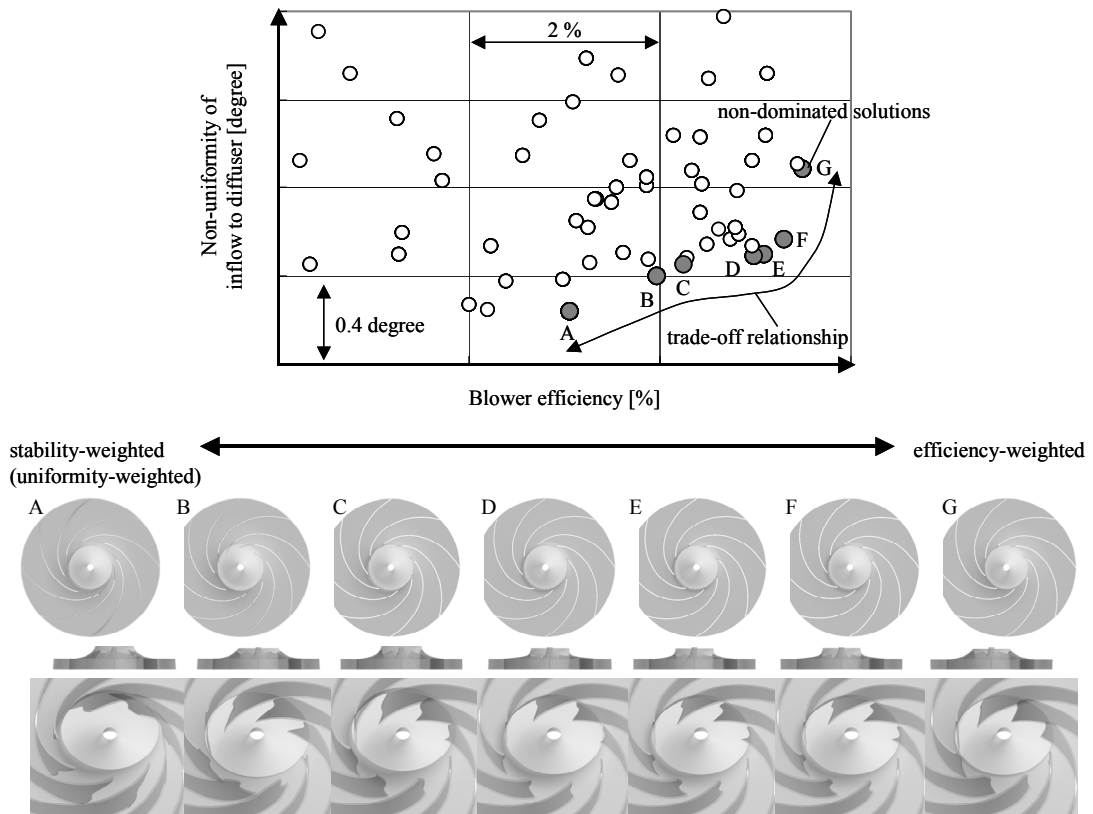
Figure 3-12 Trade-off in non-dominated solutions

Table 3-2 Coefficients of correlation

No.	1	2	3	4	5	6	7	8	9	10	11	12	13	14	15	16
DV	D_{2h}	D_{2s}	D_{0s}/D_2	r_D_{1h}	r_D_{1s}	b_2	b_0/b_2	r_R_{01}	r_R_{tan}	β_{in}	β_{max}	r_β_{max}	β_{out}	r_R_{le1}	r_R_{le2}	r_R_{le3}
η_{blower}	0.72	-0.86	0.37	0.66	0.23	0.76	0.62	-0.05	-0.55	-0.83	0.61	-0.83	-0.63	-0.10	-0.12	-0.70
$\sigma(i_b)$	-0.73	0.92	-0.26	-0.61	-0.32	-0.81	-0.45	-0.32	0.16	0.54	-0.28	0.77	0.93	-0.25	-0.23	0.36

Table 3-3 Dimensions of non-dominated solutions

	A	B	C	D	E	F	G
D_{2s}/D_{2h}	0.989	0.990	0.999	0.994	0.998	1.001	1.005
b_3/b_2	1.05	1.03	1.06	1.07	1.07	1.07	1.17
r_β_{max}	0.261	0.653	0.552	0.639	0.617	0.615	0.738
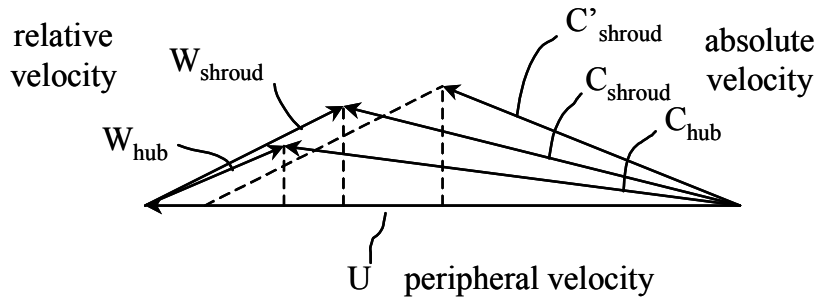
Figure 3-13 Velocity triangle at impeller exit

Table 3-3 summarizes these parameters in the normalized forms. D_{2s} / D_{2h} indicates how much the trailing edge inclines in the meridional plane. There is a tendency for efficiency-weighted designs are to be $D_{2s} > D_{2h}$ and uniformity-weighted designs to be $D_{2s} < D_{2h}$. In terms of b_3 / b_2 (b_3=constant), efficiency-weighted blowers have larger b_3 / b_2, and uniformity-weighted blowers have smaller b_3 / b_2. Regarding r_β_{max}, efficiency-weighted blowers seem to have larger r_β_{max}, but the tendency is not as clear as that of the other parameters.

Velocity triangles at the impeller exit are schematically shown in Fig. 3-13. In these low-specific-speed centrifugal impellers, the flow near the shroud surface generally has lower energy than that near the hub surface due to the effect of secondary flow (see C_{shroud} and C_{hub}). In addition, as previously mentioned, there is a meridional gap on the shroud-side in the vane-less diffuser region for this design problem and so the flow near the shroud is very diffusive. Therefore, improving pressure recovery by widening the meridional bump and injecting more energy to this diffusive region is possible. The author believes that this is why efficiency-weighted designs result in larger D_{2s} and b_3 than D_{2h} and b_2, respectively.

In the downstream vane-less diffuser region, the flow angle of C_{shroud} becomes much smaller than that of C_{hub} because of the meridional bump. Therefore, for the purpose of improving the uniformity of the flow angle, C_{shroud} must initially rise by reducing D_{2s} ($C_{shroud} \rightarrow C'_{shroud}$) in preparation for the flow angle decrease at the vane-less diffuser region.

In terms of b_3 / b_2, it is obvious that b_3 should be close to b_2 for more uniform flows. These are the reasons why D_{2s} and b_3 tend to become smaller than D_{2h} and b_2, respectively, for uniformity-weighted designs.

The last parameter r_β_{max} controls the aerodynamic load balance (distribution) of the impeller. Although its tendency is not as linear as the others, this parameter certainly affects the trade-off relationship. With these considerations, it is concluded that the trade-off between efficiency and stability is controlled by the dimensions of the vane-less diffuser and the load balance of the impeller.

As a design candidate for balancing efficiency and stability, non-dominated solution C was chosen and aerodynamic performance was measured experimentally. The solutions D, E, and F were not chosen because their b_0 and D_{0s} were considered too small to avoid the unfavorable interaction effect of separation flow with the blade leading edge. This separation flow starts from the gap between the impeller inlet and its casing, which was not incorporated in our CFD model. Figure 3-14 shows the results of the experiment, showing the current model (baseline) performance as well as a solution designed by the traditional Design-of-Experiment-based single-objective optimization method that merely optimizes efficiency. In the single-objective optimization method, we first carried out parameter surveys using an orthogonal table and then determined the optimum level combination of design variables. All the test models were mounted on the same motor. With regard to the combined vaned diffuser, the single and multi-objective designs share the same one. The diffuser used for the baseline impeller has the same vane shape as the others but different b_3 — 6.8 [mm] for the baseline and 7.3 [mm] for the others. The multi-objective design has been proven to not only improve the blower efficiency at the design point but also keep efficiency high at other flow rates. In contrast, the single-objective design suffers from aerodynamic stall at lower flow rates although it has an improved efficiency at the design point. From these results, it was confirmed the proposed multi-objective optimization method is effective for designing a centrifugal impeller that is aerodynamically efficient and stable.

Figure 3-15 compares oil flow patterns between the baseline and design C, which approximately shows secondary flow direction near the walls. Even though design C has a more diffusive vane-less diffuser due to larger b_3 than the baseline configurations, it achieves having similar oil flow patterns at the vaned-diffuser, avoiding flow separation. In the impeller region, the secondary flow of design C is more strongly restricted, resulting in more smoothed secondary flow directions.
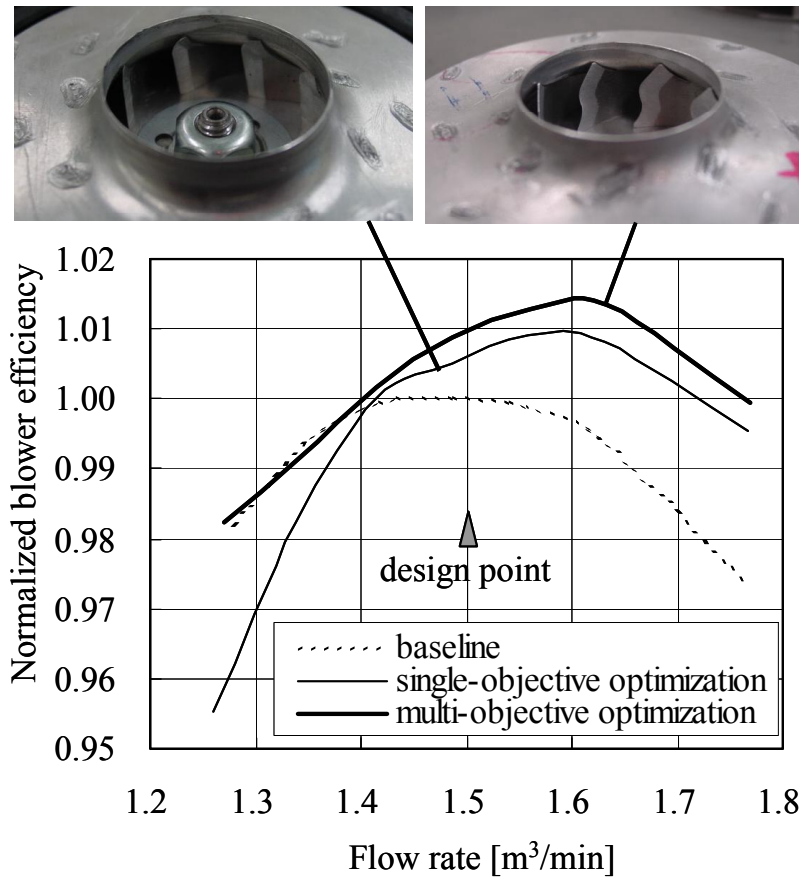
Figure 3-14 Comparison of experimental performance curves

3.4.2 Data Setup for Design Rule Mining

Although the design variables dominant to the trade-off was chosen, only their qualitative tendencies have been discussed. From industrial viewpoints, clarifying quantitative relationships between the setup of design variables and the resulting performance is needed. Hence, decision tree analysis and rough set theory were applied to obtain these quantitative design rules. These data mining techniques can be applied to either all the CFD sample data or the non-dominated solution data. The meaning of derived design rules changes depending on which data we use. In the former case, general design rules for optimality can be obtained, because the data are concerned with the global design space. In the latter case, design rules to control trade-offs that maintain optimality can be obtained, because the data are related to trade-off relationships among non-dominated solutions.

In this study, the number of non-dominated solutions was merely seven, which is not sufficient for mining design rules. In contrast, the CFD samples obtained in the first step were considered sufficient and so the data mining techniques could be applied to the CFD data. The CFD samples obtained in the first step were cleansed by eliminating duplicated data and outliers, resulting in 161 normalized data samples.

(a) baseline   (b) non-dominated solution C
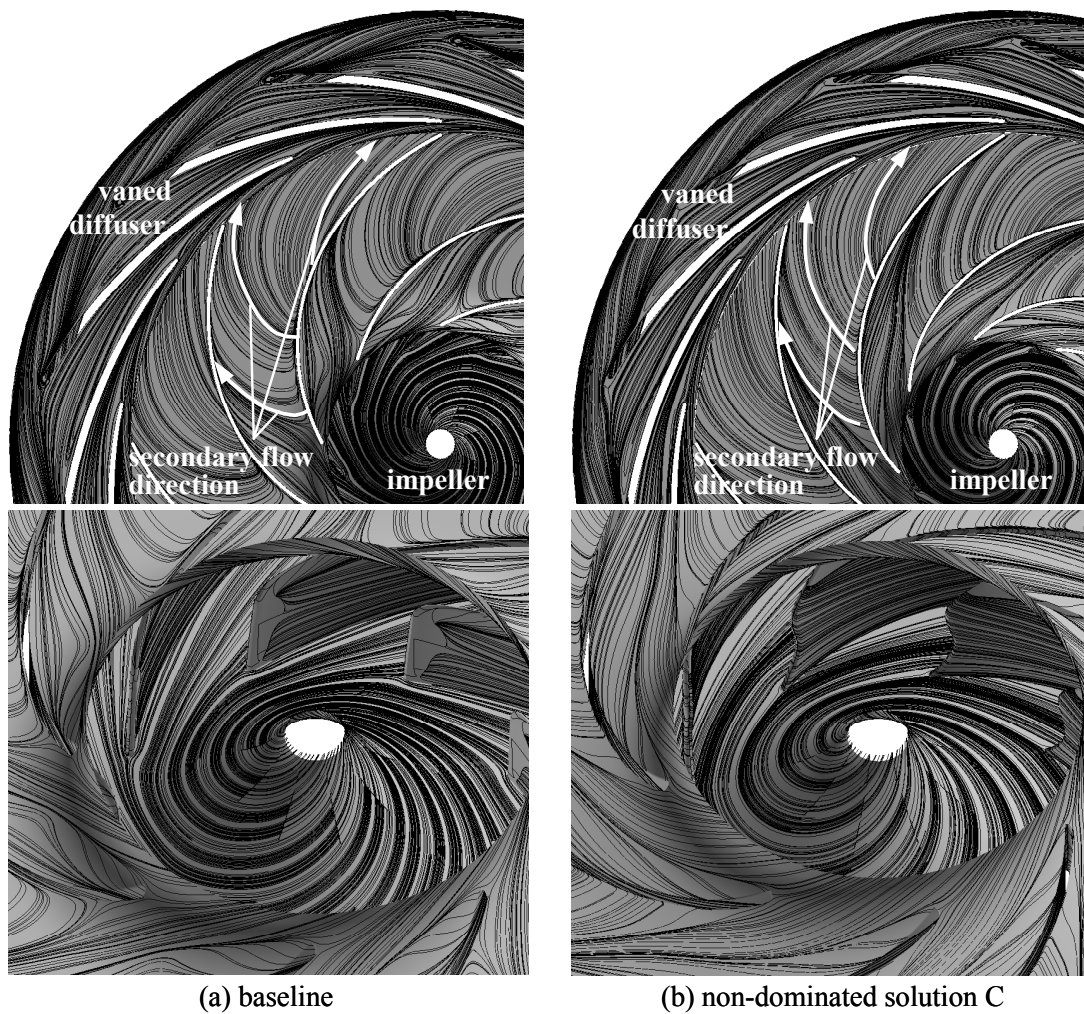
Figure 3-15 Comparison of oil flow patterns

(top: axial view from shroud side; bottom: close-up view of leading edge areas)

3.4.3 Design Rules from Decision Tree Analysis

First, decision tree analysis was applied to the CFD data. The purpose here was to find general rules to achieve extreme designs in terms of blower efficiency and stability. Figures 3-16 and 17 show decision tree diagrams obtained for η_{blower} and $\sigma(i_b)$, respectively. Each box gives a decision condition, a ratio of average of the objective function in the corresponding group to that of the top group (r_av.), and the number of data in the group. The decision conditions in the upper boxes are more important than those in the lower boxes in the sense that they are sensitive and definitive. The decision conditions in the boxes further to the right have a higher objective function value while those further to the left have a lower one. The expansion of the diagram was terminated when the number of data in a node was approximately 20% of the initial number.

The design rule to maximize η_{blower} is obtained by tracing from the top to the bottom right node, as shown in Fig. 3-16:

$$\text{if } (\beta_{in} \geqq 22.89) \text{ and } (D_{0s}/D_2 < 0.319), \text{ then (r\_av. = 1.035).} \tag{3-16}$$

This means that higher efficiency can statistically be achieved if we have a relatively large inlet blade angle β_{in} and small inlet diameter D_{0s}. Moreover, the blower efficiency is expected to improve by 3.5% on average if these quantitative conditions are satisfied. The former condition is believed to be a result of the reduction of friction loss due to the larger throat area of the impeller. The latter condition is expected to increase the total static-pressure-rise by enhancing the local static-pressure-rise at the impeller's entrance.

From Fig. 3-17, the design rule for achieving maximum uniformity is:

$$\text{if } (b_2 \geqq 6.24), (D_{2s} < 89.96), \text{ and } (D_{0s}/D_2 \geqq 0.336), \text{ then (r\_av. = 0.951).}$$

$$\tag{3-17}$$
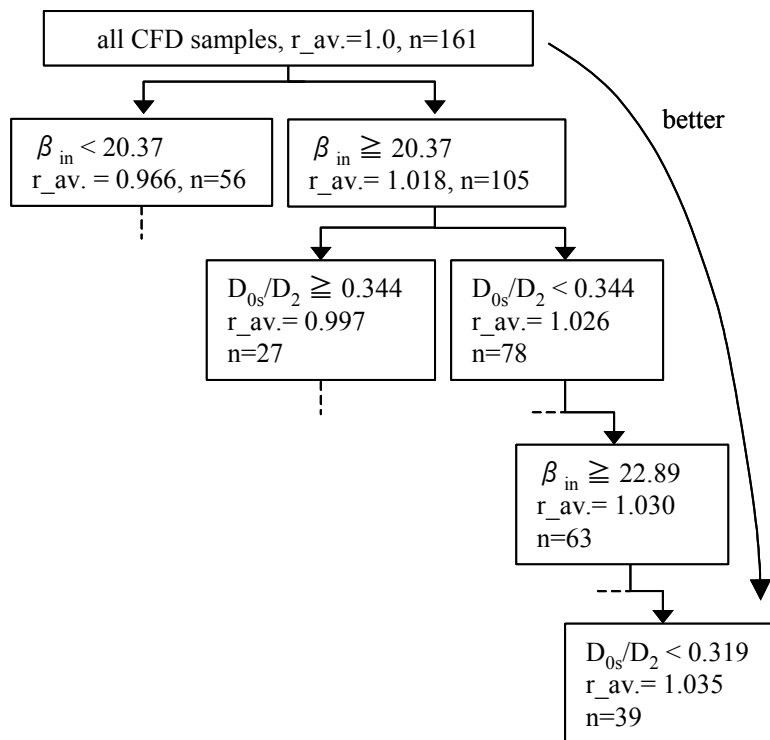
Figure 3-16 Decision tree diagram for extreme design of blower efficiency
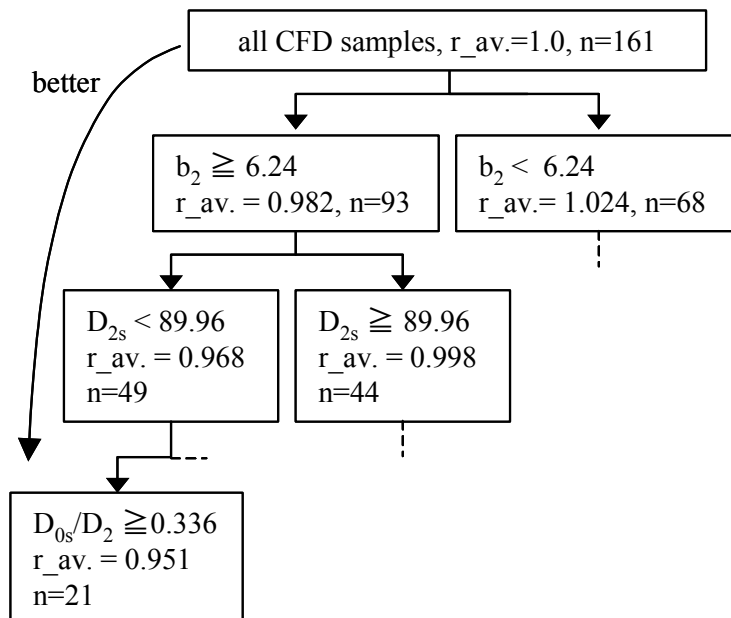
Figure 3-17 Decision tree diagram for extreme design of flow uniformity

Relatively large b_2 increases the uniformity because $b_2 < b_3 (b_3 = \text{const.})$ in this design problem. As we have already discussed with regard to Fig. 3-13, D_{2s} should be relatively small for uniform flow. In terms of D_{0s}, the opposite tendency of rule (3-16) is found. Rules (3-16) and (3-17) derived from decision tree analysis have statistical meanings as to dominant effects of these design variables including both main and interaction effects, so there can be some exceptions. However, these design rules seem understandable from a common sense in turbomachinery design.

Figure 3-18 shows a summary of the design rules derived from decision tree analysis and correlation analysis with qualitative expressions. The rule toward the extreme design regarding aerodynamic efficiency guides a move from P1 to P2 in the objective function space. Similarly, the rule toward the extreme design regarding aerodynamic stability guides a move from P1 to P3. For these moves, quantitative rules are also available. The trade-off control is made possible by applying the qualitative rules described in this figure. The rule set for the trade-off control, which is described in Fig. 3-18, is an example of moving from P3 to P2. Although these paths are schematic and do not mean that we can circulate the state of design objectives by changing only these dimensions appeared in the rules, making these general guides available and visualizing them on a map is surely useful for designers.

3.4.4 Design Rules from Rough Set Theory

Rough set theory was next applied to the CFD data to clarify general rules and compare the results with those of decision tree analysis. In applying rough set theory, each design variable is discretized to five levels in such a way that each level contains the same number of data items. The partitioning of the levels is visualized in Fig. 3-19. Notice that extreme bias was observed for D_{0s} / D_2.

The objective function η_{blower} was partitioned into 10 levels of equal width between the minimum and maximum values, and rules to be in level 10, where η_{blower} becomes the maximum, were calculated. The extracted rules are shown in Table 3-4. Rules that have been extracted fewer than six times have been filtered (see "counts" in Table 3-4). As a result of this filtering operation, 17 rules were obtained. Rule 1, for example, denotes:

if (D_{0s} / D_2 =level 1), (r_R_{01} =level 4) and (β_{out} =level 2), then (η_{blower} = level 10).

$$(3\text{-}18)$$
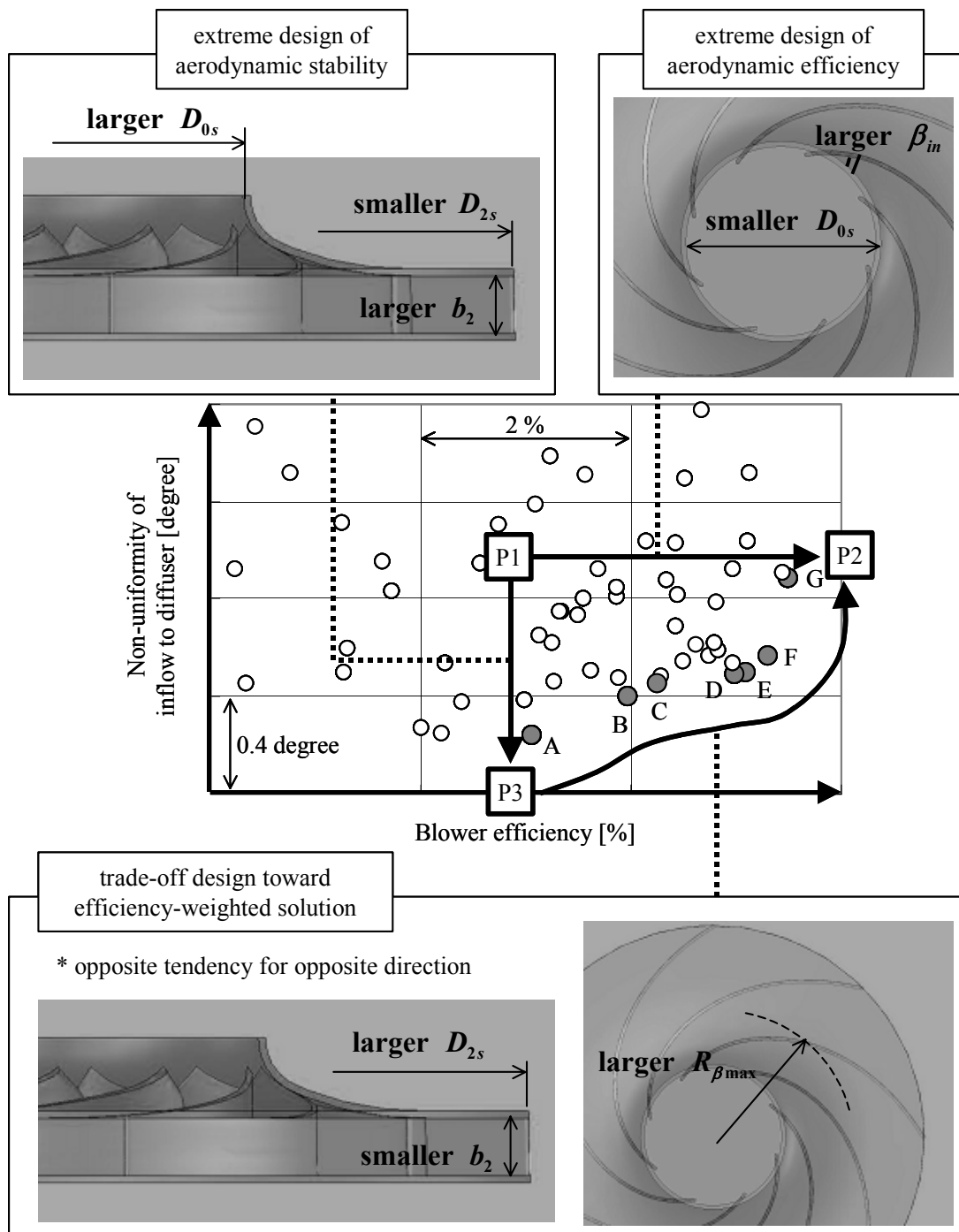
Figure 3-18 Summary of design rules

The number of conditions needed was drastically reduced from 16 to 3, resulting in a very simple rule. While decision tree analysis extracts a single rule that has statistical meaning, rough set theory extracts various deterministic rules as listed in Table 3-4. This diversity and certainty are advantages of rough set theory because the derived rules are related not only to the main effects of design variables but also to the interaction effects. Decision tree analysis cannot be used to extract the interaction effects because a data group is divided on the basis of a criterion of a single design variable.
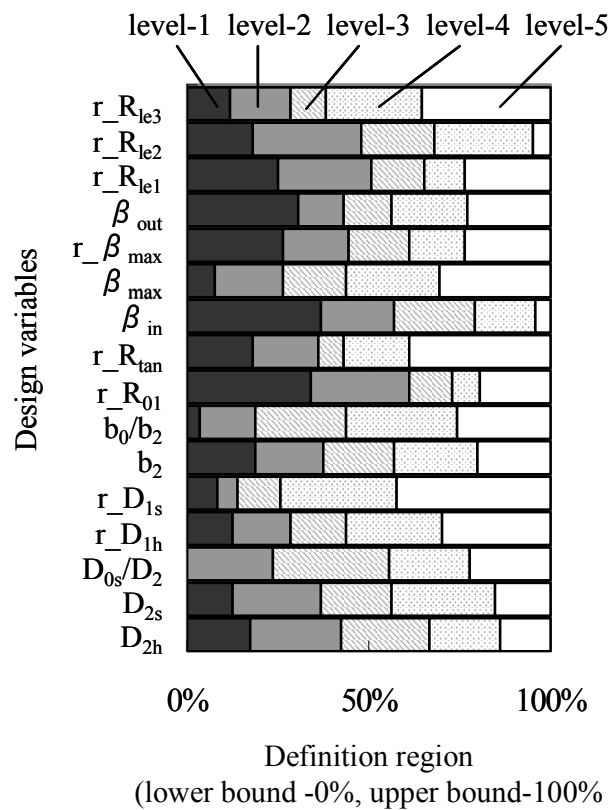
Figure 3-19 Discretized levels of design variables

Table 3-4 Rule sets for extreme design of blower efficiency

No	Design Variable	Extracted rules																	weight	avr.	stand. dev.
		1	2	3	4	5	6	7	8	9	10	11	12	13	14	15	16	17			
1	D_{2h}																3		0.02	3.0	0.0
2	D_{2s}																		0.00	NA	NA
3	D_{0s}/D_2	1	1	1		1	1		1	1		1	1	1		1			0.24	1.0	0.0
4	r_D_{1h}			3												5			0.04	4.0	1.0
5	r_D_{1s}		2					2	2				2	2	2				0.12	2.0	0.0
6	b_2				4	4				4	1		4				1		0.12	3.0	1.4
7	b_0/b_2		3		3		3	3		3						3			0.12	3.0	0.0
8	r_R_{01}	4		4	4	4	4	4											0.12	4.0	0.0
9	r_R_{tan}																		0.00	NA	NA
10	β_{in}										5	5			5			4	0.10	4.8	0.4
11	β_{max}																		0.00	NA	NA
12	r_β_{max}														4				0.02	4.0	0.0
13	β_{out}	2							2						2				0.06	2.0	0.0
14	r_R_{le1}																		0.00	NA	NA
15	r_R_{le2}													5				3	0.04	4.0	1.0
16	r_R_{le3}																		0.00	NA	NA
	extracted count	6	7	6	6	6	6	6	6	6	6	10	6	6	6	6	6	7			

However, it is difficult for rough set theory to give a statistical meaning of what these rule sets imply as a whole. Therefore, to evaluate the statistics of these rule sets, the author calculated the average and standard deviation of the level for each design variable appearing in Table 3-4. Weight index was also calculated to evaluate the relative importance of each design variable. The weight is a normalized index calculated as the "counts" in Table 3-4 multiplied by the frequency at which the rule element appears (e.g., eleven times for D_{0s}/D_2 and six times for b_0/b_2). Design variables with larger weights are considered important because their rule elements appear very frequently in decision rules.

Figure 3-20(a) shows the weights. Setting a threshold to 0.1 for the weight, design variables D_{0s}/D_2, r_D_{1s}, b_2, b_0/b_2, r_R_{01}, and β_{in} were deemed important. The calculated statistics, the averages and standard deviations, of the levels are shown in Fig. 3-20(b). The author believes that the smaller values of standard deviation reflect the generality of the rule. Although the order of importance is different from the order of results

of the decision tree analysis (Fig. 3-16), the rules that D_{0s}/D_2 should be small (level 1) and β_{in} should be relatively large (level 4 - 5) agree with the results of decision tree analysis. Other rules regarding r_D_{1s}, b_2, b_0/b_2, and r_R_{01} provide new insight as to how performance can be improved. It is also important to mention here that, in Table 3-4, the level of b_2 varies in the rule sets according to the design variables to be combined with.

Similarly, the rule sets to be in the top 20% of aerodynamic stability were analyzed by rough set theory, and the statistics of frequently extracted rules were evaluated; the results are shown in Table 3-5 and Fig. 3-21. The five most important parameters were chosen as D_{2s}, r_D_{1h}, b_2, β_{in}, and r_β_{max}. Although the order of importance is different from the order of results of the decision tree analysis again, the rules that D_{2s} should be small (level 1) and b_2 should be middle-large (level 4) agree with the result of decision tree analysis. Other rules for r_D_{1h}, β_{in}, and r_β_{max} suggest additional viewpoints to control aerodynamic stability.

Notice that, in Table 3-5, the rule set of r_β_{max} takes various levels, as observed with b_2 in Table 3-4. These parameters b_2 and r_β_{max} are considered to be related to the interaction effects of more than two design variables because the fact that their optimum levels change according to design variables to be combined with, is a typical characteristic of interaction effects.

With these findings, the author concluded that the rules for design variables related to dominant total effects can be determined as similarly as decision tree analysis by applying rough set theory and analyzing resultant rule sets statistically. It was also concluded that rough set theory can be used to extract design rules related to interaction effects by its diverse and deterministic rule extraction mechanism while decision tree analysis has the advantage of determining sensitivities of design variables.

(a) Weight of each design variable

(b) Statistics of rule elements

Figure 3-20 Design rules for extreme design of blower efficiency

(a) Weight of each design variable

(b) Statistics of rule elements

Figure 3-21 Design rules for extreme design of flow uniformity

Table 3-5 Rule sets for extreme design of flow uniformity

No	Design Variable	1	2	3	4	5	6	7	8	9	10	11	12	13	14	15	16	17	18	19	20	21	22	23	24	25	26	27	28	29	30	31	32	33	34	35	36	37	38	39	40	41	weight	avr.	stand. dev.
1	D_{2h}													5				4	4																	3					5		0.0	4.2	0.7
2	D_{2s}															1	1	1	1		1	1	1	1	1			1	1			1											0.1	1.0	0.0
3	D_{0s}/D_2				5										4	5				4		5				4				4				4									0.1	4.4	0.5
4	r_D_{1h}			5		4					4			4			4			4	4			5								5			4								0.1	4.3	0.5
5	r_D_{1s}				3	3		1					4															1															0.0	2.4	1.2
6	b_2			5		5		5			4			4			4					4			4						4				4	4	4					0.1	4.3	0.4
7	b_0/b_2									4					5	5												5						5	5	5				5		0.1	4.9	0.3
8	r_R_{01}		2					1													3									1												0.0	1.8	0.8
9	r_R_{tan}		2			2	2																																2	2		0.0	2.0	0.0
10	β_{in}	1	1		1			1			1			1						1					1	1		1	1			1				1					1	0.1	1.0	0.0
11	β_{max}							1																		1		4	4		1		4					4		0.1	2.7	1.5
12	r_β_{max}	1		1	5				4	5	5		5					1				4			4			1			4			4	3		0.1	3.3	1.6
13	β_{out}				1				3						1			4		1			1			3				0.1	2.0	1.2
14	r_R_{le1}																				4					3			3	0.0	3.3	0.5
15	r_R_{le2}	4				4		2	1			1					4					1		0.1	2.4	1.4
16	r_R_{le3}							4											3		0.0	3.5	0.5
	extracted count	3	3	3	4	3	3	3	3	3	3	3	3	3	3	4	3	3	3	4	3	3	3	3	3	3	3	3	4	3	3	3	3	4	3	3	3	3	3	4	3				

With these case studies of data mining, three types of design variables have been observed. The first one is a parameter that indicates strong main effects. D_{0s}/D_2, β_{in}, and D_{2s} are classified into this type. These design variables are sensitive and maintain certain optimum levels in design rules. The second one is a parameter that changes its level depending on the other design variables to be combined with. b_2 and r_β_{max} are among this type, which can be related to interaction effects. These parameters are also sensitive but it is difficult to identify the best level of them for better designs. The third one is a parameter that is not so sensitive but keeps its level regardless of the design variables to be combined with. These parameters concern optimality and can be detected by rough set theory as the other dominant design variables.

3.5 Conclusion

The author described multi-objective optimization and design rule mining methods for a low-specific-speed centrifugal impeller with a vaned diffuser. An efficient shape parameterization method using NURBS curve representation was used to enhance the flexibility of the geometry. The CFD evaluates time-averaged non-uniform inflow to the

diffuser so that both aerodynamic efficiency and stability had been evaluated. By carrying out multi-objective optimization aimed at improved efficiency and stability, seven non-dominated solutions were found, and design variables dominant to the trade-off were clarified to be dimensions of the vane-less diffuser and the load balance of the impeller. By experimentation, it was concluded that the proposed multi-objective optimization method is effective for designs of this type of low-specific-speed centrifugal blower.

In the subsequent step, two different data mining techniques, decision tree analysis and rough set theory, were applied to the CFD data in order to extract quantitative design rules to achieve better performance. Dominant design variables were determined together with their levels to be set. Differences in the features of the derived rules between the decision tree analysis and rough set theory were also discussed. The decision tree analysis extracts a single probabilistic rule while rough set theory mines various deterministic rules. However, statistically evaluating rough set rules makes evaluating similar probabilistic rules as a decision tree possible. As a consequence of these case studies, it is concluded that decision tree analysis is suitable for detecting the dominant total effects of design variables and interaction effects can be extracted only by using the rough set theory. It follows from these arguments that these characteristics of extracted design rules are complementary each other so that we should use both methods to understand a design problem properly. Notice that these data mining techniques can be widely applicable to any design database in the same manner as demonstrated in this paper, while the proposed multi-objective optimization method was tailored for low-specific-speed blowers.

In this study, however, the number of non-dominated solutions was not sufficient for data mining and so these data mining techniques could not be applied to them. It is our expectation that sufficient number of non-dominated solutions enables the extraction of quantitative design rules also with regard to the trade-off control. Further advancing MOGA evolutions and increasing the number of non-dominated solutions is needed. Since this approach results in an increase of the design turn around time, it should be planned to use surrogate models of design space to reduce computational cost even for higher dimensional design problems. In the next step of design exploration, the data mining techniques used in this study will be applied to various data sets obtained by surrogate model-based optimizations to clarify design space characteristics. Besides, the features of data mining techniques, including other methods that have not mentioned, will be comparatively investigated to find the best use for them in engineering designs.

References

[1] Obayashi, S., Tsukahara, T., Nakamura, T., Multiobjective Genetic Algorithm Applied to Aerodynamic Design of Cascade Airfoils, IEEE Transactions on Industrial Electronics, Vol. 47, No. 1, pp.211-216, 2000.

[2] Oyama, A., Liou, M. S., Multiobjective Optimization of Rocket Engine Pumps Using Evolutionary Algorithm, Journal of Propulsion and Power, Vol. 18, No. 3, pp.528-535, 2002.

[3] Oyama, A., Multidisciplinary Optimization of Transonic Wing Design Based on Evolutionary Algorithms Coupled with CFD Solver, Proceedings of European Congress on Computational Methods in Applied Sciences and Engineering (ECCOMAS), 2000.

[4] Sasaki, D., Obayashi, S., Nakahashi, K., Navier-Stokes Optimization of Supersonic Wings with Four Objectives Using Evolutionary Algorithm, Journal of Aircraft, Vol. 39, No. 4, pp.621-629, 2002.

[5] Benini, E. and Tourlidakis, A., Design Optimization of Vaned Diffusers for Centrifugal Compressors Using Genetic Algorithm, AIAA-2001-2583, 2001.

[6] Khelladi, S., Kouidri, S., Bakir, F., and Rey, R., Flow Study in the Impeller-Diffuser Interface of a Vaned Centrifugal Fan. Journal of Fluids Engineering, 127, 495-502, 2005.

[7] Obayashi, S., Jeong, S., Chiba, K., and Morino, H., Multi-Objective Design Exploration and its Application to Regional-Jet Wing Design, Transaction of the Japan Society for Aeronautical and Space Science, Vol. 50, No.167, pp.1-8, 2007.

[8] Gen, M. and Cheng, R., Genetic Algorithms & Engineering Optimization. New York: John Wiley & Sons, Inc., 2000.

[9] Deb, K., Multi-Objective Optimization using Evolutionary Algorithms, John Wiley & Sons, Ltd., West Sussex, England, 2001.

[10] Fonseca, C. M. and Fleming, P. J., Genetic Algorithms for Multi-objective Optimization: Formulation, Discussion and Generalization. Proceedings of the Fifth International Conference on Genetic Algorithms. San Mateo, CA: Morgan Kaufmann Publishers, Inc., 416-423, 1993.

[11] Oyama, A., Fujii, K., Shimoyama, K., and Liou, M., Pareto-Optimality-Based Constraint-handling Technique and Its Application to Compressor Design. AIAA2005-4983, 2005.

[12] Witten, I. H. and Frank, E., Data Mining. Morgan Kaufmann, chapter 6, 2005.

[13] SAS Institute, JMP 6, http://www.jmp.com/.

[14] Pawlak, Z., Rough sets. International Journal of Computer and Information Sciences, 11(5), 341-356, 1982.

[15] Obayashi S., Data Mining for Multi-Objective Optimization Using Rough Sets. Proceedings of Grant-in Aid for Scientific Research Symposium - Aerodynamics Team, 2006 (in Japanese).

[16] Øhrn, A., Discernibility and Rough Sets in Medicine: Tools and Applications, PhD thesis, Department of Computer and Information Science. Norwegian University of Science and Technology, Trondheim, Norway: NTNU report 1999:133, IDI report 1999:14, ISBN 82-7984-014-1, 1999.

[17] ROSETTA Manual, http://rosetta.lcb.uu.se/general/resources/manual.pdf, 2006.

[18] Sugimura, K., Aerodynamic Shape Optimization and Knowledge Mining of Centrifugal Fans Using Simulated Annealing Coupled With a Neural Network. ASME DETC 2006-99189, 2006.

Chapter 4

Multi-objective Robust Design Exploration using Kriging Model, Self-organizing Map, and Association Rule

4.1 Introduction

Multi-objective optimization becomes available in chapter 3, enabling to handle the uncertainty in design-decisions in practical designs. Moreover, quantitative design rules have been revealed for improving each objective function, helping designers to connect key design variables with flow physics.

However, there is different uncertainty in design-conditions, which cannot be defined as objective functions. Namely, uncertainty in design variables cannot be handled with the developed method yet. This uncertainty causes from variance in dimensions, material properties, environmental conditions and aged deteriorations. Besides, design rules for controlling trade-off balance have not been extracted yet.

Therefore, in this chapter, the previously developed method is improved to a multi-objective robust optimization method, in which the variance in design variables is modeled. A systematic way of trade-off rule mining from high-dimensional non-dominated solutions is also proposed.

Centrifugal fans used in consumer products such as washer-dryers and vacuum cleaners are typical mass-produced products. Improving the mean performance of these products and minimizing variance in their performance are important design issues for producers.

Figure 4-1 shows a washer-dryer and the centrifugal fan installed in its drying system. Reduced drying time and operating noise are features that are most important to customers. In the fan's design, a higher flow rate, i.e., higher efficiency, and lower aerodynamic noise are the keys to improving these features. It is also important to reduce variance in performance in these areas under conditions of dimensional uncertainty due to mass production.

Techniques of multi-objective optimization using evolutionary algorithms have become popular in the area of turbomachinery design because they can deal with conflicting relations

among multiple design objectives. Many previous studies [1][2][3][4] have focused on multi-objective turbomachinery designs. However, none of these studies has considered dimensional uncertainty. This is mainly because the calculation of statistical response to uncertainty has been computationally too expensive.

Regarding robust designs, Egorov [5] took a stochastic approach to the robust design of turbomachinery, but his work was not based on optimization. Lee and Park [6] incorporated uncertainty in design variables and optimized a weighted sum of mean and standard deviation of a single objective function. They used Taylor series expansion to approximate sensitivity of the objective function. In their work, simulations were directly conducted. Padmanabhan and Batill [7] used an artificial neural network as an approximation model for reducing computational cost in robust design. However, their work also used Taylor series expansion for evaluating sensitivity. Koch, et al. [8] adopted Kriging model and the descriptive Monte Carlo sampling method. They succeeded in evaluating actual variations against uncertainty in design variables, not approximated sensitivity. Robust optimization using computation fluid dynamics was started by Huyse, et al. [9], where they attempted aerodynamic robust design of two-dimensional blades. Lyu, et al. [10] studied multi-objective optimization of automotive pneumatic control valves in terms of cost and quality. They conducted Monte Carlo simulations with Radial Basis Function approximation model. It was remarkable that they defined tolerances themselves as design variables. In these ways, it has becoming possible to evaluate variations against uncertainty in design variables.

However, trade-off relations between the mean and variance of multiple objective functions have not been investigated so far, particularly for turbomachinery designs. Some researchers like Kumar et al. [12] and Shimoyama [13][14] have started to apply techniques of multi-objective optimization to robust designs as a multi-objective Six Sigma approach.

The author took a similar approach to theirs, but he instead integrated the multi-objective Six Sigma approach with the parameterization method in the Taguchi method [15], which is an acknowledged method of robust design. Within this context, the author first aimed at developing a widely applicable multi-objective robust design framework, which integrated a multi-objective genetic algorithm, Kriging models, and a generalized probabilistic representation of design parameters. Kriging models were chosen as response surface models for their excellent accuracy in prediction, which is required to evaluate robustness.

72
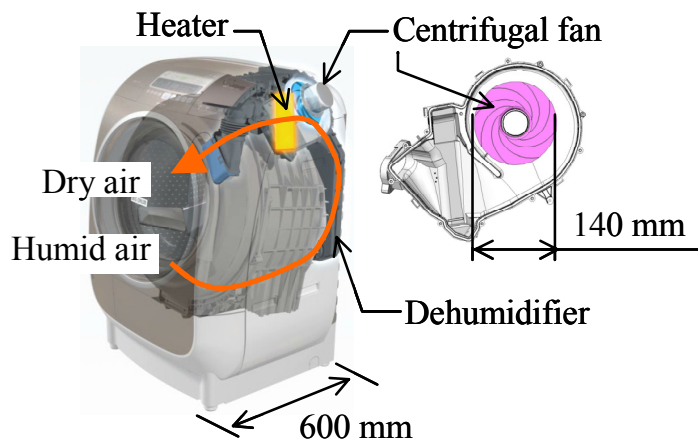
Figure 4-1 Washer-dryer and its centrifugal fan

Another difficulty in multi-objective robust optimization is higher dimensional non-dominated solutions than those from a multi-objective "non-robust" optimization. It is usually difficult to choose a proper design candidate or extract design rules from these high dimensional data if the data cannot be visualized in graphs. To overcome this problem, it was also intended to develop methods of analyzing trade-offs in this study.

Nakayama et al. [24] developed the aspiration level method that enables interactive trade-off analysis in multi-objective optimization problems. In this method, a directional vector located in high-dimensional objective function space is used for specifying a preference in a trade-off balance. The author newly applied this traditional concept of directional vector to data mining. Namely, aspiration vector concept was combined with a design rule extraction method, association rule, to find quantitative rules to control any trade-off balances.

"Multi-objective design exploration (MODE)" concept that was originally proposed by Obayashi, et al. [16] is extended to new paradigm of "multi-objective robust design exploration (MORDE)". In the following, a generalized framework of multi-objective robust optimization is first described and then methods of analyzing trade-offs are explained. MORDE's capabilities is demonstrated by applying the methods to an industrial design problem in a centrifugal fan.

Nomenclature

x : design variable

y : objective function

f : evaluation function

p : probability density function

θ : angle between aspiration vector and data vector

μ : mean

σ : standard deviation

η_s : fan efficiency

L_{tb} : turbulent noise level, dB

w : weight of objective function

4.2 Design Exploration Method

4.2.1 Generalized Multi-objective Robust Design Framework

The framework developed incorporates probabilistic representations of design parameters into a real-coded multi-objective genetic algorithm. Kriging models [17][18][19] are used to numerically evaluate these probabilistic responses between design variables and resulting variables such as objective functions and constraints. The used Kriging model tool has been developed by Jeong et al. [20]. Although Kriging models are believed to provide the most accurate predictions among available options, a great deal of computational cost is required to construct the models. However, they were worthwhile using because a number of robustness evaluations by actual simulations were more costly. It should also be noted that Kriging models are capable of optimization based on "expected improvement", which attains efficient global optimization in a high-dimensional design space [19].

Figure 4-2 shows a flowchart for the method of multi-objective robust optimization that is developed. First, the design space is sampled by Latin hypercube sampling (LHS) to collect the necessary dataset to construct Kriging models. Since a single Kriging model approximates the relation between multiple design variables and a single evaluation function, multiple Kriging models must be constructed to evaluate multiple functions.
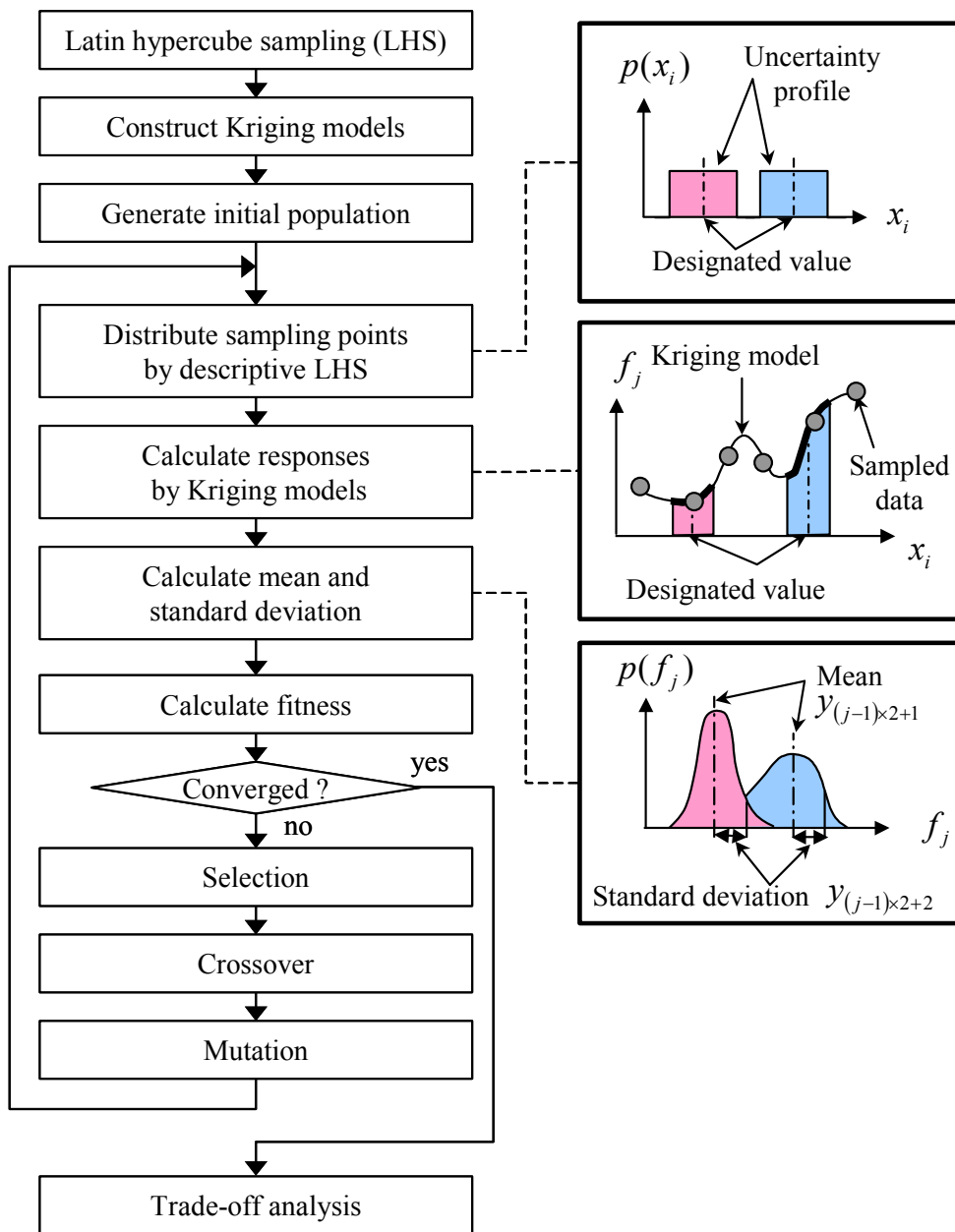
Figure 4-2 Flowchart for MORDE

(p : probability density function, x_i : i-th design variable,

f_j : j-th evaluation function, y_* : *-th objective function)

Once Kriging models are prepared, a multi-objective genetic algorithm (MOGA) solves the optimization problem using statistic parameters calculated by the Kriging models. Unlike traditional methods of non-robust optimization, each individual in MOGA only determines the representative values of uncertainty profiles of design variables, x_i, as shown in the right box at the top of Fig. 4-2. According to a prescribed uncertainty profile, a probability distribution function, $p(x_i)$, is assumed. Descriptive LHS is then done to locate sampling points according to the probability distribution for evaluations of robustness as efficiently as possible. The Kriging models are used to predict the deterministic responses of evaluation functions, f_j, to these sampling points (right box in the middle of Fig. 4-2). After that, responses are collected as $p(f_j)$ and the means and standard deviations are numerically calculated. Finally, the mean $y_{(j-1)\times 2+1}$ and standard deviation $y_{(j-1)\times 2+2}$ of each evaluation function are assigned to two objective functions (right box at the bottom of Fig. 4-2). Thus, the number of objective functions becomes twice the number of evaluation functions (Kriging models).
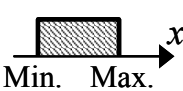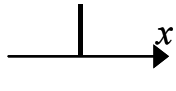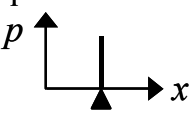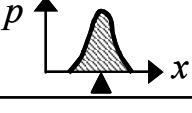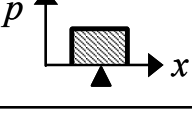
In the following sequence of genetic operations, the method explained in Chapter 3 is used. The evolutionary process is iterated until the maximum variation in the averages of objective functions become lower than a given criterion. After non-dominated solutions are obtained, the trade-off is analyzed using data-mining methods that will be explained later.

In uncertainty profiles, a rectangular and normal distribution are prepared as options for the current system. If an uncertainty profile is known through measurements, the normal or other actual distribution profiles can be used. If the profile is unknown, a rectangular profile should be used. Response calculations using the rectangular profile correspond to experiments using noise factors in the Taguchi method. Since the intention of this research was to develop a compatible method of parameterization with the philosophy of the Taguchi method, parameter representations are generalized as summarized in Table 4-1.

Table 4-1 explains the relations between the setup of design variables in our system and corresponding factors in the Taguchi method. By changing the types of uncertainty profiles and types of search regions of design variables in optimization, the roles of design variables can be assigned to the ones of the Taguchi method.

One outstanding feature of the Taguchi method is that it explicitly classifies design variables into control factors and noise factors, making designers aware of parameters' roles. While noise factors cannot be controlled by designers, control factors can be maintained in the design and manufacturing processes.

Table 4-1 Comparison of design variables with Taguchi method

Uncertainty profile \ Search region in optimization	Min. Max. Min. ≠ Max.	Min. = Max.
Deterministic profile	Control factor	Constant
Probabilistic profile (known)	Control and noise factor	Noise factor
Probabilistic profile (unknown)	Control and noise factor	Noise factor

However, in the Taguchi method, it is difficult to handle continuous uncertainty profiles like a normal distribution and the trade-off between multiple design objectives. In these areas, the multi-objective Six Sigma approach has advantages. As a result, the author combined both strengths and defined the method of parameterization summarized in Table 4-1.

4.2.2 Kriging Model

Among available approximation models such as second-order response surface, multi-layered neural network, radial basis function, and Kriging model, Kriging model is believed to be the most accurate. Although the use of it is the most computationally costly, it was chosen for the purpose of predicting not only mean but also variations against uncertainty.
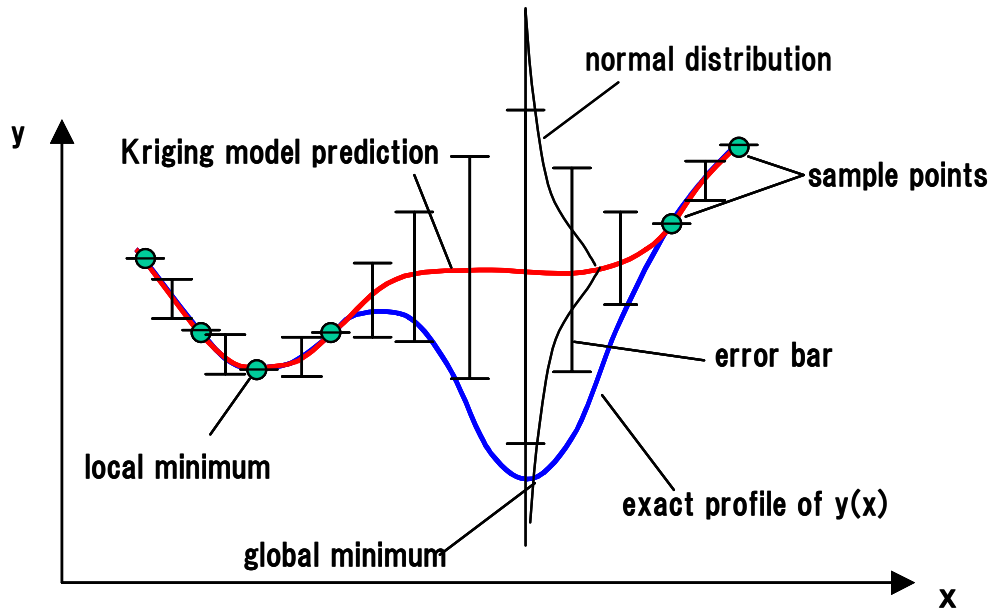
Figure 4-3 Concept of Kriging model

Figure 4-3 schematically shows the concept of Kriging model. Kriging model is an approximation function of multiple inputs and a single output. The prediction of Kriging model, denoted by red line in the figure, exactly interpolates the sample points. The model also provides normal distribution that represents prediction uncertainty. It is possible to use this uncertainty information for efficient global optimization [19].

Prediction of a function value y by a Kriging model is described as

$$y(\mathbf{x}) = \mu + z(\mathbf{x}), \tag{4-1}$$

where $\mathbf{x}$ is a vector of design variables, μ is the mean of y for all m samples, and z is a deviation from the mean. Here, the mean of z of all the samples is zero. The variance is σ^2 but covariance is not zero.

A correlation function between any two design points, $\mathbf{x}^i$ and $\mathbf{x}^j$, is defined in the form of a Gaussian function as

$$Corr\left[\mathbf{x}^i, \mathbf{x}^j\right] = \exp\left\{-\sum_{k=1}^{nDV} \theta_k \left|x_k^i - x_k^j\right|^2\right\},$$ (4-2)

where nDV is the number of design variables and θ is a Kriging parameter defined for each design variable.

The mean μ is calculated by

$$\hat{\mu} = \frac{\mathbf{1}^T \mathbf{R}^{-1} \mathbf{y}}{\mathbf{1}^T \mathbf{R}^{-1} \mathbf{1}},$$ (4-3)

where $\mathbf{1}$ is an m-vector of ones, $\mathbf{R}$ is an $m \times m$ matrix, each element of which corresponds to a correlation function $Corr\left[\mathbf{x}^i, \mathbf{x}^j\right]$ between two sample points, and $\mathbf{y}$ is the column vector of sample values.

The deviation z is calculated by the following equation:

$$z(\mathbf{x}) = \mathbf{r}^T(\mathbf{x}) \cdot \mathbf{R}^{-1} \cdot (\mathbf{y} - \mu\mathbf{1}),$$ (4-4)

where $\mathbf{r}(\mathbf{x})$ is a column vector, each element of which corresponds to a correlation function between the predicting point $\mathbf{x}$ and sample points $\mathbf{x}^i$.

A Kriging model provides a measure for uncertainty of prediction, i.e. the mean squared error,

$$s^2(\mathbf{x}) = \hat{\sigma}^2 \left[1 - \mathbf{r}^T \mathbf{R}^{-1} \mathbf{r} + \frac{\left(1 - \mathbf{1}^T \mathbf{R}^{-1} \mathbf{r}\right)^2}{\mathbf{1}^T \mathbf{R}^{-1} \mathbf{1}}\right],$$ (4-5)

where

$$\hat{\sigma}^2 = \frac{(\mathbf{y} - \hat{\mu}\mathbf{I})^T \mathbf{R}^{-1} (\mathbf{y} - \hat{\mu}\mathbf{I})}{m}.$$ (4-6)

Constructing a Kriging model is equal to calculating a set of θ that maximize the following likelihood function,

$$Ln = -\frac{m}{2}\ln\left(\hat{\sigma}^2\right) - \frac{1}{2}\ln\left(\|\mathbf{R}\|\right). \tag{4-7}$$

This is an unconstrained single-objective optimization problem and is solved by a genetic algorithm in our study.

4.2.3 Trade-off Rule Mining by Self-organizing Map and Association Rule

There are various data-mining techniques that can be applied to a design dataset, but, in this study, the author aimed to find design rules to achieve a certain trade-off balance of objective functions. For this purpose, two data-mining techniques, Self-organizing maps (SOMs) and the association rule, were used.

A SOM [21] is an unsupervised learning algorithm of neural networks, which projects high-dimensional data onto two-dimensional data (map). It converts multi-dimensional data into multiple two-dimensional data so that designers can visualize the correlation patterns of design parameters in the form of graphical maps [25]. The map has two-dimensional grids, on which data points are allocated. Each data point has meta-data of a vector, an element of which corresponds to design parameter values in the original high-dimensional space. The locations of the data points on the map are first randomly decided and then iteratively moved in a way which data points that are closer in the original space are located in a closer region on the map. The closeness is judged using the Euclidean distance of the vector data. As a result of the iteration, clusters that contain similar solutions appear on the map, enabling visualization of high-dimensional data. Commercial software, SOMine™ (Eudaptics GmbH), is used for creating the SOMs [26].

While SOMs represent a graphical and qualitative method of finding trade-off patterns, the association rule is a numerical and quantitative method of obtaining trade-off design rules. Design rules are expressed in "if-then" form that define a certain combination of levels of design variables (condition attributes) and a certain level of a design objective (decision attribute).

The author has already applied other methods of extracting design rules, decision tree analysis, and rough set theory, to a multi-objective optimization problem in the previous

chapter. Based on this work and some other preliminary investigations, it was found that decision tree analysis extracts a single probabilistic rule as a necessary condition and rough set theory extracts multiple deterministic rules as sufficient conditions. The association rule [22] is another alternative for extracting design rules with different features. The association rule has been used to find implicit rules from transaction data such as Point-of-Sales data. However, how it should be used in engineering design is still being discussed so that the author aimed to clarify this in this study.

The association rule mines design rules using a covering search algorithm, from a multivariate dataset with categorical data elements as shown in Table 4-2. In engineering data, condition attributes can be design variables x and their levels. A decision attribute can be one of objective functions y, but any other scalar variable can be chosen depending on the purpose. Because each line of the multivariate dataset represents a rule, which means if (condition attributes) then (a decision attribute), the dataset is considered to be a rule set. Consequently, the purpose of design-rule mining is to find more compact combinations of condition attributes to obtain simpler rules.

The association rule searches for all combinations of data elements, and counts up the number of times they occur. "A priori algorithm" is used to avoid redundancy in the search procedure. A rule length, which is defined as the sum of the number of necessary condition attributes and a decision attribute, must be specified in advance to restrict the search space and reduce the computational cost.

Because so many different rules can still be derived from the dataset, important rules are chosen based on the following criteria:

$$\text{support} (A \rightarrow B) = \frac{N_{A+B}}{N_{all}}, \tag{4-8}$$

$$\text{confidence} (A \rightarrow B) = \frac{N_{A+B}}{N_A}, \text{ and} \tag{4-9}$$

$$\text{lift} (A \rightarrow B) = \frac{\text{confidence}(A \rightarrow B)}{\text{support}(B)}, \tag{4-10}$$

where A, B represents a certain combination of attributes, and N_C is the number of data that satisfies the conditions denoted by C.

Table 4-2 Multivariate dataset

	Condition attributes				Decision attribute
No	x_1	x_2	x_3	x_4	y
1	Level 1	Level 2	Level 5	Level 4	Level 2
2	Level 5	Level 4	Level 1	Level 3	Level 1
3	Level 3	Level 4	Level 2	Level 2	Level 5
4	...	...	...	...	...

Because the association rule itself does not discriminate x_i from y and treats all the data elements evenly, some derived rules may have x_i in B. However, we are only interested in rules that contain y in B. Therefore, rules that do not have y in B are filtered first, and then rules are sorted or checked by using these criteria.

Support means how many times the combination of attributes A and B appear simultaneously in the dataset, indicating importance in the sense of frequent occurrence. In other words, a large value of support implies the commodity of a rule.

Confidence means how accurately the same combination of attributes A and B is repeated in the data that includes A. If confidence is equal to one or lower than one, the derived rules are sufficient conditions or necessary conditions, respectively. That is, confidence represents the accuracy of a rule.

Lift is used to check if the obtained rule is trivial. If most of the lines in Table 2 have the same decision attribute, the condition attributes in a derived rule become less meaningful. Because lower values of lift mean that the derived rules are trivial, we check if it is higher enough than the possible minimum value, i.e. one.

In the calculation of association rule, the minimum values of the "support" and "confidence" are specified in advance. The calculation was conducted with the commercial software, Visual Mining Studio^{TM} (Mathematical Systems Inc.) [27].

4.2.4 Specifications for Trade-off Balance Using Aspiration Vector

The author proposes a new definition of the decision attribute in Table 4-2, which is suitable for specifying a trade-off balance. Figure 4-4 shows the method of definition in a three-dimensional objective function space as an example. Here, the optimization problem is assumed to be a minimization problem.

First, the non-dominated solution space is normalized. The virtual point, S, corresponding to the coordinate (1,1,1), is defined as the origin for a vector to control the trade-off balance. Note that this origin can be taken in a different way depending on the purpose, e.g., the current product's performances can be assigned to the origin. An "aspiration vector" that specifies the trade-off balance is defined as:

$$\vec{a} = \begin{pmatrix} -w_1 \\ -w_2 \\ \vdots \\ -w_n \end{pmatrix}, \tag{4-11}$$

where $w_i \ (i = 1, 2, \cdots, n)$ is a positive weight for the i-th objective function, and n is the space dimension (n =3 in Fig. 4-4). Then, a vector connecting S and the j-th non-dominated solution is defined as a data vector:

$$\vec{d_j} = \overrightarrow{SD_j} = \begin{pmatrix} y_1^{(j)} - 1 \\ y_2^{(j)} - 1 \\ \vdots \\ y_n^{(j)} - 1 \end{pmatrix}, \tag{4-12}$$

where $y_i^{(j)} \ (j = 1, 2, \cdots, m)$ represents the coordinates of the j-th non-dominated solution, and m is the total number of non-dominated solutions.

The angle between the aspiration vector and the data vector is calculated to measure the proximity to the preferred balance.

$$\theta_j = \mathrm{acos}\left(\frac{\vec{a} \cdot \vec{d_j}}{\|\vec{a}\| \cdot \|\vec{d_j}\|} \right). \tag{4-13}$$
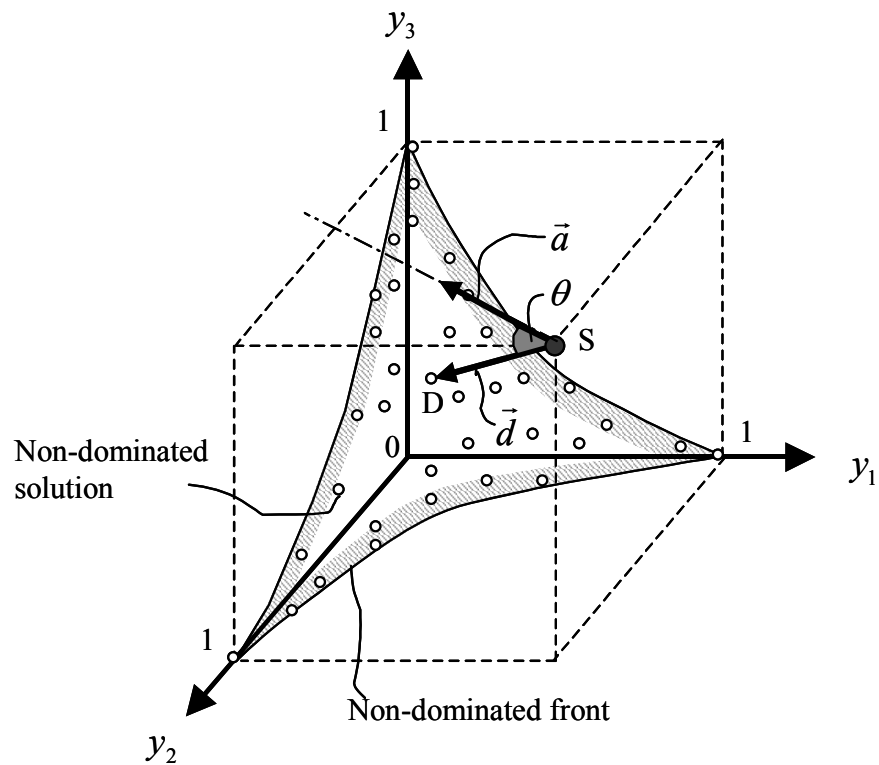
Figure 4-4 Control trade-offs using aspiration vector

The design rules to achieve the specified balance can be derived by setting θ_j to the decision attribute in Table 3 and finding rules that minimize θ_j.

4.3 Design Optimization of Centrifugal Fan with Dimensional Uncertainty

4.3.1 Shape Parameterization

In this study, the proposed methods were applied to a design problem that optimized the shapes of a centrifugal fan with dimensional uncertainty. The shape was parameterized by a method similar to those in the previous chapters. Figures 4-5 (a) and (b) briefly explain how to define the respective meridional and blade profiles of the centrifugal fan.

(a) Definition of meridional shape   (b) Definition of blade shape
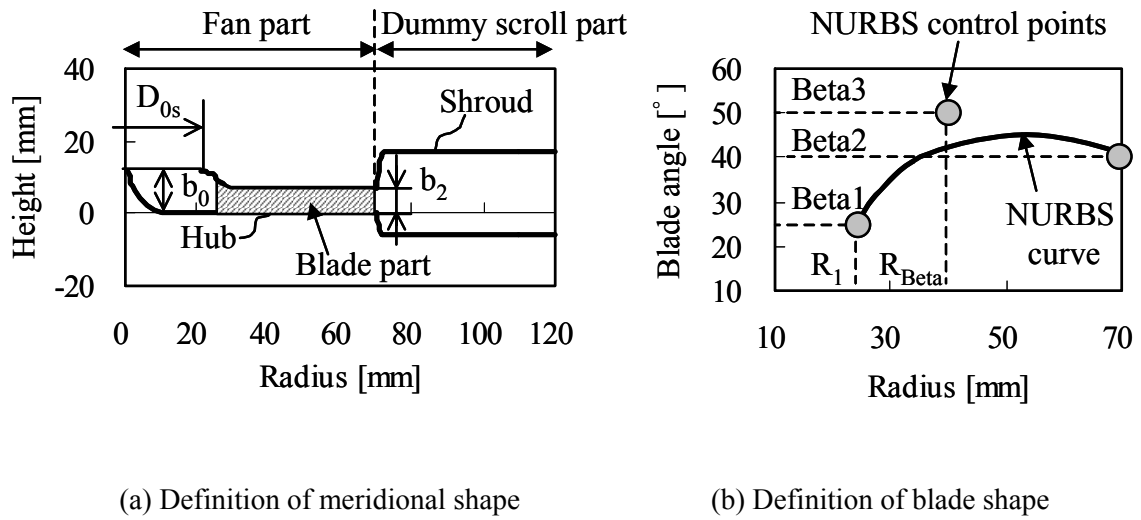
Figure 4-5 Parameterization of shape for centrifugal fan

In the definition of the meridional profile, inlet diameter D_{0s}, inlet height b_0, and outlet height b_2 are taken as design variables. Either the hub or shroud curve is modeled as a combination of a circle and a line for the fan part. The dummy scroll part is attached to the outer side of the fan part. These curves for the meridional profiles are then converted to non-uniform rational B-spline (NURBS) curves for a mesh-generation tool. The shape of the scroll is fixed during optimization.

In the definition of the blade profile, the blade angle distribution is defined by a NURBS curve with three control points, as shown in Fig. 4-5 (b). The blade camber line is then calculated according to this distribution, and the blade surface is defined by adding a constant thickness to the camber line. The blade is assumed to be two-dimensional in the axial direction due to manufacturing reasons. The design variables for the blade profile are Beta1, Beta2, Beta3, r_R_1, r_R_{Beta}, where r_R_1 and r_R_{Beta} correspond to normalized variables of R_1 and R_{Beta}. The outer radius of the fan is fixed in this problem.

4.3.2 Design Problem Definition

The objectives of this fan design were to increase fan efficiency and reduce the turbulent noise level. This aerodynamics was evaluated by a Reynolds-averaged Navier Stokes (RANS) simulation of the blade-to-blade region of the centrifugal fan. The in-house algebraic mesh generator automatically created a multi-block structural mesh of 149292 vertices and 145920 cells. Then, commercial software, STAR-CD^{TM} (CD-adapco), was used for a steady RANS. The standard k-ε turbulence model was used with a wall function model to reduce the mesh size. The discretization scheme was a spatially 2nd-order MARS scheme, and a SIMPLE algorithm solved the system of non-linear equations.

The fan efficiency is defined at the design point (flow rate: 1.5 m^3/min, number of revolutions: 19000 min^{-1}) as:

$$\eta_s = \frac{Q \cdot \Delta p}{W_{ax}}, \tag{4-14}$$

where Q, Δp, and W_{ax} correspond to the flow rate, static pressure rise at the fan part, and the shaft power.

The turbulent noise level is evaluated by the theoretical prediction model [23], which relates the noise level to the magnitudes of relative velocities in the fan:

$$L_{tb} = 10 \log_{10} \left\{ \left(W_1^6 + W_2^6 \right) \cdot D_2^2 \cdot Z \right\}, \tag{4-15}$$

where W_1, W_2, D_2, and Z correspond to the average relative velocity at the impeller inlet, the average relative velocity at the impeller outlet, the outlet diameter of the fan, and the number of blades. D_2 and Z are constant in this study.

It was attempted to evaluate the effect of the dimensional uncertainty of the fan on the aerodynamics. Therefore, the means, μ, and standard deviations, σ, of the distributions of the aerodynamics are assigned to objective functions: $-\mu(\eta_s)$, $\sigma(\eta_s)$, $\mu(L_{tb})$ and $\sigma(L_{tb})$. Note that these four objective functions are defined as a minimization problem. The μ and σ of the shaft power are also added as constraints.

Table 4-3 List of design parameters

Type	Name	Min.	Max.	Tolerance
Design variable	b_2 [mm]	6	8	0.1
	b_0/b_2	1.7	2.3	0.00719
	D_{0s}/D_2	0.33	0.36	0.000718
	r_R_1	0.001	0.08	0.00665
	r_R_{Beta}	0.05	0.95	0.0066
	Beta1 [deg.]	20	35	5
	Beta2 [deg.]	20	50	5
	Beta3 [deg.]	25	50	5
Objective function	$-\mu(\eta_s)$	Minimization		
	$\sigma(\eta_s)$	Minimization		
	$\mu(L_{tb})$ [dB]	Minimization		
	$\sigma(L_{tb})$ [dB]	Minimization		
Constraint	$\mu(W_{ax})$ [W]	517	557	-
	$\sigma(W_{ax})$ [W]	0	20	-

As dimensional uncertainty could not be measured on actual production lines, the rectangular profile in Table 1 was assumed. The width of the rectangular profile was empirically set to equal the tolerance. All the design parameters are summarized in Table 4-3 with their definition ranges.

4.4 Results and Discussion

4.4.1 Visualization of Trade-off Patterns

Using LHS, 79 valid samples were obtained by flow simulations. Three Kriging models were constructed to predict the fan efficiency, turbulent noise level, and shaft power. Cross validations of these Kriging models were conducted and the means and standard deviations of prediction errors for fan efficiency, turbulent noise level, and shaft power resulted in (0.022%, 0.44%), (0.006%, 0.30%), and (0.022%, 0.69%), respectively. Based on these results, the author considered the models were sufficiently accurate.

The optimization problem was then solved by using MOGA. The population was set to 100, and 162 generations were altered until convergence was obtained with a convergence criterion of 0.001%. The statistics of responses to uncertainty were calculated with 1000 samples of descriptive LHS, after confirming that almost the same results had been obtained as when using 2000.

1268 feasible non-dominated solutions were obtained. It took a week to sample the simulation data on a single-node dual core AMD Opteron^{TM} 2.2 GHz computer and another week to build the models, and carry out optimization and data mining. Two weeks is considered to be within a practical design lead-time.

Figure 4-6 visualizes the obtained non-dominated solutions as small black dots in scatter plots. The four-dimensional solution space is projected onto the two-dimensional plane, which has axes of mean performance.

To investigate the trade-offs, the following four representative preferences were defined as test cases:

$$\text{Solution A (weighting } \mu(\eta_s)) \qquad w_1 : w_2 : w_3 : w_4 = 1 : 0 : 0 : 0, \qquad (4\text{-}16)$$

$$\text{Solution B (weighting } \mu(\cdot)) \qquad w_1 : w_2 : w_3 : w_4 = 1 : 0 : 1 : 0, \qquad (4\text{-}17)$$

$$\text{Solution C (weighting } \sigma(\cdot)) \qquad w_1 : w_2 : w_3 : w_4 = 0 : 1 : 0 : 1, \text{ and} \qquad (4\text{-}18)$$

$$\text{Solution D (weighting equally)} \quad w_1 : w_2 : w_3 : w_4 = 1 : 1 : 1 : 1, \qquad (4\text{-}19)$$

where w_1, w_2, w_3, and w_4 correspond to weights for $\mu(\eta_s)$, $\sigma(\eta_s)$, $\mu(L_{tb})$, and $\sigma(L_{tb})$.

Solution A is an extreme design in terms of $\mu(\eta_s)$. Solution B aims to simultaneously improve mean performance $\mu(\eta_s)$ and $\mu(L_{tb})$, similar to the traditional approach in multi-objective non-robust optimization. In contrast, Solution C intends to improve standard

deviations $\sigma(\eta_s)$ and $\sigma(L_{tb})$, as a quality engineering approach like the Taguchi method does. Solution D is an equally compromised solution in terms of all the objective functions.

Solutions A, B, C, and D were first selected as ones that had the smallest θ with the aspiration vectors of Eqs. (4-16), (4-17), (4-18), and (4-19), respectively. They are indicated by the large colored circles in Fig. 4-6. In the figures, variations in these solutions due to the dimensional uncertainty are also shown as collections of small colored circles being the 1000 samples of descriptive LHS. Note that the large colored circles are mean values while the small colored circles are exact values.

It is confirmed that Solutions A, B and D are in the right balanced positions specified by the weights of mean properties w_1 and w_3 (eq. (4-16), (4-17), and (4-19)). Namely, Solution A is located in the left-end area, and Solution B and D are in the middle area in terms of the two mean properties.

It is also confirmed that the uncertainty variations of Solution C and D are smaller than those of Solution D and B, respectively (eq. (4-18) vs. (4-19) and eq. (4-19) vs. (4-17)). These are comparisons of different weights on standard deviations in the total balances. Consequently, standard deviations of Solution C, D and B increase in this order.

From these observations, it is concluded that the aspiration vector can accurately specify a trade-off balance.

The author then used SOMs to find trade-off patterns. Figure 4-7 shows SOMs created based on the similarity of the four objective functions. The locations of Solutions A, B, C, and D are indicated on the maps and the corresponding clusters are numbered from 1 to 4 in the same order.

In terms of $\mu(\eta_s)$, solutions in the bottom-right corner of the SOM are better than others (Fig. 4-7 (a)). Similarly, solutions at the top, left, and middle areas are better for $\sigma(\eta_s)$, $\mu(L_{tb})$, and $\sigma(L_{tb})$, respectively. Although there are areas where two objective functions can be improved simultaneously as in cluster 3, there are no areas that can improve all the objective functions at the same time. Therefore, the author determined that these objective functions have trade-off relations.

(a) Solution A

(b) Solution B

(c) Solution C
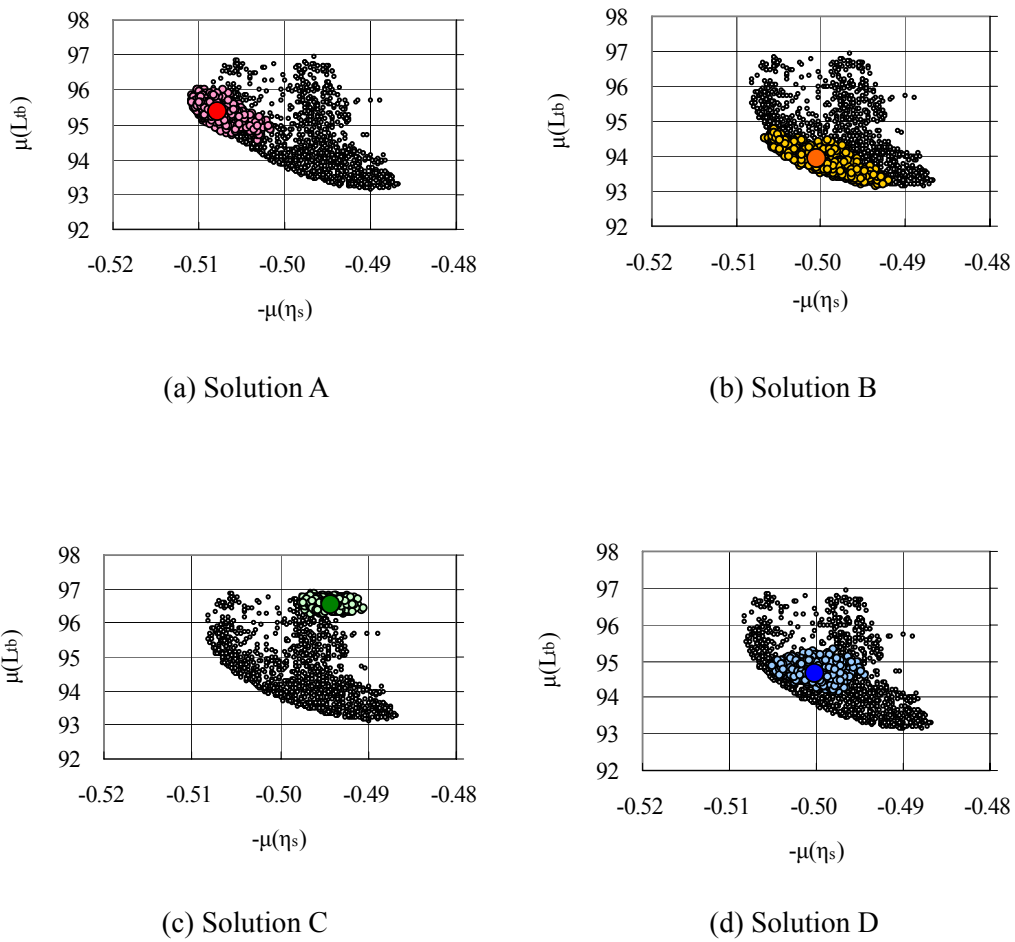
(d) Solution D

Figure 4-6 Trade-offs in non-dominated solutions

From an engineering point of view, it is beneficial to have various design candidates as obtained in these results, because we can adapt a design solution to a given design requirement afterward. For example, Solution A in cluster 1 is expected to have the best yield rate for high-efficiency fans from the four Solutions. Solution B in cluster 2 is superior in mean performance so that it is a good compromise between fan efficiency and noise level if we can restrain dimensional uncertainty as minimally as possible. In contrast, the quality of Solution C in cluster 3 is the most stable so that this is suitable for mass-produced products.

As explained above, MORDE is characterized in its diversity of solutions, which are concerned not only the mean performance but also the robustness of performance. These

different types of solutions have not been able to be obtained by using a single method of design in traditional approaches.

Figure 4-8 shows the same SOMs colored according to the values of design variables. By comparing Figs. 4-7 and 4-8, correlations patterns between objective functions and design variables can be investigated. For instance, as Fig. 4-8 (h) has a similar pattern to Fig. 4-7 (a), we can see that Beta3 plays an important role in controlling $\mu(\eta_s)$. Another resemblance in patterns is seen in Figs. 4-7 (c) and 4-8 (b).

However, this graphical approach is not always good at finding correlation patterns in analyzing trade-offs. First, recognition of the patterns may depend on a designer's subject. For example, some designers can see that Fig. 4-8 (f) has a more similar pattern to Fig. 4-7 (a) than Fig. 4-8 (h). Moreover, it is difficult to find dominant design variables for $\sigma(L_{tb})$ (Fig.4-7 (d)), because the gradation pattern is more complicated due to the effects of multiple design variables. This is generally true when we aim to find correlation patterns, where more than three parameters are concerned. Because the graphical approach is based on pattern recognition in low-order correlations, it is difficult to use the same approach in higher-order correlations. In addition, quantitative relations are difficult to examine.

It is summarized here that low-dimensional trade-off patterns can be obtained by graphical methods like SOM, but we need a method of extracting design rules that can handle high-dimensional data quantitatively, which is often obtained through multi-objective robust optimization.

4.4.2 Derivation of Quantitative Trade-off Control Rules

Quantitative design rules for controlling trade-off balance are then extracted using the multivariate data of non-dominated solutions. To apply the association rule, all the design variables are first discretized into five levels with equal intervals to obtain the categorized dataset. The θ in Eq. (4-13) was chosen as the decision attribute, and discretized into 7, 4, 5, and 4 levels for solutions corresponding to A, B, C, and D, in a way that the minimum (optimum) levels contain a sufficient amount of data.

The rule length must be given for the association rule in advance. As found in the previous chapter, another method of extracting the design rule, rough set theory, can rationally minimize the necessary number of condition attributes based on logical set operations. Thus, rough set theory was first applied to the same dataset and found that the rule length should be set to four.

(a) - $\mu(\eta_s)$ (b) $\sigma(\eta_s)$ (c) $\mu(L_{tb})$ (d) $\sigma(L_{tb})$
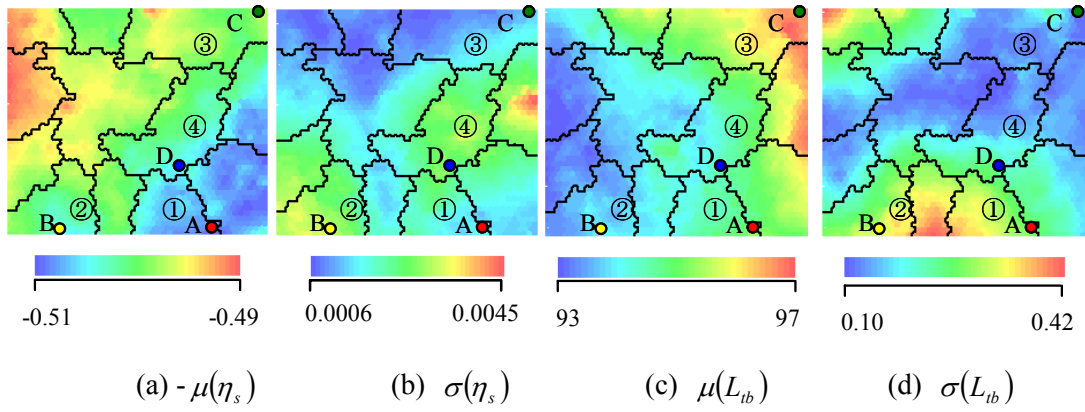
Figure 4-7 SOMs colored according to objective functions

(a) b_2 (b) b_0/b_2 (c) D_{0s}/D_2 (d) r_R_1

(e) r_R_{Beta} (f) Beta1 (g) Beta2 (h) Beta3
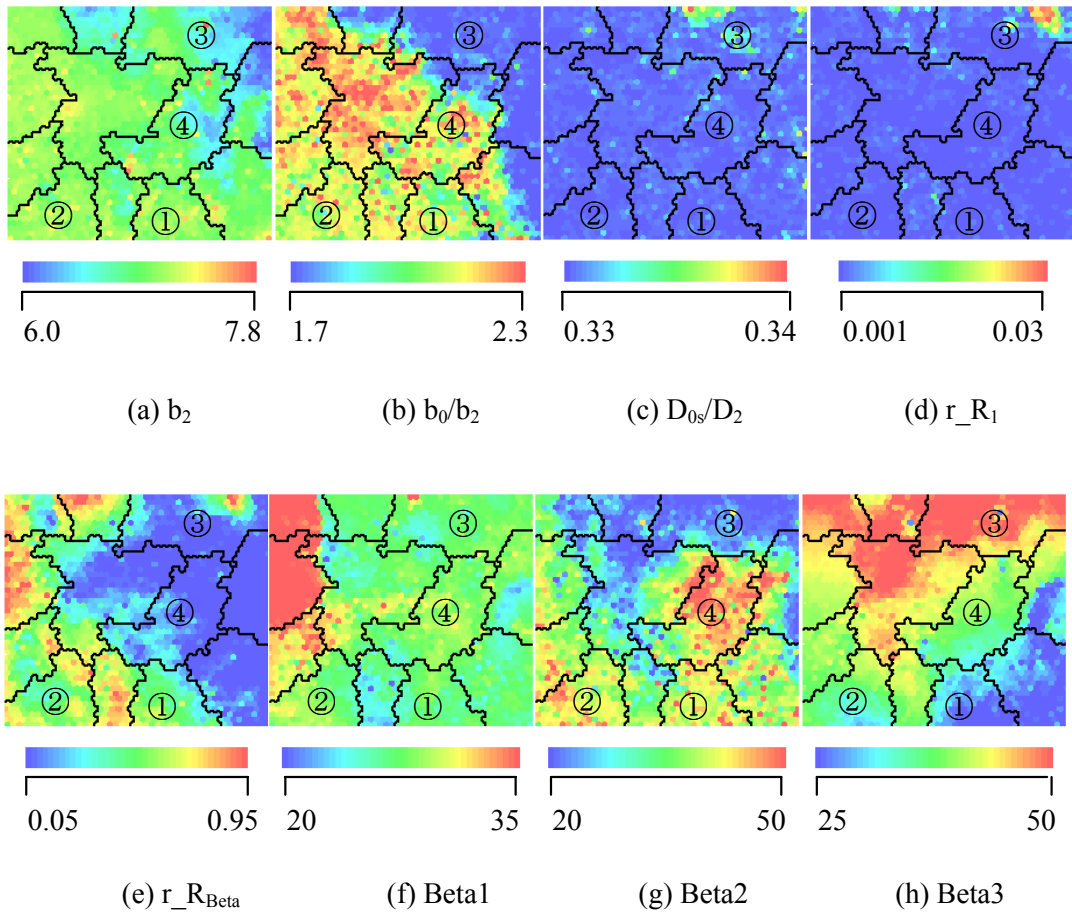
Figure 4-8 SOMs colored according to design variables

Tables 4 (a), (b), (c), and (d) respectively list extracted rules that minimize the levels of θ for Solution A, B, C, and D. Because the author intended to extracted accurate rules for sufficient conditions, rules with a confidence of one were chosen and then sorted by their values of support.

For instance, Table 4-4 (a) lists up the rules that correspond sufficient conditions to make θ for $-\mu(\eta_s)$ retain in the level 1. Thus, the rule No.1 in Table 4-4 (a) means:

if (b_2 is level 2), (b_0/b_2 is level 1), and (Beta3 is level 1),
then (θ for $-\mu(\eta_s)$ is level 1). (4-20)

As seen in Table 4-4, the association rule can extract multiple design rules to achieve prescribed trade-off balances. Another advantage of the association rule is that discrete but quantitative rules are now available. The "counts" at the right of the table are the total number of decision attributes extracted in the rule set. The counts are used to approximately determine the importance of design variables and those with larger counts are called "cores". The individual setup to achieve the trade-off balance is presented as each rule, but the average setup that all the rule sets imply is also available by examining the condition attributes of the cores.

From Table 4-4 (a), the blade angles, Beta3 and Beta1, are the main cores for $\mu(\eta_s)$. The rule sets tell us that Beta 3 should be in level 1 (0-20%) or 2 (20-40%), while Beta1 should be in levels 2 or 4, on average. From Figs. 4-7 (a) and 4-8, cluster 1 that includes Solution A certainly has smaller values for Beta3 and middle values for Beta1, so the author considered that reasonable rules had been obtained by the association rule. Small Beta3 results in a large relative velocity at the fan outlet and increases the rise in static pressure in the fan part, because the peripheral velocity is constant in this design problem. Therefore, the rules suggest that the reaction factor of the fan should be reinforced to improve $\mu(\eta_s)$.

From Table 4-4 (b), blade angle Beta3 and r_R$_{Beta}$ are determined as cores. As Solution B equally takes care of $\mu(\eta_s)$ and $\mu(L_{tb})$, Beta3 is adjusted slightly larger than that in Table 4-4 (a) as a compromise. The blade load balance, which these cores are related to, is found to be the key to improving the mean performance. If we look at cluster 2 with Solution B in Figs. 4-8 (e) and (h), we can see that it is difficult to specify quantitative conditions for these core-design variables only from SOMs.

From Table 4-4 (c), we found that b_2, D_{0s}/D_2, r_R$_{Beta}$ and Beta3 are the keys to robust designs (Solution C). The smallest level of b_2 and the largest level of Beta3 mean that the

velocity triangle at the fan outlet has a better aspect ratio and then velocity variations against dimensional uncertainty become smaller. In other words, robust solutions do not prefer skewed velocity triangles.

From Table 4-4 (d), "counts" become similar and the dominant cores are not as clear as those in Tables 4-4 (a), (b), and (c). The design variables also seem to acquire various levels. This implies that there are multiple possibilities to achieve the same trade-off balance as in Solution D. This diversity of rules is certainly confirmed as randomness of colors in SOMs (cluster 4 in Fig. 4-8).

It is interesting to see that the value of D_{0s}/D_2 remains almost at the same level in Fig. 4-8 (c) and that of r_R_1 also remains almost at the same level in Fig. 4-8 (d). This means that these design variables are only dominant for Pareto-optimality so that their values are constant in non-dominated solutions. That is, small values of D_{0s}/D_2 and r_R_1 are necessary conditions to become non-dominated solutions. Here, why do these conditions not appear as rules in Table 4-4 in a more dominant way?

The author considered that the association rule had not been able to extract rules with these design variables because only sufficient conditions were chosen in Table 4-4. To confirm this hypothesis, the same rule sets were sorted by values of support, regardless of the confidence values.

One example is presented in Table 4-5, which should be compared with Table 4-4 (a). Unlike Table 4-4 (a), the decision attributes for D_{0s}/D_2 and r_R_1 now appear frequently. The values of supports for these rules become much larger while confidence values become much smaller, suggesting these rules are necessary conditions. The lift values became smaller so that the rules are considered trivial and these conditions are very natural in non-dominated solutions.

From these investigations with the association rule above, the author concluded that the association rule can derive multiple-design rules in quantitative expressions, where even more than three parameters are related. This feature of handling high-dimensional data supports designers more in understanding the trade-offs, reinforcing graphical methods such as SOMs. Moreover, the association rule can extract both sufficient condition rules and necessary condition rules by changing levels of support and confidence criteria. This is an advantage of the association rule compared with other methods of extracting rules such as decision tree analysis and rough set theory.

Table 4-4 Rules to achieve prescribed trade-off balances

(a) Rules for Solution A

No.	Variable	1	2	3	4	5	6	7	8	9	10	11	12	13	14	15	16	17	Count
1	b_2	2		2		1		3				2	2		1		2	2	9
2	b_0/b_2	1	1		2		1					4	2						6
3	D_{0s}/D_2									1									1
4	r_R_1								1										1
5	r_R_{Beta}		2		3														2
6	Beta1					2	2	4	4	4	4				2	2	2	2	10
7	Beta2		3	4									1		1	1		3	6
8	Beta3	1		1	1	2	2	1	1	1	1	1	1	1		2	1	1	15
	Conf.	1.0	1.0	1.0	1.0	1.0	1.0	1.0	1.0	1.0	1.0	1.0	1.0	1.0	1.0	1.0	1.0	1.0	
	Supp.(%)	0.8	0.5	0.5	0.4	0.4	0.4	0.4	0.4	0.4	0.4	0.4	0.4	0.3	0.3	0.3	0.3	0.3	
	Lift	9.2	9.2	9.2	9.2	9.2	9.2	9.2	9.2	9.2	9.2	9.2	9.2	9.2	9.2	9.2	9.2	9.2	

(b) Rules for Solution B

No.	variable	1	2	3	4	5	6	7	8	9	10	11	12	13	14	15	16	17	18	19	20	21	22	Count
1	b_2			3	3								4							4		4		5
2	b_0/b_2					4						4		3					5	4			3	6
3	D_{0s}/D_2		1																					1
4	r_R_1	1																						1
5	r_R_{Beta}	3	3	3	3	4	3	3	3	3	3	4	3	3	4	3	3	3	3		4		4	20
6	Beta1							3		4					3	2		3			4	4		7
7	Beta2								4		5						3							3
8	Beta3	2	2	2	2	2	2	2	2	2	2	2	2	2	2	2	2	2	2	2	2	2	2	22
	Conf.	1.0	1.0	1.0	1.0	1.0	1.0	1.0	1.0	1.0	1.0	1.0	1.0	1.0	1.0	1.0	1.0	1.0	1.0	1.0	1.0	1.0	1.0	
	Supp.(%)	2.7	2.7	2.7	1.9	1.4	1.1	1.1	1	0.9	0.9	0.9	0.8	0.8	0.8	0.7	0.6	0.6	0.6	0.5	0.5	0.4	0.4	
	Lift	11	11	11	11	11	11	11	11	11	11	11	11	11	11	11	11	11	11	11	11	11	11	

(c) Rules for Solution C

No.	Variable	1	2	3	4	5	6	7	8	9	10	11	12	13	14	15	16	17	18	19	20	21	22	23	24	Count
1	b_2								1	1	1	1	1	1	1	1	1		1	1	1	1	1	1	1	16
2	b_0/b_2	1					1				1				1		1			1						6
3	D_{0s}/D_2		2	2	2	2	2	2						1				2	2	2	2	2	2	2		14
4	r_R_1				1													1						1		3
5	r_R_{Beta}	2		1				2	2	2	2	2	2	3	3				1					2		12
6	Beta1								3			3				4		3								4
7	Beta2	1	1					1														1				4
8	Beta3			5	5	5	5	5	5		5					5	5					5				10
	Conf.	1.0	1.0	1.0	1.0	1.0	1.0	1.0	1.0	1.0	1.0	1.0	1.0	1.0	1.0	1.0	1.0	1.0	1.0	1.0	1.0	1.0	1.0	1.0	1.0	
	Supp.(%)	1.5	0.8	0.8	0.8	0.8	0.7	0.7	0.6	0.6	0.6	0.6	0.6	0.6	0.5	0.5	0.5	0.4	0.4	0.4	0.4	0.4	0.4	0.4	0.4	
	Lift	9.9	9.9	9.9	9.9	9.9	9.9	9.9	9.9	9.9	9.9	9.9	9.9	9.9	9.9	9.9	9.9	9.9	9.9	9.9	9.9	9.9	9.9	9.9	9.9	

(d) Rules for Solution D

No.	Variable	1	2	3	4	5	6	7	8	9	10	11	12	13	14	15	16	17	18	19	20	21	Count
1	b_2	4	4	5	5	5		5								4	2			2			9
2	b_0/b_2	3	5				5		3	3	3	3	3	2	2								10
3	D_{0s}/D_2				1								1										2
4	r_R_1			1	1	1		1			1												5
5	r_R_{Beta}	1						1						2		1		2		2	2	3	8
6	Beta1								1	1	1	1	1						4				6
7	Beta2		5				2			5					4		2	2	2		3	1	9
8	Beta3			1			2			1				2	2	2	2	3	3	3	3	3	12
	Conf.	1.0	1.0	1.0	1.0	1.0	1.0	1.0	1.0	1.0	1.0	1.0	1.0	1.0	1.0	1.0	1.0	1.0	1.0	1.0	1.0	1.0	
	Supp.(%)	0.7	0.4	0.3	0.3	0.3	0.3	0.2	0.2	0.2	0.2	0.2	0.2	0.2	0.2	0.2	0.2	0.2	0.2	0.2	0.2	0.2	
	Lift	9.4	9.4	9.4	9.4	9.4	9.4	9.4	9.4	9.4	9.4	9.4	9.4	9.4	9.4	9.4	9.4	9.4	9.4	9.4	9.4	9.4	

Table 4-5 Rules for Solution A (sorted by support level)

No.	Variable	Rule no.																			Count
		1	2	3	4	5	6	7	8	9	10	11	12	13	14	15	16	17	18		
1	b_2												3	3	3	3	3	3	3		7
2	b_0/b_2																				0
3	D_{0s}/D_2		1	1			1	1			1	1	1			1	1				9
4	r_R_1	1	1		1		1		1		1			1			1	1			9
5	r_R_{Beta}																				0
6	Beta1								3	3	3	3									4
7	Beta2																				0
8	Beta3				1	1	1	1					1	1	1						7
	Conf.	0.1	0.1	0.1	0.4	0.4	0.4	0.4	0.1	0.1	0.1	0.1	0.5	0.5	0.5	0.1	0.1	0.1	0.1		
	Supp.(%)	11	11	11	8.6	8.6	8.5	8.5	7.3	7.3	7.2	7.2	7.1	7.1	7.1	7.1	7.1	7.1	7.1		
	Lift	1.0	1.0	1.0	4.0	4.0	4.1	4.0	1.3	1.3	1.4	1.3	4.4	4.3	4.3	1.0	1.0	1.0	1.0		

4.5 Conclusion

A new design paradigm called MORDE was proposed, which combines a method of multi-objective robust optimization and data mining methods.

The author first developed a generalized framework for multi-objective robust optimization. By incorporating probabilistic representation of design parameters, which is compatible with the parameterization in the Taguchi method, multi-objective robust design optimization based on Kriging models becomes feasible within a practical design lead-time.

The author then proposed a method of controlling trade-off balance using an aspiration vector, which measures the proximity to a designated preference for a trade-off balance. Using this method, the design rules to achieve the preference were extracted by applying the newly adopted association rule to a dataset of non-dominated solutions.

MORDE was applied to an industrial-design problem with a washer-dryer's centrifugal fan. This design was aimed at statistically improving both the efficiency of the fan and reducing its turbulence noise level when there was dimensional uncertainty due to mass production. It was demonstrated that it is possible to flexibly choose a design candidate and find quantitative rules to accomplish the required trade-off balance. It was also demonstrated that traditional non-robust optimal design as well as quality-weighted design like the Taguchi method could be simultaneously accomplished with MORDE approach.

The association rule can reveal multiple and quantitative design rules to achieve trade-off balances even from a high-dimensional dataset, while it is difficult for SOMs to do the same

analysis. It was also clarified that, as a method of extracting design rules, the association rule has advantage in finding both necessary and sufficient conditions.

As the author is interested in analyzing the design space to clearly understand the design problem, several data mining techniques have been incorporated into engineering design thus far. In the next step of this research, it is attempted to clarify the strengths and weakness of these techniques and develop a method that enables effective collaboration.

References

[1] Obayashi, S., Tsukahara, T., and Nakamura, T., Multiobjective Genetic Algorithm Applied to Aerodynamic Design of Cascade Airfoils, IEEE Transactions of Industrial Electronics, Vol. 47, pp.211-216, 2000.

[2] Oyama, A. and Liou, M. S., Multiobjective Optimization of Rocket Engine Pumps Using Evolutionary Algorithm, Journal of Propulsion and Power, Vol.18, pp.528-535, 2002.

[3] Pierret, S., Multi-objective Optimization of Three dimensional Turbomachinery Blades, Proceedings of International Conference on Computational Methods for Coupled Problems in Science and Engineering, 2005.

[4] Huppertz, A., Flassig, P., Flassig, R., and Swoboda, M., Knowledge-Based 2D Blade Design Using Multi-Objective Aerodynamic Optimization And A Neural Network, ASME Paper No. GT2007-28204, 2007.

[5] Egorov, I. N., Optimization of a Multistage Axial Compressor Stochastic Approach, ASME Paper No. 92-GT-163, 1992.

[6] Lee, K. H., Park, G. J., Robust Optimization Considering Tolerances of Design Variables, Computers and Structures, Vol. 79, pp.77-86, 2001.

[7] Padmanabhan, D., Batill, S. M., An Iterative Concurrent Subspace Robust Design Framework, AIAA 2000-4841, 2000.

[8] Koch, P. N., Wujek, B., Golovidov, O., Facilitating Probabilistic Multidisciplinary Design Optimization Using Kriging Approximation Models, AIAA 2002-5415, 2002.

[9] Huyse, L., Padula, S. L., Lewis, R. M., Li, W., Probabilistic Approach to Free-Form Airfoil Shape Optimization Under Uncertainty, AIAA Journal, Vol. 40, No. 9, pp.1764-1772, 2002.

[10] Lyu, N., Shimura, A., Saitou, K., Optimal Tolerance Allocation of Automotive Pneumatic Control Valves Based on Product and Process Simulations, ASME Paper DETC2006-99592, 2006.

[11] Lee, J., AHN, B., DOE Based Robust Optimization Considering Tolerance Bands of Design Parameters, JSME International Journal, Series C, Vol. 49, No. 4, pp.1223-1231, 2006.

[12] Kumar, A., Keane, A., Nair, P., and Shahpar, S., Robust Design of Compressor Blades Against Manufacturing Variations, ASME Paper No. DETC2006-99304, 2006.

[13] Shimoyama, K., Robust Aerodynamic Design of Mars Exploratory Airplane Wing with a New Optimization Method, Ph.D thesis, University of Tokyo, Japan, 2006.

[14] Shimoyama, K., Oyama, A., Fujii, K., Multi-Objective Six Sigma Approach Applied to Robust Airfoil Design for Marts Airplane, AIAA 2007-1966, 2007.

[15] Taguchi, G., Chowdhury, S., Wu, Y., Taguchi, S., and Yano, H., Taguchi's Quality Engineering Handbook, John Wiley & Sons, Inc., Hoboken, New Jersey, 2004.

[16] Obayashi, S., Jeong, S., Chiba, K., and Morino, H., Multi-Objective Design Exploration and its Application to Regional-Jet Wing Design, Transaction of the Japan Society for Aeronautical and Space Science, Vol. 50, No.167, pp.1-8, 2007.

[17] Sacks, J., Welch, W., Mitchell, T., and Wynn, H., Design and Analysis of Computer Experiments, Statistical Science, Vol. 4, pp. 409-s435, 1989.

[18] Simpson, T. W., Mauery, T. M., Korte, J. J., Mistree, F., Kriging Models for Global Approximation in Simulation-Based Multidisciplinary Design Optimization, AIAA Journal, Vol. 39, No. 12, pp. 2233-2241, 2001.

[19] Jones, D. R., Schonlau, M., Welch, W. J., Efficient Global Optimization of Expensive Black-Box Functions, Journal of Global Optimization, Vol. 13, pp. 455-492, 1998.

[20] Jeong, S., Murayama, M., and Yamamoto, K., Efficient Optimization Design Method Using Kriging Model, Journal of Aircraft, Vol. 42, pp.413-420, 2005.

[21] Kohonen, T., Self-Organizing Maps, Springer, Berlin, Heidelberg, 1995.

[22] Witten, I. H. and Frank, E., Data Mining, Morgan Kaufmann, San Francisco, CA, 2005.

[23] Watanabe, M., Takada, and Y., Satou, R., Prediction Model for Aeroacoustic Noise from Low-Speed Fans, AIAA-99-1983, 1999.

[24] Nakayama, H., and Sawaragi, Y., Satisfying Trade-off Method for Interactive Multiobjective Programming Methods, Proceeding of an International Workshop on Interactive Decision Analysis and Interpretative Computer Intelligence, Springer, pp. 113-122, 1984.

[25] Obayashi, S., Sasaki, D., and Oyama, A., Finding Tradeoffs by Using Multiobjective Optimization Algorithms, Transactions of the Japan Society for Aeronautical and Space Sciences, Vol. 47, No. 155, pp.51-58, 2004.

[26] Viscovery SOMine, Mindware Inc., http://www.mindware-jp.com/somine/.

[27] Visual Mining Studio, Mathematical Systems Inc., http://www.msi.co.jp/english/.

Chapter 5

A New Design Method based on

Cooperative Data Mining

from Multi-objective Design Space

5.1 Introduction

Up to the previous chapter, a computationally inexpensive design optimization method, which can handle the both uncertainties in design-decisions and design-conditions, has been developed. Besides, quantitative design rules have been extracted not only for achieving extreme design regarding each objective function, but also for controlling trade-off between multiple objective functions. Based on these developments, the design optimization becomes practical.

Several data mining methods have been introduced in this study so far. These methods have been used for analyzing multi-objective design space and yielding design knowledge, which is oriented to knowledge-based design. The author considers that knowledge-based design is an alternative of practical design method because the essential idea in these design knowledge can be applied to other design problems without any additional expensive computations. Therefore, in this chapter, the author attempts to develop a new multi-objective parameter design method that uses data mining method in cooperative way.

It has become common to design products using parameter surveys and optimizations that use simulations and experiments. The resultant data obtained with a large amount of trial and error can be captured as a design database. Designers are likely interested only in the final solution but the author believes that it is important to analyze such databases to deepen understanding of design problems. Namely, we should decide on a final design solution after reviewing the sum of the design knowledge obtained from the design database. Therefore, it is believed that a parameter design method that is used to practice this idea should be developed.

A parameter design method is used to decide how to provide design variables to achieve the desired product performance. In one parameter design method, the Taguchi method [1], the best setup of design variable levels that should be set is determined by evaluating

sensitivities and signal-noise ratios (SNRs) of the design variables to a single objective function. Since the Taguchi method aims at doing robust designs, the level combination of design variables in which the SNR is at the maximum is first chosen, and the level combination of other design variables with relatively larger sensitivities is then adjusted for obtaining the preferred level of the objective function. Although the Taguchi method is a systematic and reasonable method for robust designs, it cannot be used to optimize multiple objective functions.

In contrast, numerical optimization methods [2][3][4] that are used to evaluate trade-offs between multiple objective functions, including performance robustness, determine the optimum level combinations of design variables for achieving any prescribed balances of multiple objective functions. In these methods, both the designs that value robustness and limit performance regardless of robustness are possible, depending on the aims of the designs. This flexibility is an advantage over the Taguchi method. However, these numerical optimization methods yield many optimum solutions, i.e. a database that corresponds to different balances of objective functions. Because a database cannot be easily analyzed due to its high-dimensionality, data mining techniques are necessary.

Various data mining techniques have been applied to multi-objective optimization databases to clarify the relationship of design variables with multiple objective functions. For example, Jeong et al. [5] applied functional analysis of variance (ANOVA) to analyze different types of design variable effects on objective functions and their contribution ratios. Obayashi et al. [6] applied Self-organizing map (SOM) to visualize high-dimensional data on two-dimensional maps for finding correlation patterns between design variables and objective functions. Lim et al. [7] and Sugimura et al. [4][8] applied design rule extraction methods, decision tree analysis, rough set theory, and association rule, to the design database for determining the quantitative relationships of design variables and objective functions. The features of the individual data mining technique have become clear based on these previous works. However, there are strong and weak points in each individual technique; thus, it is beneficial to develop a method combining these techniques based on comparative studies.

The author proposes "a multi-objective parameter design method" consisting of these data mining techniques in a collaborative manner. This method is used for first analyzing the design database by using a series of data mining techniques, and then using design rules obtained as a result of data mining for determining the optimum level combination of design variables to achieve a desired balance between multiple objective functions. This method is different from the Taguchi method in that it uses both main and interaction effects of design variables and can handle multiple objective functions.

In the followings, the proposed method is first explained. After that, it is demonstrated with an application to a multi-objective robust design optimization problem of an industrial fan, for demonstrating its capability and discussing how the collaboration of data mining techniques

5.2 Multi-Objective Parameter Design Method

5.2.1 Parameter Design Using Both Main and Interaction Effects

The purpose of multi-objective parameter design is to obtain combinations of design variable levels that simultaneously optimize multiple objective functions as much as possible.

$$\text{minimize} \quad y_1 = f_1(x_1, x_2, \cdots, x_n),$$

$$\text{minimize} \quad y_2 = f_2(x_1, x_2, \cdots, x_n),$$

$$\cdots$$

$$\text{minimize} \quad y_m = f_m(x_1, x_2, \cdots, x_n), \tag{5-1}$$

where n and m are the numbers of design variable and objective function, respectively.

There are two types of design variable effects of on an objective function, main and interaction effects. The main effect is an independent contribution of a single design variable to an objective function. The interaction effect is a synergistic contribution of more than two design variables, which is obtained after subtracting the main effects from the total effect. Any high-order interaction effect can be defined, but only the interaction effects of two design variables are considered in this study.

Figure 5-1 describes the relationship between the design variables, x_1 and x_2, and the objective function y_1, (a) without and (b) with the interaction effect between x_1 and x_2. The optimum level of x_1 that minimizes y_1 is maintained regardless of levels of x_2 with no interaction effect, as shown in Fig. 5-1 (a). In contrast, the optimum levels of x_1 changes depending on the combined levels of x_2 with interaction effect, as shown in Fig. 5-1 (b).

(a) Without interaction effect   (b) With interaction effect
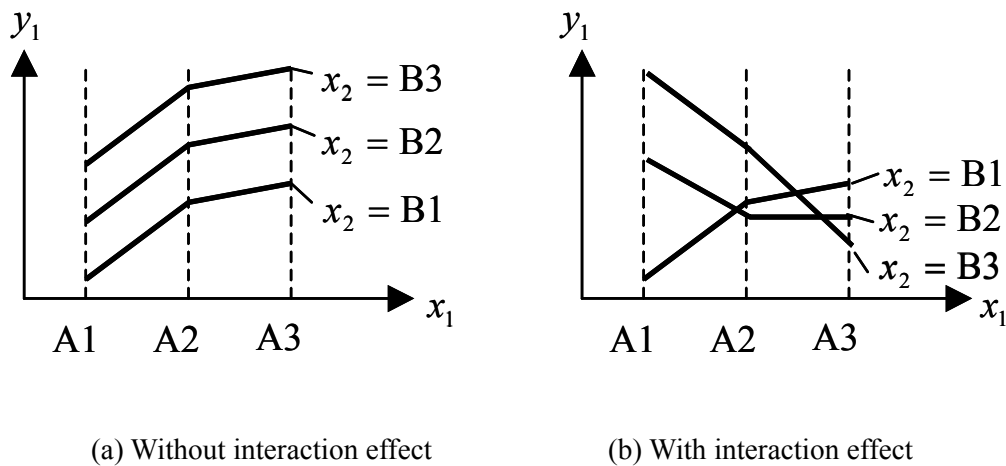
Figure 5-1 Responses with and without interaction effect

Since interaction effects make design problems difficult to understand, they have been avoided in traditional parameter design methods such as the Taguchi method. However, interaction effects can be keys to solving conflict in multi-objective designs. For instance, if x_1 has predominant main effects for two objective functions y_1 and y_2, with opposite signs of responses, y_1 and y_2 cannot be improved at the same time. However, if there was also a predominant interaction effect between x_1 and x_2 for y_2, it then became possible to improve y_1 by adjusting x_1, and improve y_2 by adjusting x_2, using the same x_1 as with y_1. In this way, the possibility of design extends if interaction effects can be determined and applied.

Based on the above, a multi-objective parameter design method should use both main and interaction effects to effectively achieve a prescribed balance in multiple objective functions. In this context, the final goal of data mining is to obtain various quantitative design rules that represent level combinations of design variables to be set for achieving a design preference.

5.2.2 Data Mining Process for Finding Design Rules

Figure 5-2 shows the proposed flowchart of data mining for obtaining design rules and determining an optimum design candidate. First, a design database is prepared in the multivariate data format. The database can be acquired using parameter surveys. Although the

original database usually consists of continuous parameters, discretization of the database is necessary for processes of the rough set theory and the association rule.

The design space is then investigated macroscopically. ANOVA reveals different types of design variable effects and their contribution ratios to each objective function. The results from ANOVA are used for interpreting results of the following data mining processes. SOM or alternative visualization methods are used for visualizing the relationship between design parameters, particularly trade-off patterns between multiple objective functions.
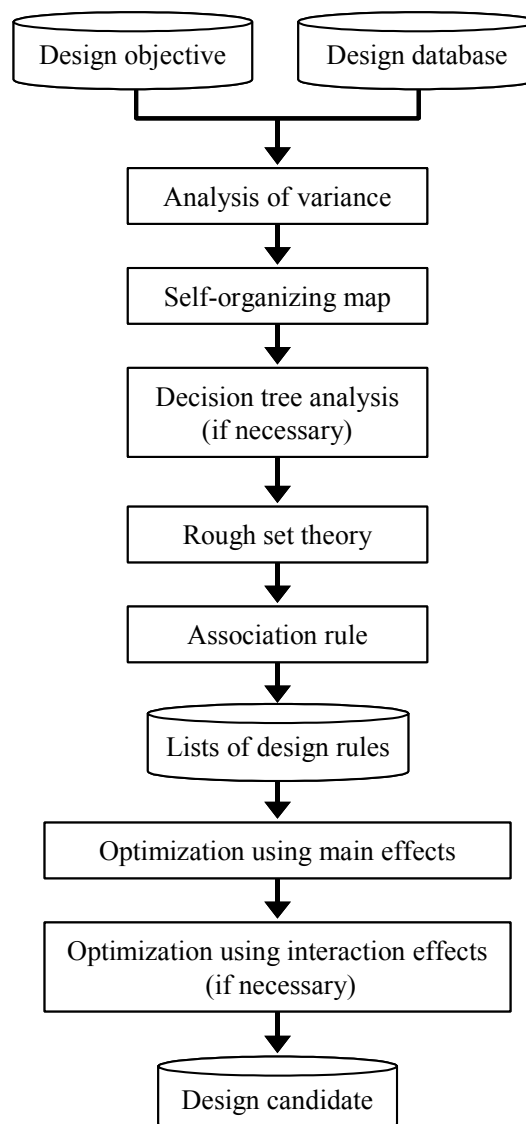
Figure 5-2 Flowchart of data mining

Table 5-1 Summary of data mining techniques

Data mining method	Capability	Feature of design rules
ANOVA	● type of effect ● contribution ratio	
SOM	● clustering ● visualization of correlation pattern	● qualitative rules (pattern recognition)
Decision tree analysis	● single probabilistic rule ● localized rule	● quantitative rules ● necessary condition
Rough set theory	● multiple deterministic rules ● reduction (simplification)	● quantitative rules ● sufficient condition
Association rule	● multiple rules ● support and confidence	● quantitative rules ● necessary ～ sufficient condition (controllable)

After that, the design space is investigated microscopically. Quantitative design rules that optimize each objective function are extracted using three different design rule extraction methods, decision tree analysis, rough set theory, and association rule. Methods are chosen according to the number and features of design rules to be extracted. For example, decision tree analysis yields a single rule of necessary condition. The rough set theory is used to extract many rules of sufficient condition, while the association rule is used to extract many rules of both sufficient and necessary conditions depending on the purpose. Here, decision tree analysis process can be skipped for parameter design because a single rule is not sufficient for solving a conflicting multi-objective design problem. However, this rule is useful for understanding the design problem because the simple rule represents the average structure of the design space.

The capability of each data mining technique and the features of the derived design rules are summarized in Table 5-1. Details of collaboration between these data mining techniques with their application are discussed in the next chapter.

At this stage, multiple design rules for improving each objective function are obtained. Finally, we choose one optimum design candidate by searching for a compatible design rule

that simultaneously improves all objective functions. The first effort that should be done in the search process is to improve each objective function by using the dominant main effects of different design variables. Then, the remaining conflicts (if any) are resolved by using the dominant interaction effects, and an optimum solution is chosen.

In the next section, ANOVA is reviewed briefly. For Self-organizing map and association rule, see Chapter 4. For decision tree analysis and rough set theory, see Chapter 3.

5.2.3 Analysis of Variance

ANOVA [5] is a method for quantitatively analyzing the effects of design variables on an objective function. The Kriging surrogate model is used to approximate the design space, and creates fine and uniform data samples in the design space for enabling the following statistical calculations. The mean and variance of all the data samples are calculated as:

$$\hat{\mu}_{total} = \int_{n} \cdots \int_{1} f(x_1, x_2, \ldots, x_n) dx_1 dx_2 \cdots dx_n \text{ , and} \tag{5-2}$$

$$\hat{\sigma}_{total}^2 = \int_{n} \cdots \int_{1} \{f(x_1, x_2, \ldots, x_n) - \hat{\mu}_{total}\}^2 dx_1 dx_2 \cdots dx_n \text{ .} \tag{5-3}$$

Design variables are normalized here.

The total variance $\hat{\sigma}_{total}^2$, which corresponds to the total effect, is decomposed into the variance due to each effect. The main effect of x_i and the interaction effect between x_i and x_j are calculated as:

$$\hat{\mu}_i(x_i) \equiv \int_{n} \cdots \int_{1} f(x_1, x_2, \cdots, x_n) dx_1 dx_2 \cdots dx_{i-1} dx_{i+1} \cdots dx_n - \hat{\mu}_{total} \text{ , and} \tag{5-4}$$

$$\hat{\mu}(x_i, x_j) \equiv \int_{n} \cdots \int_{1} f(x_1, x_2, \cdots, x_n) dx_1 dx_2 \cdots dx_{i-1} dx_{i+1} \cdots dx_{j-1} dx_{j+1} \cdots dx_n$$
$$- \hat{\mu}_i(x_i) - \hat{\mu}_j(x_j) - \hat{\mu}_{total} \text{ .} \tag{5-5}$$

The contribution ratio of each main effect to the total effect is calculated as:

$$P = \frac{\hat{\sigma}^2_{x_i}}{\hat{\sigma}^2_{total}}, \tag{5-6}$$

where

$$\hat{\sigma}^2_{x_i} = \int_i \{\hat{\mu}_i(x_i)\}^2 dx_i . \tag{5-7}$$

The contribution ratio of interaction effect is calculated similarly.

5.3 Multi-objective Parameter Design of Centrifugal Fan

The proposed parameter design method was applied to the design problem in the previous chapter [4] that numerically optimized the shape of a centrifugal fan installed in drying system of washer-dryer. In this design optimization problem, it was assumed that the fan had dimensional uncertainty due to mass production. The objectives of this fan design were to improve fan efficiency and the turbulent noise level under dimensional uncertainty. Thus, the following four objective functions were defined: the mean and standard deviation of the fan efficiency, and the mean and standard deviation of turbulent noise level. The fan efficiency and the turbulent noise level were evaluated using results from steady flow simulations.

The fan's shape was parameterized as a combination of meridional and blade profiles (Fig. 4-5). In the definition of the meridional profile, inlet diameter D_{0s}, inlet height b_0, and outlet height b_2 were taken as design variables. In the definition of the blade profile, the blade angle distribution was defined by a non-uniform rational B-spline curve with three control points. The design variables for the blade profile were assigned to these control points, Beta1, Beta2, Beta3, r_R$_1$, r_R$_{Beta}$, where r_R$_1$ and r_R$_{Beta}$ correspond to normalized variables of R$_1$ and R$_{Beta}$.

A probability density function for representing the dimensional uncertainty in these design variables is modeled with a rectangular function, the width of which was set equal to the tolerance. All the design parameters are summarized in Table 4-3.

The design space defined in Table 4-3 was sampled using the Latin hypercube sampling

method (LHS) with actual flow simulations. 79 valid data points were obtained, and Kriging models were constructed to approximate the global design space with these data. Using LHS again, new 1000 data points were collected, which the author considers as a sufficient number of data points for data mining. The proposed flowchart of data mining was applied to this database, and the multi-objective parameter design that takes into account performance robustness was demonstrated. Note that the database was the result of Design of Experiments, not the non-dominated solutions. Collaboration between these data mining methods is discussed in the next section.

5.4 Results and Discussion

First, ANOVA was conducted on the database. Figure 5-3 shows the calculated contribution ratios of the effects to each objective function. In the legends of Fig. 5-3, the name of a single design variable is the main effect, and a combination of two different design variables is the interaction effect from these design variables.

It was found that the main effects are dominant for $\mu(\eta_s)$, $\mu(L_{tb})$ and $\sigma(L_{tb})$, while interaction effects play an important role for role for $\sigma(\eta_s)$. Regarding the former three objective functions, design variables of the predominant main effects are different from each other, namely, b_2 for $\mu(\eta_s)$, r_R_1 for $\mu(L_{tb})$, and r_R_{Beta} for $\sigma(L_{tb})$. Therefore, it is possible to improve these three objective functions simultaneously by controlling these design variables independently.

In contrast, $\sigma(\eta_s)$ shares the dominant main effect of design variable b_2 with $\mu(\eta_s)$. This means that simultaneous improvement with these main effects would be impossible in terms of the mean and standard deviation of fan efficiency if these objective functions were in a trade-off relationship. However, it was found that there are also interaction effects relating to b_2, namely, b_2-Beta1 and b_2-Beta3, which can be used for solving a conflict between $\mu(\eta_s)$ and $\sigma(\eta_s)$.

(a) $\mu(\eta_s)$ (b) $\sigma(\eta_s)$

(c) $\mu(L_{tb})$ (d) $\sigma(L_{tb})$
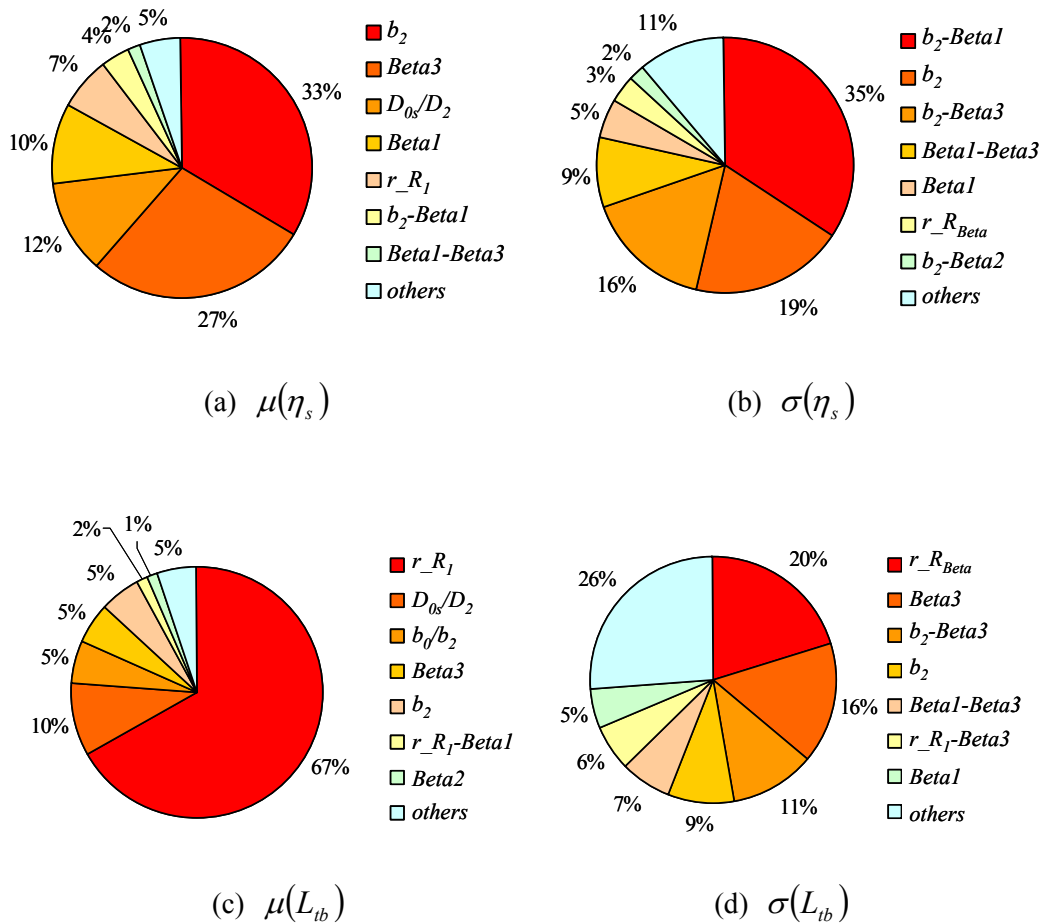
Figure 5-3 Contribution ratios of effects analyzed using ANOVA

ANOVA reveals dominant effects in the global design space and extracts design variables for careful investigation afterwards. However, ANOVA cannot clarify how these design variables and objective functions are correlated. Therefore, the author applied SOM to visualize the correlation patterns. Because SOM analysis is based on human recognition of patterns, it is necessary to create SOMs with the simplest clusters pattern as possible for avoiding misjudgments. This is possible by creating SOMs based on the similarity of the objective functions and dominant design variables, which are determined using ANOVA. In this design problem, the dominant design variables were chosen as b_2, D_{0s}/D_2, r_R_1, r_R_{Beta}, Beta1 and Beta3, which are in 75% of the contributions in Fig. 5-3.
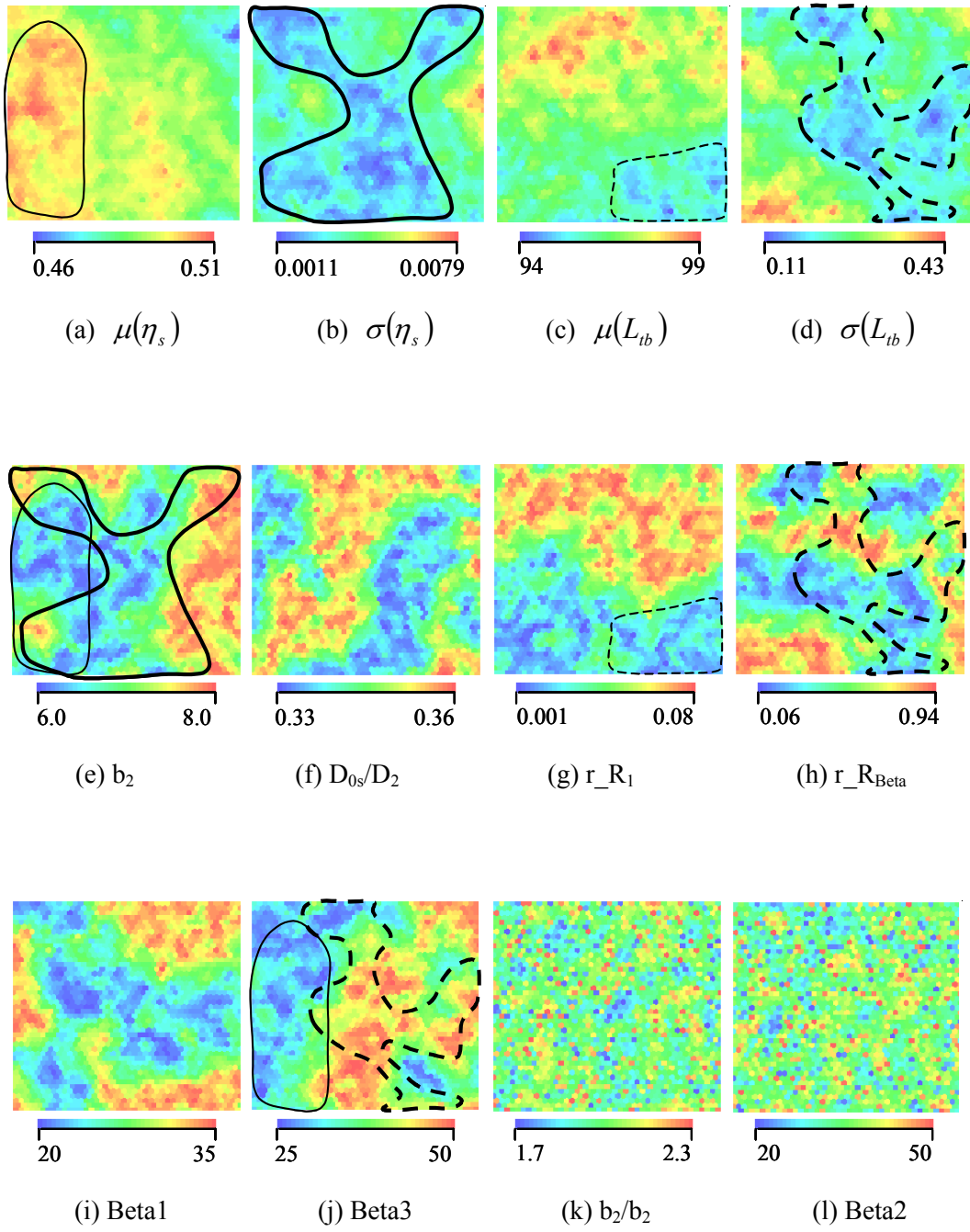
Figure 5-4 SOMs colored using design parameter values

Figure 5-4 shows SOMs created and colored with corresponding parameter values. It was confirmed that better $\mu(\eta_s)$ approximately corresponds to smaller values of the corresponding dominant design variables b_2 and Beta3 (areas inside thin solid lines in Figs. 5-4 (a), (e), and (j)). For improving $\sigma(\eta_s)$, the most dominant main effect of b_2 should be relatively smaller (areas inside thick solid lines in Figs. 5-4 (b) and (e)). Similarly, better $\mu(L_{tb})$ is related to small values of r_R$_1$ (areas inside thin dotted lines in Figs. 5-4 (c) and (g)). For improving $\sigma(L_{tb})$, r_R$_{Beta}$ and Beta3 may take smaller and larger values, respectively, although these correlations are not as clear as those of other objective functions (areas inside thick dotted lines in Figs. 5-4 (d), (h), and (j)). From Figs. 5-4 (a) and (b), it was recognized that the trade-off between $\mu(\eta_s)$ and $\sigma(\eta_s)$ is not strong, but careful choosing of design candidates is necessary.

As shown in Fig. 5-4, low-order qualitative correlations can be determined with SOMs as far as the cluster patterns remain simple. It is because of the strength of SOMs that we can examine correlations of more than four-dimensional data with maps. However, it was also concluded that it is difficult to detect low-order correlations from complicated cluster patterns as well as higher-order correlations with more than three parameters. To clarify these correlations, particularly quantitative ones, design rule extraction methods were adopted.

Decision tree analysis was then applied to the database, and a corresponding decision tree diagram to each objective function was obtained. From these diagrams, the following rules for extremely improving corresponding objective functions were obtained.

■ Rule for maximizing $\mu(\eta_s)$

if ($b_2 < 0.57$), (Beta3 < 0.16) and ($D_{0s}/D_2 < 0.53$) then (avg. $0.49 \rightarrow 0.50$) (5-8)

■ Rule for minimizing $\sigma(\eta_s)$

if ($0.16 \leqq b_2 < 0.65$) and (Beta3 $\geqq 0.74$) then (avg. $0.0033 \rightarrow 0.0024$) (5-9)

■ Rule for minimizing $\mu(L_{tb})$

if (r_R$_1 < 0.25$), ($b_2 \geqq 0.37$) and ($D_{0s}/D_2 < 0.33$) then (avg. $96.4 \rightarrow 94.7$) (5-10)

■ Rule for minimizing $\sigma(L_{tb})$

if (r_R$_{Beta}$ < 0.59), (Beta3 $\geqq$ 0.52) and (Beta1 < 0.24) then (avg. 0.25 → 0.19)

(5-11)

In "if" terms of Eqs. (5-8)-(5-11), the definition region of the design variables is normalized. The "avg." term means the change in the average of the corresponding objective function before and after applying the conditions represented in "if" terms. As already mentioned above, a single rule of necessary condition is obtained for each objective function.

The order of design variable appearing in the condition terms represents the order of sensitivities to the corresponding objective function. It is strength of decision tree analysis that both extraction of a simple rule and detection of the sensitive design variables are possible. In fact, design variables in the first condition terms exactly coincide with those in the ANOVA results.

However, the orders of design variables appearing after the second terms do not always match with those in ANOVA. Decision tree analysis extracts dominant design variables in each divided sub-group of data, while ANOVA detects dominant design variables in the global design space. This difference in target data results in the difference in dominant design variables. In this context, a rule derived from decision tree analysis can be defined as a localized rule.

A more important fact is that it is impossible to distinguish interaction effects from main effects from decision tree analysis, as expressed in Eq. (5-9), which has interaction effects as shown in Fig. 5-4 (b). This is because decision tree analysis is used to evaluate the sum of the effects.

Despite this weak point in decision tree analysis, the simple rule is useful to estimate the essence of the design problem. For example, for improving $\mu(\eta_s)$, levels of b$_2$ and Beta3 must be small, suggesting that a fan with a large reaction factor is crucial. To improve $\sigma(\eta_s)$, it was found that a better aspect ratio of the velocity triangle at the impeller exit is necessary to minimize the effect of dimensional uncertainty on the velocity profiles as much as possible. To improve $\mu(L_{tb})$, the maximum relative velocity at the blade inlet must be suppressed by reducing r_R$_1$ and increasing b$_2$. For improving $\sigma(L_{tb})$, design variable r_R$_{Beta}$ related to the blade load balance is the key issue.

In summary of ANOVA, SOM and decision tree analysis, it was concluded that the objective functions $\mu(\eta_s)$, $\mu(L_{tb})$, and $\sigma(L_{tb})$ can be controlled by the main effects of

different design variables. Regarding $\sigma(\eta_s)$, we need to use the interaction effect because the main effect of the same design variable was detected for $\mu(\eta_s)$ and $\sigma(\eta_s)$, which are in a trade-off relationship. Although a necessary condition to simultaneously improve $\mu(\eta_s)$ and $\sigma(\eta_s)$ was analyzed as $0.16 \leqq b_2 < 0.57$ from Eqs. (5-8) and (5-9). This condition is merely a necessary condition and the interaction effect was not distinguished.

Then, the rough set theory was applied to extract multiple design rules of sufficient conditions discriminating between main and interaction effects. In applying the rough set theory, definition ranges of design variables are discretized into five levels with equal widths. The ranges of the objective functions are also equally divided into five levels in a way that the optimum level contains enough data samples to be analyzed.

Tables 5-2 (a), (b), (c), and (d) show lists of derived rules for obtaining the optimum level of the corresponding objective functions, $\mu(\eta_s)$, $\sigma(\eta_s)$, $\mu(L_{tb})$, and $\sigma(L_{tb})$. The obtained rules are sorted in order of frequency of extracting the same rules. One column corresponds to one of the obtained rules. For instance, rule No. 1 in Table 5-2 (a) is

if (b_2 = level 1), (Beta1 = level 2), and (Beta3 = level 1)

then ($\mu(\eta_s)$= level 5). (5-12)

The strength of the rough set theory is that it can be used to extract many rules with minimum rule lengths automatically by the reduction mechanism. The weak point, unlike ANOVA and decision tree analysis, is that the importance of the obtained rules and design variables cannot be easily evaluated.

The "count" number on the far right of each table shows how many times each design variable appears in the rule elements. This index can be used to estimate the importance of the design variables. The design variables with larger count numbers are called "cores" in rough set theory. In fact, the cores in Tables 5-2 (a), (b), (c), and (d) roughly agree with the dominant design variables in ANOVA (Fig. 5-3). The author considers the reason the similar tendency was obtained is that the original data was uniformly sampled using LHS. Conversely, careful judgment is necessary when the sampling is not uniform.

The results from the rough set theory were compared with those from decision tree analysis. For example, the decision tree's rule for optimizing $\mu(\eta_s)$ in Eq. (5-8) signifies that levels of b_2, Beta3, and D_{0s}/D_2 should at least be within 1-3, 1, and 1-3, respectively.

Table 5-2 Design rules derived from rough set theory

(a) Rules for optimizing $\mu(\eta_s)$ (conditions for setting $\mu(\eta_s)$ in level 5)

No.	Variable	1	2	3	4	5	6	7	8	9	10	11	12	13	14	15	16	17	18	19	20	21	22	23	24	25			count
1	b_2	1	1	1	2	1	1	1	1	1	1	1	2	1		1	1	1			2	1	3	1					20
2	b_0/b_2		1				2					5		5															4
3	D_{0s}/D_2				1	1								2				1	1	2		3			4				8
4	r_R_1													1								1		1	1				4
5	r_R_{Beta}						2	1				3														2			4
6	$Beta1$	2		3						2						4	1	1			3				2				8
7	$Beta2$								4	1						2							3	1					5
8	$Beta3$	1	1	1	1	1	1	1	1	1	1	1	1	1	1	1	2	1	1	1	1	2	1	1	1	2			25

(b) Rules for optimizing $\sigma(\eta_s)$ (conditions for setting $\sigma(\eta_s)$ in level 1)

No.	variable	1	2	3	4	5	6	7	8	9	10	11	12	13	14	15	16	17	18	19	20	21	22	23	24			count
1	b_2	5	2	1	3	3	2	4	2	1		2	1				3	3	2	2	4		1	1				18
2	b_0/b_2								2	4		4		4		2				4								6
3	D_{0s}/D_2		1													3	3	1		2	5		2	5				8
4	r_R_1							4		4						2	1	3	2			2						7
5	r_R_{Beta}					4				2	4	2	2								4							6
6	$Beta1$	2		2	5	2	2	2	2	3	1	1	3	2	3		2		1		2	1	3		3			19
7	$Beta2$													2					5									2
8	$Beta3$	1	5	5	5	2		1		1				1	2	1			5		2	1	3					14

(c) Rules for optimizing $\mu(L_{tb})$ (conditions for setting $\mu(L_{tb})$ in level 1)

No.	Variable	1	2	3	4	5	6	7	8	9	10	11	count
1	b_2		3				3			3		4	4
2	b_0/b_2			3	3	3	4	3	3		4		7
3	D_{0s}/D_2	1		1		1		1				1	5
4	r_R_1	1	1	1	1	1	1	1	1	1	1	2	11
5	r_R_{Beta}		3			3	3			3			4
6	$Beta1$							4	4	5	2		4
7	$Beta2$		4		4								2
8	$Beta3$	3		2	4			4		5	3		6

(d) Rules for optimizing $\sigma(L_{tb})$ (conditions for setting $\sigma(L_{tb})$ in level 1)

No.	Variable	1	2	3	4	5	6	7	8	9	10	11	12	13	14	15	16	17	18	19	20	21	22	23	24	25	26	27	28	count
1	b_2	5		5	5		1		5	5	5	5		5			3	2	5		1		5	5	5	5	5	2	5	20
2	b_0/b_2								1			3	1		2					1	2			3						7
3	D_{0s}/D_2	5		2			3		3	5			5									2	2							8
4	r_R_1		1	4	5	3		1		5	5	4		5	2	3				4					5		5	4	4	16
5	r_R_{Beta}		1			2	1	1			4		1		1	2	2	2	5	2	1		5			1	4	2		17
6	$Beta1$	3		1		1		3			1	3		1	1	1	1	1	1			1	1		3	1	1	1	1	19
7	$Beta2$			1		1	4				5	1		5				3			2		3			5				10
8	$Beta3$		5		1	5	4		1	1							5	4		4	5	4		3					2	13

The rules from the rough set theory, which are related to the same design variables, are Nos. 4, 5, 14, 19, and 21 in Table 5-2 (a). It was confirmed that the rules' conditions from the rough set theory are more limited than those from the decision tree analysis. Moreover, some rough set's rules like Nos. 19 and 21 represent conditions that do not satisfy the rule from decision tree analysis. This relationship is also true for $\mu(L_{tb})$ and $\sigma(L_{tb})$. These are because the rules from the rough set theory are of sufficient conditions while the rule from decision tree is of a necessary condition.

For $\sigma(\eta_s)$, which is concerned with the interaction effect, b_2-Beta1, many rules that are related to this combination can be found from Table 5-2 (b). Figure 5-5 is a bubble chart of the possible level combinations of these design variables. The bubble size refers to the frequency of rule extraction. In this way, the interaction effects are distinguished from the main effects using the rough set theory. Moreover, possible combinations are determined quantitatively, unlike with SOM and decision tree analysis. Since we already know that b_2 should be in levels 1 - 3 for improving $\mu(\eta_s)$, it is concluded that Beta1 should be set in level 2 or 3. This corresponds to rule No. 9 in Table 5-2 (b).
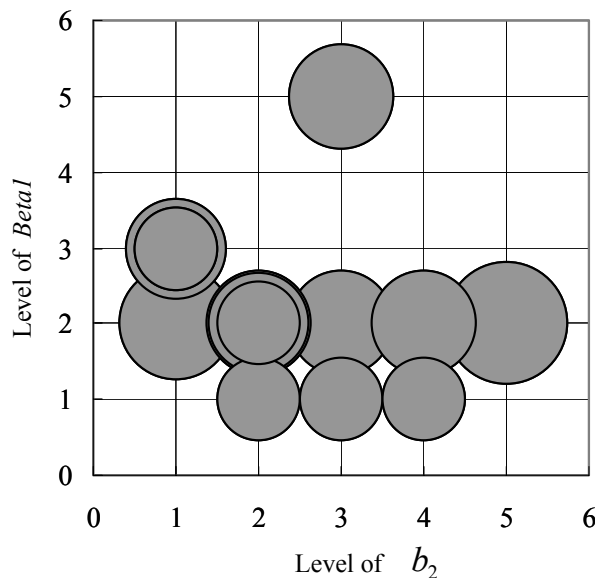

Figure 5-5 Possible level combinations between *b2* and *Beta1* for optimizing $\sigma(\eta_s)$

Finally, the association rule was applied to the database. As mentioned before, the association rule is used to derive multiple rules of both necessary conditions and sufficient conditions by changing the confidence parameter. Since obtaining necessary conditions was not the intention in this study, only the rules of sufficient condition were extracted by setting the confidence parameter to one, and compared the results with those from the rough set theory. For extraction of rules of necessary conditions using the association rule, please see the previous chapter.

Although the strength of the association rule is that the accuracy of rules is changeable, the rule length must be manually specified in advance. At this point, the rough set theory has an advantage over the association rule. Thus, the author referred the rule length in the results from the rough set theory (Table 5-2), and determined it as four for $\mu(\eta_s)$ and $\sigma(\eta_s)$, and as five for $\mu(L_{tb})$ and $\sigma(L_{tb})$. Table 5-3 summarizes the obtained rules with a confidence of one, sorted by magnitude of support.

By comparing Tables 5-2 and 5-3, it was confirmed that similar rules were obtained. In terms of interaction effect, b$_2$-Beta1, rule No. 9 in Table 5-2 (b) corresponds to rule No. 9 in Table 5-3 (b). The association rule provides almost the same rules sets as those with the rough set theory if the confidence is set to one and the same rule length is specified.

As discussed above, data mining methods have both strengths and weaknesses. Thus, their complementary use is necessary. By following the data mining process described in Fig. 5-2, and as demonstrated in this chapter, we can extract dominant effects using ANOVA, find trade-off patterns using SOM, and extract design rules using decision tree analysis, rough set theory, and association rule. In extracting multiple design rules, association rule should use the same rule length obtained from rough set theory. Based on the lists of multiple design rules finally obtained using the rough set theory or association rule, we can find a proper design candidate that solves the conflict between multiple objective functions. In this way, multi-objective parameter design is possible.

Table 5-3 Design rules derived from association rule

(a) Rules for optimizing $\mu(\eta_s)$ (conditions for setting $\mu(\eta_s)$ in level 5)

No	Variable	1	2	3	4	5	6	7	8	9	10	11	12	13	14	15	16	17	18	19	20	21	22	count
1	b_2	1	1	2	1	1	1	1	1	1	1	1		1	1	1	1	1	2	1			1	18
2	b_0/b_2		1						2			5												3
3	D_{0s}/D_2			1			1							2				2		1		1		6
4	r_R_1												1								1			2
5	r_R_{Beta}				1	2								3					2					4
6	$Beta1$	2									3					4			1		2	3		6
7	$Beta2$						4			1				2	3					1				5
8	$Beta3$	1	1	1	1	1	1	1	1	1	1	1	1	1	1	2	1	1	1	2	1	1	2	22
	confidence	1	1	1	1	1	1	1	1	1	1	1	1	1	1	1	1	1	1	1	1	1	1	
	support(%)	0.8	0.8	0.7	0.7	0.7	0.7	0.7	0.7	0.7	0.7	0.6	0.6	0.6	0.6	0.5	0.5	0.5	0.5	0.5	0.5	0.5	0.5	

(b) Rules for optimizing $\sigma(\eta_s)$ (conditions for setting $\sigma(\eta_s)$ in level 1)

No	variable	1	2	3	4	5	6	7	8	9	10	11	12	13	14	15	16	17	18	19	20	21	22	23	24	count
1	b_2	5	2	1	2	4	3	3	2	1		2	3		1	1	1		2				3	4	1	18
2	b_0/b_2								2										1					4	4	4
3	D_{0s}/D_2		1									2				5	2		1			1		1		7
4	r_R_1							4		4				2									1			4
5	r_R_{Beta}				4								2		4			1			4	2				6
6	$Beta1$	2		2	2	2	2	5	2	3	1			3	3	3	3	4		1	2	3	2		3	19
7	$Beta2$																			2						1
8	$Beta3$	1	5	5		1	2	5		1		5	1	1				5		1	1					13
	confidence	1	1	1	1	1	1	1	1	1	1	1	1	1	1	1	1	1	1	1	1	1	1	1	1	
	support(%)	1.1	0.9	0.9	0.8	0.8	0.8	0.8	0.7	0.7	0.6	0.5	0.5	0.5	0.5	0.5	0.5	0.4	0.4	0.4	0.4	0.4	0.4	0.4	0.4	

(c) Rules for optimizing $\mu(L_{tb})$ (conditions for setting $\mu(L_{tb})$ in level 1)

No	Variable	1	2	3	4	5	6	7	8	9	10	11	count
1	b_2				3	3	3		4				4
2	b_0/b_2	3	3	3	4			4		3	3		7
3	D_{0s}/D_2		1					1	1	1	1		5
4	r_R_1	1	1	1	1	1	1	1	2	1	1	1	11
5	r_R_{Beta}				3	3	3				3		4
6	$Beta1$	4	4				5	2					4
7	$Beta2$			4		4							2
8	$Beta3$	4		4				5	3	2		3	6
	confidence	1	1	1	1	1	1	1	1	1	1	1	
	support(%)	0.4	0.4	0.4	0.4	0.4	0.4	0.4	0.4	0.4	0.4	0.4	

(d) Rules for optimizing $\sigma(L_{tb})$ (conditions for setting $\sigma(L_{tb})$ in level 1)

No	Variable	1	2	3	4	5	6	7	8	9	10	11	12	13	14	15	16	17	18	19	20	21	22	23	24	25	26	27	28	29	30	31	32	33	34	count
1	b_2	5			5	5	5	1	2			3	5			1	1				5	5	5	5	5	5	5	5	5	5	5	5	5	5	2	25
2	b_0/b_2										2			2			1	1				1	3	3								4				8
3	D_{0s}/D_2	5			2		2								3					3	5					5		5	2	5	5	5	5			13
4	r_R_1		1	5	4					4					2	1	1			3	3	5			4	5	5	5	4		5		4		4	18
5	r_R_{Beta}		1			5		1	2	2		2	1	1	1	1	1	1	2	2							4	4			5			2		18
6	$Beta1$	3			1	1	1			1	1	1	1	3	1				3	1	1		3	3	1		1			1	3	1	3	3	3	24
7	$Beta2$		1		3	3	1				2		5		4			5		5											1			5		11
8	$Beta3$		5	1				4	4	4	4	5				5	5		5		1	1	1		3			2	2							16
	confidence	1	1	1	1	1	1	1	1	1	1	1	1	1	1	1	1	1	1	1	1	1	1	1	1	1	1	1	1	1	1	1	1	1	1	
	support(%)	0.7	0.5	0.4	0.4	0.3	0.3	0.3	0.3	0.3	0.3	0.3	0.3	0.3	0.3	0.3	0.3	0.3	0.3	0.3	0.3	0.3	0.3	0.3	0.3	0.3	0.3	0.3	0.3	0.3	0.3	0.3	0.3	0.3	0.3	

5.5 Conclusion

A new multi-objective parameter design method was proposed, which can be used to solve conflicting trade-off problems between multiple objective functions. This method uses lists of design rules obtained by a combination of the following data mining techniques: analysis of variance, self-organizing map, decision tree analysis, rough set theory, and association rule. The derived database of the design rules distinguishes main and interaction effects of design variables. The proposed method first uses the predominant main effects of different design variables for controlling each objective function. Then, it uses predominant interaction effects to resolve the remaining trade-offs if there are any. The proposed method is applied for not only to better understanding design problems through data mining but also to reusing the design rules for establishing a more generalized robust parameter design method than a traditional ones like the Taguchi method.

The author also summarized the capabilities of each data mining technique to clarify their strengths and weaknesses for facilitating their combined use. ANOVA should be first applied to determine important main and interaction effects, which are used in the later process of data mining. SOM or alternative visualization methods should be used for finding qualitative low-order correlations, particularly for determining the trade-off relationship between objective functions. Then, design rule extraction methods should be applied to obtain quantitative design rules for solving the trade-off problems. A decision tree analysis can be applied to extract an easy-to-understand single rule of necessary condition, but it cannot handle main and interaction effects discriminately. Both the rough set theory and the association rule can be applied to extract multiple design rules that distinguish main and interaction effects. While the rough set theory is used to only extract rules of sufficient conditions, the association rule is used to extract rules of both sufficient and necessary conditions. However, the rough set theory has advantages in finding the minimum rule length, which has to be specified in advance for the association rule. Therefore, use of the association rule, after obtaining the proper rule length with the rough set theory, is recommended.

References

[1] Taguchi, G., Chowdhury, S., Wu, Y., Taguchi, S., and Yano, H., Taguchi's Quality Engineering Handbook, John Wiley & Sons, Inc., Hoboken, New Jersey, 2004.

[2] Kumar, A., Keane, A., Nair, P., and Shahpar, S., Robust Design of Compressor Blades Against Manufacturing Variations, ASME Paper No. DETC2006-99304, 2006.

[3] Shimoyama, K., Robust Aerodynamic Design of Mars Exploratory Airplane Wing with a New Optimization Method, Ph.D thesis, University of Tokyo, Japan, 2006.

[4] Sugimura, K, Jeong, S, Obayashi, S., and Kimura, T, Kriging-Model-Based Multi-Objective Robust Optimization and Trade-Off Rule Mining of a Centrifugal Fan with Dimensional Uncertainty, JSME Journal of Computational Science and Technology, Vol.3, No.1, 2008.

[5] Jeong, S., Murayama, M., and Yamamoto, K., Efficient Optimization Design Method Using Kriging Model, Journal of Aircraft, Vol. 42, pp.413-420, 2005.

[6] Obayashi, S., Sasaki, D., and Oyama, A., Finding Tradeoffs by Using Multiobjective Optimization Algorithms, Transactions of the Japan Society for Aeronautical and Space Sciences, Vol. 47, No. 155, pp.51-58, 2004.

[7] Lim, J. N., Sasaki, D., Jeong, S., and Obayashi, S., Application of Fuzzy Decision Tree to Datasets Obtained by Evolutionary Algorithms, JSME Proc. of annual meeting, Vol. 7, pp.9-10, (in Japanese), 2005.

[8] Sugimura, K., Obayashi, S. and Jeong, S., Multi-objective Design Exploration of a Centrifugal Impeller Accompanied with a Vaned Diffuser, ASME Paper No. FEDSM 2007-37502, 2007.

Chapter 6

Concluding Remarks

6.1 Conclusion of Chapter 2

An efficient shape parameterization method was developed for centrifugal turbomachinery configurations. Non-uniform rational B-Spline curves were used and assigned only to the enclosing boundaries of the blades consisting of the hub, shroud, leading edge, and trailing edge profiles. That is, traditional multi-sectional definition of the blade profile was avoided and the number of design variables required was reduced.

A hybrid optimization algorithm was developed by combining simulated annealing with an artificial neural network for efficient, global, and single-objective optimization. The neural network adaptively learned the simulation results collected by simulated annealing. The trained neural network, as an approximation model, periodically predicted a possible global optimum. Simulated annealing itself explored the design space independently of the neural network in case the neural network learning failed, which ensured a robust and fully automatic optimization. The approximated design space was then analyzed by regression analysis to determine the sensitivity and non-linearity of each design variable, which helps the designer understand the global characteristics of the design space.

The methods developed here were applied to design problems of centrifugal impeller and diffuser. The optimized impeller had a unique S-shaped leading edge profile, which effectively controlled secondary flows and improve the flow uniformity at the impeller exit. The optimized diffuser had a unique bending trailing edge with a wedge-shaped gap, which generated a streamwise vortex and prevented boundary layer separation. In both designs, the design turnaround times were accelerated, although the degree of speedup depended on how much design space was non-linear. Regression analysis revealed important design variables that were related to these unique shapes of the optima.

Based on these results, it was concluded that the proposed single-objective design exploration methods enabled efficient global optimization of centrifugal turbomachinery configurations. It was also concluded that the revealed characteristics of the design space helped designers to understand design problems at a macroscopic level.

6.2 Conclusion of Chapter 3

The single-objective optimization method developed in Chapter 2 had defects in decision-making under the uncertainty in trade-off balance among multiple design objectives. Thus, a multi-objective optimization method was developed using a multi-objective genetic algorithm to obtain widespread non-dominated solutions. Multiple non-dominated solutions then became available, with which a designer could adaptively choose a solution to a design requirement specified afterwards. To analyze microscopic structures of the design space, decision tree analysis and rough set theory were adopted as data mining methods. These methods were used to extract quantitative design rules to achieve extreme design in terms of each objective function.

The developed methods were applied to the design of a low-specific-speed centrifugal impeller with a vaned diffuser. The design objectives were set to improve both aerodynamic efficiency and aerodynamic stability. Seven non-dominated solutions were obtained, and simultaneous improvements were confirmed by experiments with a selected non-dominated solution. Data mining methods indicated that dimensions such as inlet blade angle, vane-less diffuser height, and blade load balance were important for extreme designs. Decision tree analysis generally extracts a single rule of necessary condition, while rough set theory mines multiple rules of sufficient conditions. Decision tree analysis extracts a single rule but it is easy to understand, while rough set theory extracts complicated multiple rules, some of which are concerned with interaction effects of design variables.

Based on these results, it was concluded that the multi-objective design exploration methods were capable of handling the uncertainty in design decisions and revealing key reasons for achieving extreme designs.

6.3 Conclusion of Chapter 4

The multi-objective optimization method developed in Chapter 3 was deterministic and could not be used when the degree of uncertainty in design conditions was not negligible. Therefore, this method had been extended to a probabilistic method that enables robust optimization with uncertainty in design conditions.

First, a generalized framework for multi-objective robust optimization was developed by incorporating probabilistic representation of design parameters, which was compatible with parameterization in the Taguchi method. Multi-objective robust design optimization became feasible within a practical design turnaround time using Kriging models that can rapidly calculate significant number of statistical responses among design parameters. In terms of data mining, extraction of design rules for achieving any trade-off balance were investigated. The aspiration vector concept was introduced to represent the designer's preference of trade-off balance, and the combined use of association rule and the aspiration vector was proposed for design rule extraction.

The integrated method of multi-objective robust optimization and trade-off rule mining was named MORDE (Multi-objective Robust Design Exploration), and was applied to an industrial design problem of a centrifugal fan used for a washer-dryer. The design was aimed toward improving the means and standard deviations of resultant statistical distributions of fan efficiency and turbulence noise level under conditions of dimensional variances due to mass production. It was demonstrated that designers could flexibly choose a design candidate and find quantitative rules to accomplish the required trade-off balance. It was also clarified that association rules can reveal multiple and quantitative design rules, while it is difficult to performed the same analysis with a Self-organizing map. Rules from association rules can be either necessary or sufficient conditions depending on control parameters for rule extraction.

Based on these results, it was concluded that MORDE was capable of design optimization within a practical design turnaround time taking both uncertainties in design decisions and design conditions into account. It was also concluded that MORDE revealed key reasons for achieving arbitrary trade-off balance.

6.4 Conclusion of Chapter 5

Practical design exploration methods were developed as described in the previous chapters. As design rules extracted by data mining methods represent key structures in multi-objective design space, it seemed beneficial to use these design rules for parameter design. Thus, a new rule-based multi-objective parameter design method was proposed in this chapter.

This new method used a database of design rules obtained by the following data mining methods: analysis of variance, Self-organizing map, decision tree analysis, rough set theory, and association rule. The design rules distinguished main and interaction effects of design variables. The method first used the predominant main effects of different design variables for optimizing different objective functions. Then, it used predominant interaction effects to resolve any remaining trade-off conflicts.

The strengths and weaknesses of each data mining method were clarified and a systematic procedure of cooperative data mining was established. Analysis of variance was first applied to determine the important main and interaction effects, which were used in the later process of data mining. Self-organizing maps or alternative visualization methods were used to find qualitative low-order correlations, particularly to determine the trade-off relationships between objective functions. Then, design rule extraction methods were applied to obtain quantitative design rules for solving the trade-off problems. Decision tree analysis could be applied to extract a single easy-to-understand rule of necessary conditions, but could not distinguish main and interaction effects. Therefore, decision tree analysis could be skipped depending on the purpose of parameter design. Both rough set theory and the association rule were applied to extract multiple design rules that distinguished main and interaction effects. While rough set theory was used to extract rules of sufficient conditions, association rules were used to extract rules of either sufficient or necessary conditions. However, rough set theory had an advantage in finding the minimum rule length, which had to be specified in advance for association rules. Therefore, the use of association rules, after obtaining the proper rule length by rough set theory, was recommended.

The proposed method was applied to the same design optimization problem as that discussed in Chapter 4 and showed advantages over traditional parameter design methods, such as the Taguchi method, in that it could handle multiple design objectives and interaction effects.

6.5 Conclusion of Thesis

The objective of this research was to develop and propose design optimization and data mining methods that were efficient and practical for designing centrifugal turbomachinery for

consumer products. It was necessary to conduct efficient global optimization as well as deal with the uncertainties in design decisions and design conditions. It was also necessary to facilitate knowledge reinforcement in design routines.

With regard to efficient global optimization, a shape representation method tailored for centrifugal turbomachinery configurations was developed, and hybrid methods that use global optimization algorithms (simulated annealing and multi-objective genetic algorithm) and approximation models (neural network and Kriging model) were developed. Design turnaround time was then reduced in such a way that the optimization methods can be used in designs for consumer products.

With regard to uncertainty handling, a multi-objective robust optimization method was developed. By modeling variances in design parameters in a multi-objective optimization framework, practical designs with uncertainties became feasible with various non-dominated solutions.

With regard to knowledge reinforcement, several data mining methods were applied and the characteristics of each method were clarified by comparative studies. Design rules for any prescribed trade-off balance could be obtained by cooperative use of design rule extraction methods and aspiration vectors. Moreover, the obtained design rules were reused in a newly proposed multi-objective parameter design method.

The designs from Chapters 3 and 4 were applied to actual products of a vacuum cleaner and a washer-dryer manufactured by Hitachi Ltd. in 2006 and 2007, respectively. Thus, the capability of the proposed methods was successfully demonstrated in real-world applications.

6.6 Future Work

The following topics have arisen from this research as future work.

■   Verification of results of multi-objective robust design optimization

With regard to the centrifugal fan for a washer-dryer discussed in Chapters 4 and 5, it was impossible to measure the actual variance in dimensions and resulting performance of all the products for economic reasons. That is, the resultant statistics of multi-objective robust

design optimization have not yet been verified. This may remain difficult for this product in the near future. Thus, verification of this design method should be conducted with a different product, such as a semi-conductor device, the performance of which can be measured on the production line.

■ Design rule extraction related to physics

In this research, only design parameters such as design variables, constraints, and objective functions were defined as targets of data mining. However, designers are also interested in physical mechanisms of performance improvement. Therefore, it is expected that some indexes representing flow physics should also be added to the design parameters.

Recent developments in scientific visualization techniques have made it possible to extract dominant vortex structures and topological structures of flow fields. Thus, the information from these results should be added to the design parameters.

■ Efficient multi-objective global optimization in large design space

When the design space becomes high-dimensional, it generally becomes difficult to search for optimum solutions. This is typically true with multi-objective robust optimization with large number of design variables. In this research, the dimensions of design space were relatively low (between 8 and 27). However, these sizes are not sufficient for conducting design optimization of a product system comprised of several numbers of turbomachinery. Therefore, a more efficient optimization method must be developed.

Kriging models can provide an Expected Improvement (EI) index that enables probability-based efficient global optimization. However, EI is tailored for single- and not multi-objective objective optimization problems. Therefore, this approach should be extended to multi-objective optimization in future studies.

Appendix A
Non-uniform Rational B-Spline Curve

NURBS (Non-uniform Rational B-Spline) curve is a generalized form of various parameter curves. Its definition contains B-Spline curves and Bezier curves as special cases. NURBS curve definition is associated with (1) position vectors of defining polygon vertices, (2) basis function to define how to interpolate the vertices to make a smooth curve, (3) a parameter to designate locations along the curve, (4) NURBS degree or order, and (5) knot vector.

An arbitrary point on a NURBS curve is defined as:

$$\vec{X}(t) = \frac{\sum_{i=0}^{n} \left\{ N_{i,p}(t) \cdot w_i \cdot \vec{x}_i \right\}}{\sum_{i=0}^{n} \left\{ N_{i,p}(t) \cdot w_i \right\}}, \tag{A-1}$$

$$\vec{U} = \left\{ u_0, u_1, \cdots, u_m \right\}, \tag{A-2}$$

where

n : $n+1$ is number of control points (polygon vertices),

m : $m+1$ is number of components in knot vector,

p : NURBS degree $\left(k = p + 1 \text{ is called NURBS order} \right)$,

$\vec{x}_i$: $i-th$ control point $\left(i = 0,1,\cdots,n \right)$,

w_i : weight for $i-th$ control point $\left(i = 0,1,\cdots,n \right)$,

$N_{i,p}$: basis function,

$\vec{U}$: knot vector,

t : parameter.

Note there is a constraint among m, n and p,

$$m = n + p + 1. \tag{A-3}$$

In practice, the knot vector and the parameter are usually defined within the range from 0.0 to 1.0. NURBS basis function is defined in the following recursive form.

$$N_{i,p}(t) = \frac{t - u_i}{u_{i+p} - u_i} \cdot N_{i,p-1}(t) + \frac{u_{i+p+1} - t}{u_{i+p+1} - u_{i+1}} \cdot N_{i+1,p-1}(t), \tag{A-4}$$

$$\begin{matrix} N_{i,0}(t) = 1 & \left(u_i \leq t < u_{i+1} \right) \\ 0 & \left(otherwise \right) \end{matrix}. \tag{A-5}$$

The conventional rule $\dfrac{0}{0} \equiv 0$ is adopted.

The sum of basis functions is equivalent to 1.

$$\sum_{i=0}^{n} N_{i,p}(t) = 1 \tag{A-6}$$

The last basis function, $N_{n,p}(t)$, cannot be calculated with the above definition because $t = u_m$ is out of the definition. Then,

$$N_{n,p}(t) = 1 - \sum_{i=0}^{n-1} N_{i,p}(t) \tag{A-7}$$

To make the edges of a NURBS curve coincide with the first and the last control points, some components of the knot vector are overlapped as

$$\vec{U} = \left\{ \underbrace{u_p, u_p, \cdots, u_p}_{p+1}, \underbrace{u_{p+1}, u_{p+2}, \cdots, u_n}_{n-p}, \underbrace{u_{n+1}, u_{n+1}, \cdots, u_{n+1}}_{p+1} \right\}. \tag{A-8}$$

The components in the middle part are evenly increased. This type of knot vector is called an open uniform knot vector.

Acknowledgements